Measurement of Branching Fractions and Form Factor Parameters of $B \to D\ell\nu$ and $B \to D^*\ell\nu$ Decays at BaBar

by

Kenji Hamano

BSc, Osaka University, 1983
MSc, Osaka University, 1985

A Dissertation Submitted in Partial Fulfillment of the
Requirements for the Degree of

Doctor of Philosophy

in the Department of Physics and Astronomy

University of Victoria

Measurement of Branching Fractions and Form Factor Parameters of $B \to D\ell\nu$ and $B \to D^*\ell\nu$ Decays at BaBar

by

Kenji Hamano

BSc, Osaka University, 1983
MSc, Osaka University, 1985

Supervisory Committee

Dr. R. V. Kowalewski, Supervisor (Department of Physics and Astronomy)

Dr. D. Karlen, Member (Department of Physics and Astronomy)

Dr. J. M. Roney, Member (Department of Physics and Astronomy)

Dr. F. van Veggel, Outside Member (Department of Chemistry)

Dr. D. Asner, External Examiner (Department of Physics, Carleton University)

Supervisory Committee

Dr. R. V. Kowalewski, Supervisor (Department of Physics and Astronomy)

Dr. D. Karlen, Member (Department of Physics and Astronomy)

Dr. J. M. Roney, Member (Department of Physics and Astronomy)

Dr. F. van Veggel, Outside Member (Department of Chemistry)

Dr. D. Asner, External Examiner (Department of Physics, Carleton University)

Abstract

We use a global fit to determine the form factor slopes and branching fractions of the decays $B \to D\ell\nu$ and $B \to D^*\ell\nu$. We reconstruct $D\ell$ pairs and construct a 3-dimensional distribution binned in lepton momentum, D momentum and $\cos\Theta_{B-D\ell}$. These kinematic variables provide good separation between the signal and background. We fit electron and muon samples separately and combine them after calculating systematic uncertainties. The form factor slopes, ρ_D^2 for $B \to D\ell\nu$ and ρ^2 for $B \to D^*\ell\nu$ decays, are measured to be $\rho_D^2 = 1.22 \pm 0.04 \pm 0.07$ and $\rho^2 = 1.21 \pm 0.02 \pm 0.07$, where the errors are statistical and systematic, respectively. Branching fractions are fitted to be $\mathcal{B}(B^+ \to \bar{D}^0\ell^+\nu) = (2.36 \pm 0.03 \pm 0.12)$ % and $\mathcal{B}(B^+ \to \bar{D}^{*0}\ell^+\nu) = (5.37 \pm 0.02 \pm 0.21)$ %. We use these results to determine the products, $\mathcal{G}(1)|V_{cb}| = (43.8 \pm 0.8 \pm 2.3) \times 10^{-3}$ and $\mathcal{F}(1)|V_{cb}| = (35.7 \pm 0.2 \pm 1.2) \times 10^{-3}$

of the form factors at zero recoil and the CKM matrix element $|V_{cb}|$, from which $|V_{cb}|$ can be extracted using theoretical input.

Table of Contents

List of Tables

List of Figures

Acknowledgements

I am indebt to many people. Dr. Robert V. Kowalewski guided me throughout my graduate study. Dr. Vera Luth has provided great effort during the review process of this analysis. Dr. Zoltan Ligeti offered me valuable theoretical advices. I thank Florian Bernlochner for his collaboration in systematic studies of this analysis.

I am also grateful to people in the Physics and Astronomy department at University of Victoria. I have received many academic and clerical support during the course of my graduate study. I thank professors who offered useful and inspiring lectures. I would like particularly to recognize Dr. Charles Picciotto and Dr. Michel Lefebvre. University of Victoria BaBar group gave me valuable advises. I owe a great deal to Dr. J. Mike Roney, Dr. Randal J. Sobie, Dr. Swagato Banerjee and Dr. Bipul Bhuyan. I have received generous computing support from Dr. Ashok Agarwal. I am grateful to Dr. Richard K. Keeler who helped me to get into graduate study. Fellow graduate students gave me delightful moments when I was struggling with my research. Special thanks to Ian Nugent and Tayfun Ince

The BaBar collaboration and SLAC accelerator colleagues deserve special acknowledgments. The excellent beam condition, the computing support and the expertise of the semileptonic working group made this analysis possible.

I also have received generous support from the University of Victoria, Geoffrey and Elise Fox, Patricia Pearce and Charles S. Humphrey.

To my wife Mari

Chapter 1

Introduction

The Standard Model of particle physics describes the properties and the interactions of fundamental particles. Although it is very successful, it is incomplete. It fails to account for most of the mass in the universe called the dark matter, which is inferred from observations in astrophysics. It also fails to account for non-zero neutrino masses, which are implied by neutrino oscillation experiments. Even within the domains of its applicability, it has about two dozen free parameters to be determined by experiment. Quantitative tests of the Standard Model, as well as the searches for physics beyond the standard model, require precise knowledge of these parameters. This thesis address the determination of one of these parameters and lays a ground work of improved determination of another parameter.

In the Standard Model, there are three families of fundamental particles. The second and the third families behave as more massive partners of the first. The families are classified by a quantity called "flavor". Among the fundamental interactions of the Standard Model, only the charged weak interaction can change flavor. This interaction is responsible for the radioactive decay of nuclei, which is the result of a transition between two different quark flavors. The flavor changing interaction produces many fascinating phenomena : particle-antiparticle oscillations, neutrino oscillations and particle-antiparticle (CP) symmetry violation. These phenomena

in the quark sector are related to the complex 3×3 CKM matrix in the Standard Model. This matrix mixes different flavors of quarks and the non-vanishing phase of the matrix is responsible for the violation of CP (particle-antiparticle) symmetry.

Particle-antiparticle oscillations and CP violation have been observed in K mesons, and similar observations in B mesons were expected. A B meson is composed of an anti-bottom quark and either an up or down quark. Two experimental facilities were built in 1990s to investigate the properties of B mesons. One is the BaBar experiment at SLAC (Stanford Linear Acceleration Center, California, USA) and the other is the BELLE experiment at KEK (High Energy Accelerator Research Organization, Tsukuba, Japan). They have tuned their accelerators, PEP-II at SLAC and KEKB at KEK, to produce B meson pairs for more than 9 years. These machines are called B-factories because they produce B mesons with a higher rate than other experiments have ever done. The primary targets of B-factories are to quantitatively determine the mechanism of CP-violation in B mesons and to measure the fundamental parameters of the Standard Model related to B physics with high precision.

In this dissertation, we are interested in semileptonic decays of the type $B \to X_c \ell \nu$. Here, ℓ is an electron or a muon, ν is a neutrino and X_c is a hadronic system including a charm quark. Details of these particles and semileptonic decays are explained in chapter 2. The main features of these decays are

- They are experimentally accessible and theoretically clean.
- We can measure one of the fundamental parameters of the Standard Model, $|V_{cb}|$, through these decays.

There remain problems in our understanding of these decays :

- $B^0 \to D^{*-} \ell^+ \nu$ decay [1] branching fraction measurements disagree.

  Existing measurements are summarized in Table 1.1. The results vary from

[1] Charge conjugate modes are implied throughout this text

Branching Fraction	Experiment (year)
$0.0459 \pm 0.0023 \pm 0.0040$	BELLE (2002) [1]
$0.0470 \pm 0.0013^{+0.0036}_{-0.0031}$	DELPHI (2001) [2]
$0.0490 \pm 0.0007^{+0.0036}_{-0.0035}$	BABAR (2005) [3]
$0.0526 \pm 0.0020 \pm 0.0046$	OPAL (2000) [4]
$0.0553 \pm 0.0026 \pm 0.0052$	ALEPH (1997) [5]
$0.0590 \pm 0.0022 \pm 0.0050$	DELPHI (2004) [6]
$0.0609 \pm 0.0019 \pm 0.0040$	CLEO (2003) [7]

Table 1.1: [$B^0 \to D^* \ell\nu$ **BF**] $B^0 \to D^{*-}\ell^+\nu$ branching fractions from different experiments. The first uncertainty is statistical and the second one is systematic.

ρ^2_D	Experiment (year)	Decay mode
$0.97 \pm 0.98 \pm 0.38$	ALEPH (1997) [5]	$B^0 \to D^-\ell^+\nu$
$1.12 \pm 0.22 \pm 0.14$	BELLE (2002) [8]	$B^0 \to D^-\ell^+\nu$
$1.27 \pm 0.25 \pm 0.14$	CLEO (1999) [9]	$B^0 \to D^-\ell^+\nu$ and $B^+ \to \bar{D}^0\ell^+\nu$

Table 1.2: [$B \to D\ell\nu$ **FF slope**] Form factor slope ρ^2_D from different experiments. The first uncertainty is statistic and the second one is systematic.

0.0459 (BELLE) to 0.0609 (CLEO), and those measurements are not consistent with each other.

- $B \to D\ell\nu$ decay form factor slope is not well measured.

  Existing measurements are listed in Table 1.2. The best measurement from BELLE has a 23 % uncertainty.

- There is a discrepancy between the inclusive and the sum of exclusive branching fractions. In principle, the sum of the branching fractions of exclusive modes is equal to the inclusive branching fraction. The inclusive branching fraction as well as the two major exclusive modes $B \to D\ell\nu$ and $B \to D^*\ell\nu$ have been measured by many experiments. In addition, recently the $B \to D^{(*)}\pi\ell\nu$ mode was measured [10,11] with good precision. However, these three exclusive modes do not add up to inclusive branching fraction. It is evident something is missing. The most probable candidates are decays of the type of $B \to D^{(*)}\pi\pi\ell\nu$

and $B \to D_s^{(*)} K^{(*)} \ell\nu$, which have never been measured.

The $B \to D^* \ell\nu$ decay mode has the largest branching fraction of any B decay. Thus, it is important to solve the above problems.

In existing measurements, each decay mode is reconstructed exclusively to measure branching fractions or form factor parameters. However, the above problems are related with each other and cannot easily be solved by looking at a single decay mode. For example, to reconstruct D^*, we need to reconstruct its decay product π. However the π moves very slowly and is difficult to detect. All existing measurements of $B \to D^* \ell\nu$ decays have uncertainties related to this issue. Moreover, the $B \to D \ell\nu$ measurements suffer from large background from mis-reconstructed $D^* \ell\nu$ decays. We use a global fit to pairs of D mesons and leptons to measure simultaneously the branching fractions and form factor parameters of the principal semileptonic decay modes $B \to D \ell\nu$ and $B \to D^* \ell\nu$. The two decay modes are distinguished from each other and from backgrounds via their different kinematic signatures in a 3-dimensional space. As a result, the measurements have no uncertainty related to slow pion reconstruction.

The measurement described in Ref. [11] takes similar approach. It simultaneously determines the $B \to D \ell\nu$, $B \to D^* \ell\nu$ and $B \to D^{(*)} \pi \ell\nu$ branching fractions. In that analysis, they fully reconstruct one B meson and look at semileptonic decays of the other B. They reconstruct all particles except the neutrino. Thus, they can use the conservation of 4-momentum to separate signal, where the only missing particle is the massless neutrino, from background. The measurement is complementary to ours because it uses explicit D^* reconstruction and does not measure form factor parameters due to the limited statistics of the fully reconstructed samples.

In order to measure another parameter, $|V_{ub}|$, of the Standard Model, semileptonic decays of the type $B \to X_u \ell\nu$ is used. Here X_u is a hadronic system including a up quark. The dominant background in the measurements is $B \to X_c \ell\nu$ decays and

uncertainties related to this background is one of the dominant systematic errors in $|V_{ub}|$. Thus, a better understanding and precise measurements of $B \to X_c \ell \nu$ decays is a major factor to further improve the determination of $|V_{ub}|$.

Chapter 2

Theory

2.1 The standard model of particle physics

The Standard Model (SM) of particle physics [12–14] is a very successful theory. It has survived many experimental tests in the past three decades. In this theory matter consists of three families of quarks and leptons and forces or interactions between them are mediated by gauge bosons. There are four types of fundamental interactions : gravity, electromagnetic, weak and strong. Gravity is too small and usually plays no role in particle physics at currently accessible energies. Strong interactions are mediated by gluons, weak interactions by weak bosons (W and Z) and electromagnetic interactions by photons. These are listed in Table 2.1.

Each particle has an associated anti-particle. Anti-particles have opposite quan-

Family	First	Second	Third
Leptons	electron e^-	muon μ^-	tau τ^-
	neutrino ν_e	ν_μ	ν_τ
Quarks	up (u)	charm (c)	top (t)
	down (d)	strange (s)	bottom (beauty b)
Interactions	Electromagnetic	Weak	Strong
Gauge bosons	photon γ	weak bosons $W^\pm$, Z^0	gluon g

Table 2.1: [**Fundamental constituents**] Fundamental constituents in the Standard Model.

	mass	charge	spin
e	0.511 MeV	-1	1/2
μ	106 MeV	-1	1/2
τ	1777 MeV	-1	1/2
ν_e	0	0	1/2
ν_μ	0	0	1/2
ν_τ	0	0	1/2
u	$(1.5 - 3.0) \times 10^{-3}$ GeV	+2/3	1/2
c	1.25 ± 0.09 GeV	+2/3	1/2
t	172.5 ± 2.7 GeV	+2/3	1/2
d	$(3 - 7) \times 10^{-3}$ GeV	-1/3	1/2
s	0.95 ± 0.25 GeV	-1/3	1/2
b	4.20 ± 0.07 GeV	-1/3	1/2
γ	0	0	1
$W^\pm$	80.4 GeV	$\pm$1	1
Z	91.2 GeV	0	1
g	0	0	1

Table 2.2: [**Mass, charge and spin**] Mass, charge and spin of fundamental constituents in the Standard Model. Charges are given in the unit of proton charge. Neutrino mass is not zero. However, massive neutrinos have not yet been integrated into the Standard Model.

tum numbers. For example, anti-muons have positive charge. The mass, charge and spin of the fundamental constituents are listed in Table 2.2. It has recently been established through measurements that at least two of the neutrino species have non-zero mass [15], but we did not include the new discovery in the Table. Note that we use natural units ($\hbar = 1$ and $c = 1$); thus, energy, momentum and mass have the same unit.

2.1.1 Strong Interactions

Strong interactions are the interactions between quarks and gluons and are governed by Quantum Chromo-Dynamics (QCD), which is a part of the Standard Model. No single quark has ever been isolated. This is called confinement, which is a feature of QCD. In QCD, quarks and gluons have a charge called color. There are three fundamental color charges, red, green and blue, and QCD has a group structure

meson	quark contents
π^0	$u\bar{u}$ or $d\bar{d}$
π^+	$u\bar{d}$
K^0	$d\bar{s}$
K^+	$u\bar{s}$
D^0	$c\bar{u}$
D^+	$c\bar{d}$
B^0	$d\bar{b}$
B^+	$u\bar{b}$

Table 2.3: [**Quark contents**] Quark contents of mesons.

$SU(3)_c$; the c stands for color. If you could isolate a bare quark, you would see its color charge. However, QCD allows only color-less combinations of quarks to exist in isolation. If we combine red and anti-red quarks, the pair is color-less, as is the combination of red, green and blue quarks. Thus, quarks always appear as a quark - anti-quark pair or a combination of three quarks. Quark - anti-quark pairs form mesons, and combinations of three quarks form baryons. For example, a B^0 meson consists of d and $\bar{b}$ (anti-b) quarks, and a B^+ meson of u and $\bar{b}$ quarks. Other mesons are listed in Table 2.3. A proton is a baryon and is made of two u quarks and one d quark. Baryons and mesons are both called hadrons. As quarks are confined in hadrons, all fundamental particles we can isolate are divided into two categories : leptons and hadrons.

2.1.2 Electroweak interactions

Electromagnetic and weak interactions are unified into electroweak interactions, whose group structure is $SU(2) \times U(1)_Y$. This Y represents the weak hypercharge and the charge of $SU(2)$ is called weak isospin. Weak hypercharge and weak isospin are not conserved because the $SU(2) \times U(1)_Y$ symmetry is broken. The only conserved charge is the electric charge. However, the properties of $SU(2)$ can be seen, for example, in the interactions between weak bosons and photons. The mechanism to break electroweak symmetry has not yet known. Among many theoretical predictions, the

most popular one is so called Higgs mechanism.

There are two types of weak interactions : neutral weak interactions, which are mediated by Z^0 and charged weak interactions, which are mediated by $W^{\pm}$. The charged weak interaction is the only fundamental interaction which violates flavor conservation and CP symmetry. This is done by coupling up-type and down-type quarks as explained in the following section. The neutral weak interaction couples up-type quarks with up-type quarks and down-type with down-type, thus, does not change flavor and conserves CP symmetry.

2.2 Charged weak interactions and CKM matrix

An interesting property of the charged weak interactions is that the weak eigenstates of quarks and leptons differ from their mass eigenstates. When a quark couples to a weak boson, the quark is not in its mass eigenstate. Instead, the quark is a superposition of the three families of quark mass eigenstates. This is expressed by the following equation [16, 17]:

$$\begin{pmatrix} d' \\ s' \\ b' \end{pmatrix} = \begin{pmatrix} V_{ud} & V_{us} & V_{ub} \\ V_{cd} & V_{cs} & V_{cb} \\ V_{td} & V_{ts} & V_{tb} \end{pmatrix} \begin{pmatrix} d \\ s \\ b \end{pmatrix} \tag{2.1}$$

The primed states of the left hand side are the weak eigenstates of down-type quarks and those on the right hand side are the mass eigenstates. This matrix which mixes the different flavors of down-type quarks is called the Cabibbo-Kobayashi-Maskawa (CKM) Matrix. The matrix elements of the CKM matrix are free parameters of the Standard Model to be determined by experiments. Determination of the magnitude of the CKM matrix elements $|V_{cb}|$ and $|V_{ub}|$ is one of the principal goals of the BaBar experiment.

Figure 2.1 is an example of the charged current weak interactions which is me-

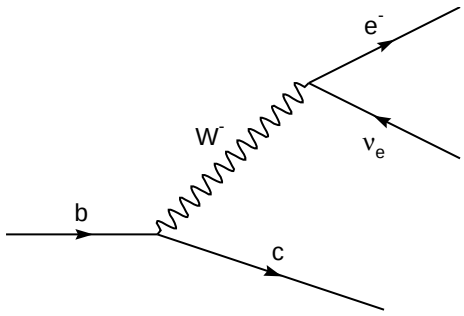

Figure 2.1: [**Quark level weak interaction**] Weak interaction via W boson.

diated by a charged weak boson W^-. In this case, a bottom quark changes into a charm quark and produces a electron-neutrino pair. When W interacts with c, the W couples with the weak eigenstate of the quark in the same family, namely s'

$$s' = V_{cd}d + V_{cs}s + V_{cb}b \tag{2.2}$$

Since initial quark is b, the interaction picks up only b component of s'. Thus, the amplitude of this interaction is proportional to V_{cb}.

CP-transformation changes a charged weak decay of a particle into the decay of its anti-particle. The amplitude of the decay remains unchanged, by CP-transformation, if the elements of the CKM matrix are all real numbers. Thus the imaginary phase of the CKM matrix is responsible for CP violation [18]. In case of decays or mixing of mesons, their charge asymmetry is strongly suppressed [19]. In order for charge asymmetry to be observable, for example in B decays, interference between two different decay processes is necessary.

2.3 Semileptonic decays of B mesons

Hadrons including u, d, s and c quarks have been measured with good precision because they can be produced at lower center-of-mass energy. In order to get a

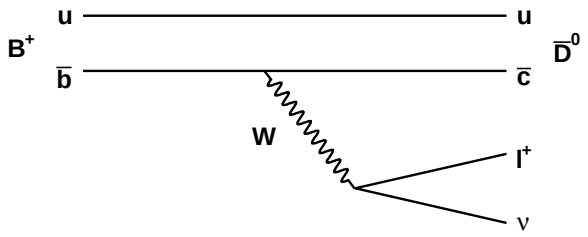

Figure 2.2: [**Weak decay of B meson**] Weak decay of a B meson.

complete picture of the three families of the Standard Model, the properties of quarks b and t need to be understood. This is one of the reasons B-factories were built. B-factories copiously produce pairs of B mesons and we can investigate the properties of B mesons (or b quarks) through their decays. Decay modes are categorized into hadronic, leptonic and semileptonic decays.

- Hadronic decays : decays into only hadrons. For example, $B^0 \to D^-\pi^+$
- Leptonic decays : decays into only leptons. For example, $B^+ \to e^+\nu_e$
- Semileptonic decays : decays into a combination of hadrons and leptons. For example, $B^0 \to D^-e^+\nu_e$

Among these three modes, semileptonic decays are the best for measuring CKM matrix elements $|V_{cb}|$ and $|V_{ub}|$.

As described in the previous section, the amplitude of the decay $b \to c\ell\nu$ is proportional to V_{cb}, which means the decay rate is proportional to $|V_{cb}|^2$. Since bare quarks do not exist in nature, the process given in Figure 2.1 is possible only with hadrons. One example is shown in Figure 2.2. This time, a B^+ meson decays into a $\bar{D}^0$ meson and a ℓ^+-neutrino pair. Here ℓ denotes a charged lepton, which is either electron or muon throughout this document unless otherwise stated.

In the case of semileptonic $B \to X_c\ell\nu$ decays (X_c denotes a meson or a meson system including one c quark), there are the following decay modes (see also

Appendix A):

- For B^+
  - $B^+ \to \bar{D}^0 \ell^+ \nu$
  - $B^+ \to \bar{D}^{*0} \ell^+ \nu$
  - $B^+ \to \bar{D}^{(*)} \pi \ell^+ \nu$

    This includes
    - Excited charm mesons : $B^+ \to \bar{D}_0^{*0} \ell^+ \nu$, $B^+ \to \bar{D}_1^0 \ell^+ \nu$, $B^+ \to \bar{D}_1'^0 \ell^+ \nu$ and $B^+ \to \bar{D}_2^{*0} \ell^+ \nu$
    - Non-resonant decays : $B^+ \to D^- \pi^+ \ell^+ \nu$, $B^+ \to \bar{D}^0 \pi^0 \ell^+ \nu$, $B^+ \to D^{*-} \pi^+ \ell^+ \nu$ and $B^+ \to \bar{D}^{*0} \pi^0 \ell^+ \nu$
  - $B^+ \to \bar{D}^{(*)} \pi\pi \ell^+ \nu$
  - $B^+ \to D_s^{(*)-} K^{(*)+} \ell^+ \nu$
- For B^0
  - $B^0 \to D^- \ell^+ \nu$
  - $B^0 \to D^{*-} \ell^+ \nu$
  - $B^+ \to \bar{D}^{(*)} \pi \ell^+ \nu$

    This includes
    - Excited charm mesons : $B^0 \to D_0^{*-} \ell^+ \nu$, $B^0 \to D_1^- \ell^+ \nu$, $B^0 \to D_1'^- \ell^+ \nu$ and $B^0 \to D_2^{*-} \ell^+ \nu$
    - Non-resonant decays : $B^0 \to D^- \pi^+ \ell^+ \nu$, $B^0 \to \bar{D}^0 \pi^0 \ell^+ \nu$, $B^0 \to D^{*-} \pi^+ \ell^+ \nu$ and $B^0 \to \bar{D}^{*0} \pi^0 \ell^+ \nu$
  - $B^0 \to \bar{D}^{(*)} \pi\pi \ell^+ \nu$
  - $B^0 \to D_s^{(*)-} \bar{K}^{(*)0} \ell^+ \nu$

The D_0^*, D_1, D_1' and D_2^* are called D^{**} as a whole. These D^* and D^{**} are excited charm mesons. The D meson is spin zero whereas the spin of D^* meson is 1. The D^{**} have 1 unit of orbital angular momentum (see Appendix B). The D^* and D^{**} decay into either D^0 or D^+ plus some pions (see Appendix A). Since D^* and D^{**} are exited states, they have the same quark content as D. Thus, for example, the $B^+ \to \bar{D}_1^0 \ell^+ \nu$ decay diagram is just like Figure 2.2. The D_s^+ meson consists of c and $\bar{s}$ quarks and does not decay into D^0 or D^+. The $B \to D^{(*)}\pi\pi\ell\nu$ and $B \to D_s^{(*)}K^{(*)}\ell\nu$ modes have never been measured.

2.4 Heavy Quark Effective Theory (HQET) and decay rates

For a free quark, as shown in Figure 2.1, it is possible to calculate decay rates [12]. The amplitude is given by

$$\mathcal{M} = -i\frac{G_F}{\sqrt{2}} V_{cb} L^\mu H_\mu \tag{2.3}$$

where G_F is the Fermi constant. The amplitude is proportional to V_{cb}. Here, L^μ is called the leptonic current because it expresses the flow of weak hypercharge from ν_e to e^-. H_μ is the quark current in this example because it represents the flow from b to c. These currents have Lorentz index μ because the amplitude is expressed in a Lorentz invariant form. Since we are dealing with relativistic velocities, the Lorentz invariant form is more convenient than other forms.

The leptonic current can be written in terms of Dirac spinors of the charged lepton u_l and the neutrino v_ν

$$L^\mu = \bar{u}_l \gamma^\mu (1 - \gamma_5) v_\nu \tag{2.4}$$

where γ^μ and γ_5 are the 4-dimensional Dirac gamma matrices. The quark current H_μ can be written in terms of quark spinors b and c

$$H^\mu = \bar{c} \gamma^\mu (1 - \gamma_5) b \tag{2.5}$$

There is no complication and we can calculate the decay rates.

However in reality, there are no bare quarks, and b and c quarks are confined inside of hadrons B and $\bar{D}$ as shown in Figure 2.2. This complicates the decay process because it is possible to have interactions between u and $\bar{b}$ quarks and so on. These interactions are strong interactions and cannot be calculated from first principles in the Standard Model. In reactions involving momentum transfers that are large compared to the QCD scale, $\Lambda \simeq 0.5$ GeV, the strong forces between quarks are not so strong and their cross sections can be calculated perturbatively, but this does not apply in the present case. Now, H^μ is not a simple quark current but a complicated hadronic current. It is written in the following form

$$H^\mu =< D|\bar{c}\gamma^\mu(1-\gamma_5)b|B >=< D|V^\mu|B > - < D|A^\mu|B > \tag{2.6}$$

where

$$\begin{aligned} V^\mu &= \bar{c}\gamma^\mu b \quad \text{(vector current)} \\ A^\mu &= \bar{c}\gamma^\mu\gamma_5 b \quad \text{(axial-vector current)} \end{aligned} \tag{2.7}$$

These $< D|$ and $|B >$ include the complication. Since we cannot easily calculate the matrix elements $< D|V^\mu|B >$ and $< D|A^\mu|B >$, we express them in terms of unknown functions called form factors. For example, for $B \to D\ell\nu$ decays, the matrix elements are given by

$$< D(p')|V^\mu|B(p) >= f_+(p+p')^\mu + f_-(p-p')^\mu \tag{2.8}$$

$$< D(p')|A^\mu|B(p) >= 0 \tag{2.9}$$

where f_+ and f_- are form factors. This means that we push complications into form factors and express decay rates using form factors. Then we can concentrate on how to calculate form factors.

Since we cannot calculate form factors from first principles, we need models or extra symmetries to calculate them. One successful method is to use Heavy Quark Effective Theory (HQET) [20, 21]. This theory can be applied to mesons consisting of a heavy quark, Q, and a light quark, q. Since the mass of c and b quarks are much heavier than u and d quarks (Table 2.2), the decays involving D and B mesons are ideal places to apply this theory. This theory uses extra symmetries [20] that are exact in the limit of infinitely heavy quark mass m_Q :

- Heavy quark flavor symmetry

  The dynamics is unchanged under the exchange of heavy quark flavors.

- Heavy quark spin symmetry

  The dynamics is unchanged under arbitrary transformations on the spin of the heavy quark.

The exchange of heavy quark flavors means, for example, an exchange of a b quark by a c quark. One important consequence of the Heavy Quark Symmetry on decay amplitudes is the prediction of the existence of a single and universal form factor, which is called the Isgur-Wise Function [21, 22]. Since $m_Q < \infty$, these are only approximate symmetries. HQET provides us with corrections to the heavy quark limit in a systematic way.

In the following sections, we give the decay rate formulae of the two major decay modes $B \to D\ell\nu$ and $B \to D^*\ell\nu$ based on HQET [21, 22]. $B \to D^{**}\ell\nu$ decay rates are given in Appendix G.

2.4.1 $B \to D\ell\nu$

The differential decay rate is given by

$$\frac{d\Gamma(B \to D\ell\nu)}{dw} = \frac{G_F^2 |V_{cb}|^2 m_B^5}{48\pi^3} r^3 (w^2-1)^{3/2} \mathcal{J}_D(w) \tag{2.10}$$

where

$$\mathcal{J}_D(w) = [(1+r)h_+ - (1-r)h_-]^2 \tag{2.11}$$

w is the velocity transfer defined by

$$w \equiv v_B \cdot v_D \tag{2.12}$$

where v_B and v_D are 4-velocities of B and D mesons. w can be understood as the relativistic boost of the D in the B rest frame. w is Lorentz invariant and linearly related to the momentum transfer q^2 :

$$w = \frac{m_B^2 + m_D^2 - q^2}{2m_B m_D} \tag{2.13}$$

More details are in Appendix E. r is the mass ratio

$$r = \frac{m_D}{m_B} \tag{2.14}$$

In heavy quark limit, the form factors $h_+(w)$ and $h_-(w)$ are

$$h_+(w) = \xi(w), \;\; h_-(w) = 0 \tag{2.15}$$

where $\xi(w)$ is the Isgur-Wise Function and can be expanded in the powers of $(w-1)$ because $0 \leq (w-1) < 0.6$

$$\xi(w) = \xi(1)[1 - \rho_D^2(w-1) + ...] \tag{2.16}$$

where ρ_D^2 is the form factor slope. This form factor slope is one of the parameters we try to determine in our analysis. $h_+(1) = \xi(1)$ can be calculated by the Lattice

QCD [23].

Caprini, Lellouch and Neubert proposed a better way to parametrize the Isgur-Wise Function [24]. They include higher order in the $(w-1)$ expansion and relate the curvature and slope using unitarity bounds of the decay amplitude. Thus, $h_+(w)$ can be expressed by one parameter ρ_D^2 that includes higher order terms :

$$h_+(z) = h_+(1)[1 - 8\rho_D^2 z + (51\rho_D^2 - 10)z^2 - (252\rho_D^2 - 84)z^3 + ...] \tag{2.17}$$

where

$$z = \frac{\sqrt{w+1} - \sqrt{2}}{\sqrt{w+1} + \sqrt{2}} \tag{2.18}$$

We call this the CLN parametrization. In the CLN parametrization, $h_+(w)$ is expanded in powers of z instead of $(w-1)$. Since $0 \leq z < 0.06$, higher order terms are more suppressed.

2.4.2 $B \to D^* \ell \nu$

The kinematic variables in $B \to D^* \ell \nu$ decays are shown in Figure 2.3.

- θ_ℓ : Angle between the directions of "the ℓ in the W rest frame" and "the W in the B rest frame".
- θ_V : Angle between the directions of "the D in the D^* rest frame" and "the D^* in the B rest frame".
- χ : Azimuthal angle between the planes formed by "W-ℓ system" and "$D^* - D$ system".

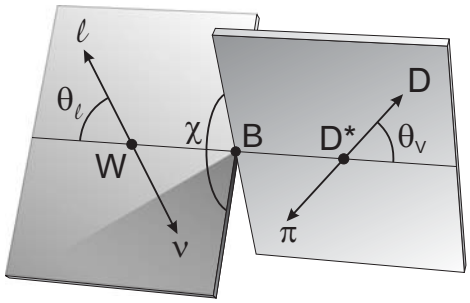

Figure 2.3: [$B \to D^*\ell\nu$ **decay geometry**] Geometry of $B \to D^*\ell\nu$ decays.

The differential decay rate is given by

$$\begin{aligned}
\frac{d\Gamma(B\to D^*\ell\nu)}{dw\,d\cos\theta_V\,d\cos\theta_\ell\,d\chi} &= \frac{3G_F^2}{4(4\pi)^4}|V_{cb}|^2 m_B m_{D^*}^2\sqrt{w^2-1}(1-2wr+r^2)\times \\
&\quad [(1-\cos\theta_\ell)^2\sin^2\theta_V|H_+(w)|^2 \\
&\quad +(1+\cos\theta_\ell)^2\sin^2\theta_V|H_-(w)|^2 \\
&\quad +4\sin^2\theta_\ell\cos^2\theta_V|H_0(w)|^2 \\
&\quad -4\sin\theta_\ell(1-\cos\theta_\ell)\sin\theta_V\cos\theta_V\cos\chi H_+(w)H_0(w) \\
&\quad +4\sin\theta_\ell(1+\cos\theta_\ell)\sin\theta_V\cos\theta_V\cos\chi H_-(w)H_0(w) \\
&\quad -2\sin^2\theta_\ell\sin^2\theta_V\cos 2\chi H_+(w)H_-(w)]
\end{aligned}$$

where $H_i(w)$ are called the helicity form factors. These form factors are related to another set of form factors, $h_V(w)$, $h_{A_1}(w)$, $h_{A_2}(w)$ and $h_{A_3}(w)$, as follows.

$$H_i = -m_B\frac{R(1-r^2)(w+1)}{2\sqrt{1-2wr+r^2}}h_{A_1}(w)\widetilde{H}_i(w) \tag{2.19}$$

where $\widetilde{H}_i(w)$ are given by

$$\begin{aligned}
\widetilde{H}_\pm(w) &= \tfrac{\sqrt{1-2wr+r^2}}{1-r}\left(1\mp\sqrt{\tfrac{w-1}{w+1}}R_1(w)\right) \\
\widetilde{H}_0(w) &= 1+\tfrac{w-1}{1-r}\left(1-R_2(w)\right)
\end{aligned} \tag{2.20}$$

where $R_1(w)$ and $R_2(w)$ are the form factor ratios.

$$R_1(w) = \frac{h_V(w)}{h_{A_1}(w)}, \quad R_2(w) = \frac{h_{A_3}(w) + r h_{A_2}(w)}{h_{A_1}(w)} \tag{2.21}$$

and

$$r = \frac{m_D^*}{m_B}, \;\; R = \frac{2\sqrt{m_B m_D^*}}{m_B + m_D^*} \tag{2.22}$$

In the first approximation, $R_1(w)$ and $R_2(w)$ has no w dependence

$$\begin{aligned} R_1(w) &= R_1 \\ R_2(w) &= R_2 \end{aligned} \tag{2.23}$$

and $h_{A_1}(w)$ is given by

$$h_{A_1}(w) = h_{A_1}(1)\left[1 - \rho^2(w-1) + ...\right] \tag{2.24}$$

where ρ^2 is the form factor slope. These ρ^2, R_1 and R_2 are the parameters we try to determine in the fit.

With the CLN parametrization [24]

$$\begin{aligned} R_1(w) &= R_1 - 0.12(w-1) + 0.05(w-1)^2 \\ R_2(w) &= R_2 + 0.11(w-1) - 0.06(w-1)^2 \\ h_{A_1}(w) &= h_{A_1}(1)\left[1 - 8\rho^2 z + (53\rho^2 - 15)z^2 - (231\rho^2 - 91)z^3\right] \end{aligned} \tag{2.25}$$

It is convenient to use integrated form of the differential decay rate in some calculations (see section 4.4 and 5.5). If we integrate the differential decay rate over angles, we get

$$\frac{d\Gamma(B \to D^* \ell \nu)}{dw} = \frac{G_F^2 |V_{cb}|^2 m_B^5}{48\pi^3} r^3 (w^2-1)^{1/2} \mathcal{J}_{WD}(R_1, R_2, \rho^2) \tag{2.26}$$

where

$$\mathcal{J}_{WD}(R_1, R_2, \rho^2) = (w+1)^2 [h_{A_1}]^2 (\tilde{h}_+^2 + \tilde{h}_-^2 + \tilde{h}_0^2) \tag{2.27}$$

and

$$\begin{aligned} \tilde{h}_\pm(w) &\equiv (1-r)\widetilde{H}_\pm(w) = \sqrt{1-2wr+r^2}\left(1 \mp \sqrt{\tfrac{w-1}{w+1}} R_1(w)\right) \\ \tilde{h}_0(w) &\equiv (1-r)\widetilde{H}_0(w) = (1-r) + (w-1)\left(1 - R_2(w)\right) \\ &= (w-r) - (w-1)R_2(w) \end{aligned} \tag{2.28}$$

2.5 Isospin symmetry

Isospin symmetry is an approximate symmetry due to the similar mass of u and d quarks. The strong interaction couples only to the color charge and is independent of the electric charge or flavor of the quarks. Thus, the quarks with the same mass and color have strong interactions of identical strength. This is the basis of isospin symmetry. Isospin has the same mathematical structure as spin or angular momentum. For example, when its magnitude is 1 its z-component can be either -1, 0, or +1. The u and d quarks are treated as a doublet and isospin is assigned such that

$$u : |1/2, +1/2>, \quad d : |1/2, -1/2> \tag{2.29}$$

where numbers are |magnitude, z-component>. The isospin of s, c, b and t quarks are all zero.

The isospin conservation of semileptonic B decays is not obvious because those decays are weak decays. Weak interactions are flavor-dependent and isospin is not necessarily conserved. We take $B^0 \to D^{*-}\ell^+\nu$ and $B^0 \to D^{*-}\ell^+\nu$ decays as an example to consider isospin symmetry. In Figure 2.2, if u is replaced by d, the diagram represents the $B^0 \to D^{*-}\ell^+\nu$ decay. From heavy quark symmetry, the weak decay part $\bar{b} \to \bar{c}$ occurs independently. Thus, the weak decay does not distinguish

between the two decay amplitudes. Since the remainder of the process involves strong interactions, the corrections to the picture of the weak decay of a free heavy quark conserve isospin.

We can determine the isospin of hadrons from their constituent quarks, for example,

$$\begin{aligned} B^+(u\bar{b}) &: |1/2, +1/2>, \quad \bar{D}^0(u\bar{c}) : |1/2, +1/2> \\ B^0(d\bar{b}) &: |1/2, -1/2>, \quad D^-(d\bar{c}) : |1/2, -1/2> \end{aligned} \tag{2.30}$$

Thus, from isospin symmetry, the partial decay rates of the two decays $B^+ \to \bar{D}^0 \ell^+ \nu$ and $B^0 \to D^- \ell^+ \nu$ are the same :

$$\Gamma(B^+ \to \bar{D}^0 \ell^+ \nu) = \Gamma(B^0 \to D^- \ell^+ \nu) \tag{2.31}$$

However, since total decay rates of B^+ and B^0 are different [10], branching fractions of the above two decay modes are different because

$$\text{Branching fraction} = \frac{\text{Partial rate}}{\text{Total rate}} \tag{2.32}$$

As total decay rates are inverse of lifetimes, the ratio of the branching fractions is given by

$$\frac{\mathcal{B}(B^+ \to \bar{D}^{*0} \ell^+ \nu)}{\mathcal{B}(B^0 \to D^{*-} \ell^+ \nu)} = \frac{\Gamma(B^+ \to D^* \ell \nu)\tau_{B^+}}{\Gamma(B^0 \to D^* \ell \nu)\tau_{B^0}} = \frac{\tau_{B^+}}{\tau_{B^0}} \tag{2.33}$$

where τ_{B^+} and τ_{B^0} are the lifetimes of B^+ and B^0. More calculations of isospin are given in Appendix C.

Chapter 3

BaBar data and Event selection

3.1 BaBar data

We use a data sample of approximately 230 million $B\bar{B}$-pairs, collected by the BaBar detector. This corresponds to an integrated luminosity of 207 fb^{-1}. The $B\bar{B}$-pairs are produced from the decay of the $\Upsilon(4S)$ resonance created by the asymmetric e^+e^- collider, PEP-II [25], at the Stanford Linear Accelerator Center (SLAC). We also use 21.5 fb^{-1} of off-resonance data collected 40 MeV below the $\Upsilon(4S)$ resonance. The off-resonance data are used to subtract the background from the process $e^+e^- \to f\bar{f}$, where f is a lighter quark (u, d, s or c) or a charged lepton (e, μ or τ). We also use Monte Carlo (MC) simulated events. In BaBar, the package EvtGen [26] is used to generate MC events. The GEANT4 software [31] is used to simulate the response of the BaBar detector. The generated particles are tracked through the detector material where they lose energy, interact with detector materials and leave signals in the active detector elements. To reconstruct particles from the detector signals, the same program is used for both BaBar data and simulated events.

The ISGW2 model [27, 28] is used to generate $B \to D\ell\nu$ and $B \to D^{**}\ell\nu$ events. These are re-weighted to HQET-inspired models as described in section 5.5. The Goity-Roberts model [29, 30] is used to simulate non-resonant $B \to D^{(*)}\pi\ell\nu$ decays. For $B \to D^*\ell\nu$ events, the HQET-based model, as described in chapter 2, is employed.

3.2 BaBar detector

A detailed description of the BaBar detector can be found elsewhere [32]. Here, we give a brief summary relevant to our analysis. In the following a cylindrical coordinate system is used. The z-axis coincides with beam axis and the origin with the beam collision point.

The BaBar detector consists of different components. From inside to outside :

- Silicon Vertex Tracker (SVT)

  SVT is composed of five layers of double-sided silicon strip detectors. Each layer has two sides : one with strips parallel to the beam axis (to measure ϕ coordinate) and one with strips perpendicular to the beam axis (to measure the z coordinate).

- Drift Chamber (DCH)

  DCH is composed of 40 layers of small hexagonal cells providing position and ionization loss (dE/dx) measurements for charged particles. The charged particles, moving through the helium-isobutane (He, C_4H_{10}) gas in the DCH, ionize the gas. The electrons produced by the ionization drift to the anode wires because of the high voltage (usually 1930 V) between the wires. The drift time determines the distance from the anode and the total charge gives dE/dx.

  SVT and DCH are both charged particle tracking systems which can measure the z coordinate and azimuthal angle θ. They are in a 1.5 T axial magnetic field. We can determine the momentum of charged particles from the curvature of their tracks.

- Cerenkov Detector (Detector of Internally Reflected Cerenkov light, DIRC)

  The silica bars of DIRC produce Cerenkov light from charged particles. DIRC can measure the angle of the Cerenkov cone (Cerenkov angle). The Cerenkov

light is produced when the speed of the charged particle v is larger than the speed of the light in the silica bar c/n, where n is the index of refraction of the silica. We can determine the speed of the charged particle from the Cerenkov angle Θ_C using the following relation :

$$v \cos \Theta_C = \frac{c}{n} \tag{3.1}$$

This speed combined with the momentum from the tracking systems gives the mass of the charged particle.

- Electromagnetic Calorimeter (EMC)

  EMC is a finely segmented array of thallium-doped cesium iodide (CsI(Tl)) crystals. EMC can measure the energy of electrons and photons (γ). An electron or a photon, which entered a crystal in the EMC, produces an electromagnetic shower in the crystal. The scintillation light produced by the shower is collected by the silicon photo-diode. The number of collected photons is proportional to the energy deposited in the crystal.

- Instrumented Flux return (IFR)

  IFR is designed to identify muons and to detect neutral hadrons such as K^0 and neutrons.

With the combination of above components, we can identify particles with relatively long lifetime such as electrons, muons, photons, pions (π), kaons (K), and protons. As an example, Figure 3.1 shows how dE/dx can distinguish different types of particles. We can also measure particle energies and momenta. The resolution in transverse momentum of charged particles is 0.7 % at 2 GeV. The photon energy resolution is 3 % at 1 GeV.

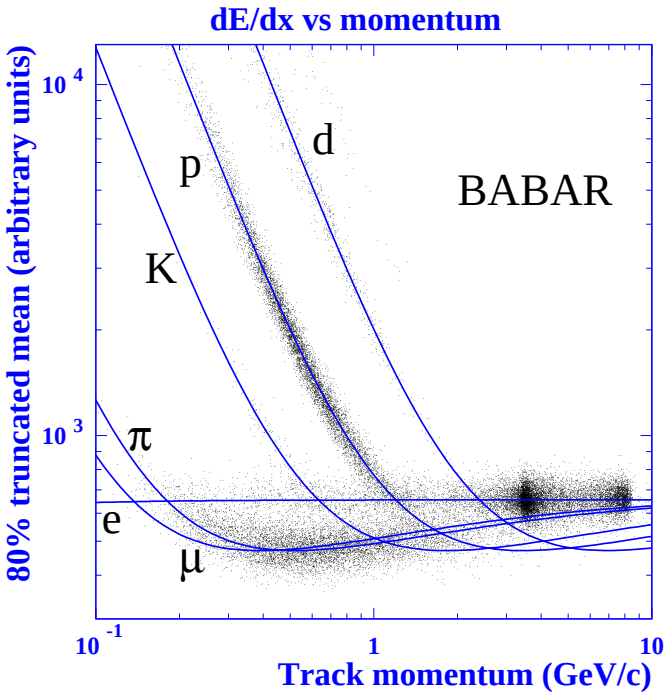

Figure 3.1: [dE/dx **vs momentum**] dE/dx vs momentum plot showing the ability of particle identification.

3.3 Signal and background events

The $B \to X_c \ell \nu$ decays are what we are interested in (see section 2.3). We call them signal. To access these events, we reconstruct a charged lepton and a D meson (D^0 or D^+) and form a $D\ell$ candidate. Since neutrinos escape undetected, we cannot fully reconstruct B mesons. Only one true $D\ell$-pair can be produced from one B meson. We do not explicitly reconstruct D^* or D^{**}. However we can access those decay modes which include D^* or D^{**} because D^* and D^{**} eventually decay into either D^0 or D^+ (see Appendix A). D^0 and D^+ are reconstructed from two and three charged tracks, respectively, using the decay modes :

- $D^0 \to K^- \pi^+$
- $D^+ \to K^- \pi^+ \pi^+$

The masses of reconstructed $D^0(K^-\pi^+)$ and $D^+(K^-\pi^+\pi^+)$ are distributed as shown in Figure 3.2. The OnPeak data events are the events produced by the colliding beam at the energy of $\Upsilon(4S)$ resonance. These events include

- $B\bar{B}$ events, because $\Upsilon(4S)$ decays into a $B\bar{B}$-pair with almost 100% probability. We can simulate these $B\bar{B}$ events with Monte Carlo (MC) simulation.

- $u\bar{u}$, $d\bar{d}$, $s\bar{s}$, and $c\bar{c}$ events which do not come from $\Upsilon(4S)$ resonance.
  These events are called $q\bar{q}$ or continuum events as a whole. We can estimate the amount of $q\bar{q}$ events from OffPeak data which is taken 40 MeV below the resonance. OffPeak data does not include $B\bar{B}$ events since this is below the energy threshold for $B\bar{B}$ production.

Typical cross sections at $\Upsilon(4S)$ energy are 1.05 nb for $B\bar{B}$ events and 3.39 nb for $q\bar{q}$ events. In Figure 3.2 (left), black points are OnPeak data, colored histograms are produced from $B\bar{B}$ MC and the dark gray histogram at the bottom is OffPeak data. This shows that OnPeak data consists of $B\bar{B}$ events and $q\bar{q}$ events. We subtract continuum events using OffPeak data. The continuum-subtracted plots are shown on the right hand side.

3.3.1 Signal events

Signal events are categorized into four components :

- $B \to D\ell\nu$ events (Red histograms in Figure 3.2 and 3.3).

- $B \to D^*\ell\nu$ events (Green histograms in Figure 3.2 and 3.3).

- $B \to D^{(*)}\pi\ell\nu$ events (Blue histograms in Figure 3.2 and 3.3).
  This includes $B \to D^{**}\ell\nu$ and non-resonant $B \to D^{(*)}\pi\ell\nu$ events

- $B \to D^{(*)}\pi\pi\ell\nu$ events (Magenta histograms in Figure 3.3).
  This includes $B \to X_c\ell\nu$ events other than $B \to D\ell\nu$, $B \to D^*\ell\nu$ and $B \to D^{(*)}\pi\ell\nu$ events.

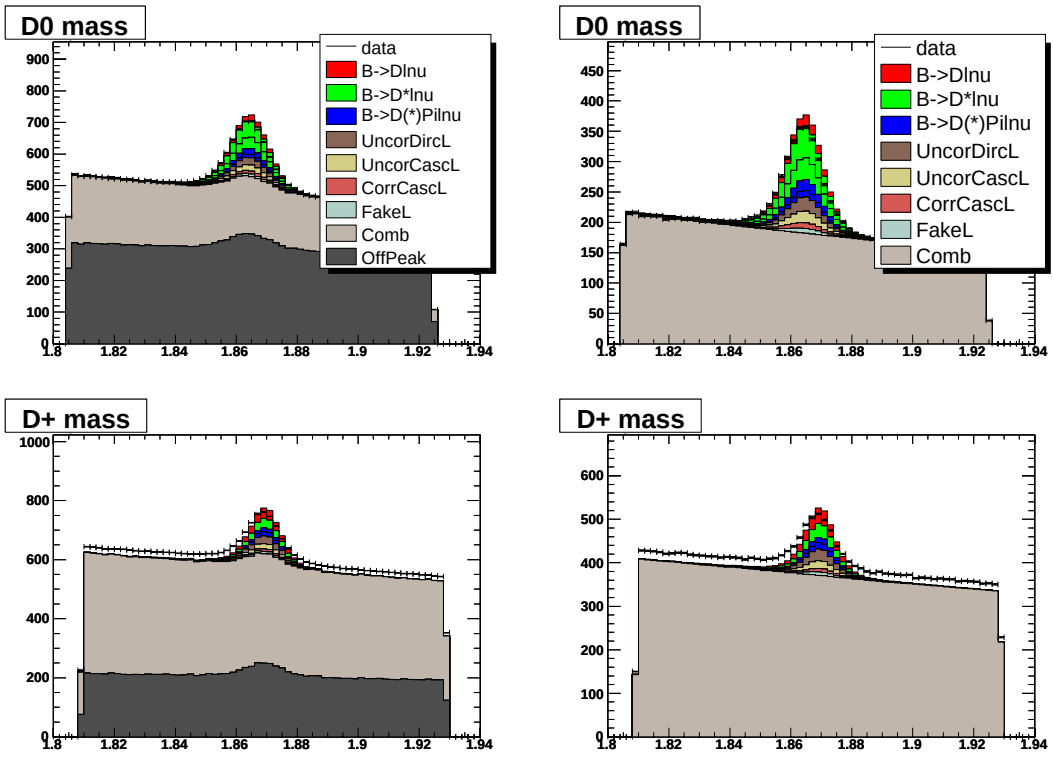

Figure 3.2: [D **mass distribution**] Typical D mass distributions before (left) and after (right) continuum subtraction. The top is D^0 and the bottom is D^+. Black points are OnPeak (or OnPeak - OffPeak) data. Red is $B \to D\ell\nu$, green is $B \to D^*\ell\nu$, blue is $B \to D^{(*)}\pi\ell\nu$, the rest is background. Dark brown is Uncorrelated Direct Lepton, light brown is Uncorrelated Cascade Lepton, dark red is Correlated Cascade Lepton, blue gray is Fake Lepton, light gray is Combinatorial, and dark gray is OffPeak data. $B \to D^{(*)}\pi\pi\ell\nu$ component is not included in these plots.

name	mass	width	spin
X	2.61	0.3	0
X^*	2.61	0.3	1
Y	2.87	0.1	0
Y^*	2.87	0.1	1

Table 3.1: [X_c **states**] X_c states used to generate $B \to D^{(*)}\pi\pi\ell\nu$ events.

Not much is known about $B \to D^{(*)}\pi\pi\ell\nu$ events and these events were not included in our original MC. However it is evident that these events should exist [10,11]. Thus, we generated events in this category using an ad-hoc model. We assumed four broad intermediate X_c states, namely X, X^*, Y and Y^* states, as listed in Table 3.1.

- These states are treated as heavier D or D^* according to the spin. The mass and spin of the X_c state determine, for example, the lepton momentum and D momentum spectrum.

- The X and X^* states are decayed into D or D^* (with equal branching fractions) and two pions according to phase space.

- The Y and Y^* states are decayed as two-body $D^{(*)}\rho$ states, and ρ subsequently decays to two pions. The $Y^{(*)}$ mass is chosen to be just above the threshold for this decay.

3.3.2 $B\bar{B}$ background events

$B\bar{B}$ events also produce backgrounds. $B\bar{B}$ background events are categorized into five different types.

- **Uncorrelated Direct Lepton** (Dark brown histograms in Figure 3.2 and 3.3.)

  Uncorrelated means D and ℓ come from different B. The ℓ comes directly from a B.

We have this kind of background because we have two B mesons in one event. The most typical example of this type of background is

- $B^+ \to \bar{D}^0 \ell^+ \nu$
- $B^- \to D^{*0} D^{*-} K^0$ with $D^{*-} \to D^- \pi^0$ or $D^{*-} \to D^- \gamma$

These ℓ^+ from B^+ and D^- from B^- form a $D\ell$ candidate. Note that in order for a B meson to produce a D meson (in addition to usual $\bar{D}$ meson), the W in the Figure 2.2 has to produce $c\bar{q}$ pair (instead of $\bar{\ell}\nu$ pair).

Another typical example is $B^0 \bar{B}^0$ mixing.

- $B^0 \to X^- \ell^+ \nu$
- $\bar{B}^0 \to B^0 \to D^- X'^+$

These ℓ^+ from B^0 and D^- from $\bar{B}^0$ form a $D\ell$ candidate.

- **Uncorrelated Cascade Lepton** (Light brown histograms in Figure 3.2 and 3.3.)

  D and ℓ came from different B, and cascade means ℓ does not directly come from B. In most of the cases, the ℓ come from a $D^{(*)}$ meson which is a decay product of one B.

  The most typical example is

  - $B^+ \to \bar{D}^0 X_1$
  - $B^- \to D^0 X_2$ with $D^0 \to K^- \ell^+ \nu$

  These $\bar{D}^0$ from B^+ and ℓ^+ from $B^-(D^0)$ form a $D\ell$ candidate.

- **Correlated Cascade Lepton** (Dark red histograms in Figure 3.2 and 3.3.)

  Correlated means D and ℓ come from the same B. But, ℓ does not directly come from B.

  A typical example is

– $B^+ \to \bar{D}^0 D^{*0} K^+$ with $\bar{D}^0 \to K^+ \ell^- \bar{\nu}$ and $D^{*0} \to D^0 \pi^0$

These ℓ^- and D^0 form a $D\ell$ candidate.

Another typical example is

– $B^+ \to \bar{D}^0 \tau^+ \nu$ with $\tau^+ \to \ell^+ \nu_\ell \bar{\nu}_\tau$

These $\bar{D}^0$ and ℓ^+ form a $D\ell$ candidate.

- **Fake Lepton** (Blue gray histograms in Figure 3.2 and 3.3.)

  The lepton in a $D\ell$ candidate is a mis-identified K, π or p.

  90 % of mis-identification is between μ and π.

- **Combinatorial** (Light gray histograms in Figure 3.2.)

  The D in a $D\ell$ candidate is not correctly reconstructed.

  Typical mis-reconstructions are that the kaon and the pion do not come from same D or not directly come from D. In our analysis, D^0 has much less combinatorial background than D^+ because D^0 is reconstructed from two particles (one K and one π) whereas D^+ is reconstructed from three particles (one K and two π) as described above. The combinatorial background can be statistically removed as described in the next section.

3.3.3 D mass sideband subtraction

As can be seen in Figure 3.2, the combinatorial background does not have a peak in the D mass distribution. Thus we can remove combinatorial $B\bar{B}$ background by subtracting the number of candidate with invariant masses in the D mass sidebands. We define the D mass peak region and sidebands as follows :

- D^0 mass

  peak : 1.840 - 1.888 GeV

  side bands : 1.816 - 1.840 and 1.888 - 1.912 GeV

- D^+ mass

  peak : 1.845 - 1.893 GeV

  side bands : 1.821 - 1.845 and 1.893 - 1.917 GeV

We count the number of $D\ell$ candidates in both peak, N_{peak} and sidebands, N_{side}. Then subtract N_{side} from N_{peak} to remove the combinatorial background. Figure 3.3 shows a typical lepton momentum and D momentum distribution after event selection and D mass sideband subtraction. The correlated cascade lepton, the fake lepton and the combinatorial background are too small to be visible. Based on MC studies, approximately 4.6 % of true $D\ell$ candidates enter the sidebands. The sideband subtraction, therefore, slightly lowers the signal efficiency.

3.4 Event selection

To reduce backgrounds, we apply a few selection criteria. We consider the statistical uncertainty on the signal

$$\frac{\sigma_S}{S} = \frac{\text{Statistical uncertainty on } S}{\text{Signal yield}} \tag{3.2}$$

to optimize our cuts. This analysis is systematics limited; thus, obtaining minimum σ_S/S is not always the optimum choice. In many cases we chose a looser cut than would be obtained from the minimum σ_S/S point.

3.4.1 BToDlnu skim

First, the collected data is processed to select only events with $D\ell$ candidates. This processing is done centrally within the BaBar collaboration and the produced data set is called the BToDlnu skim. In this section, we summarize the selection criteria of the BToDlnu skim.

Good quality charged tracks are used to reconstruct D and ℓ. The good quality charged tracks must satisfy the following conditions :

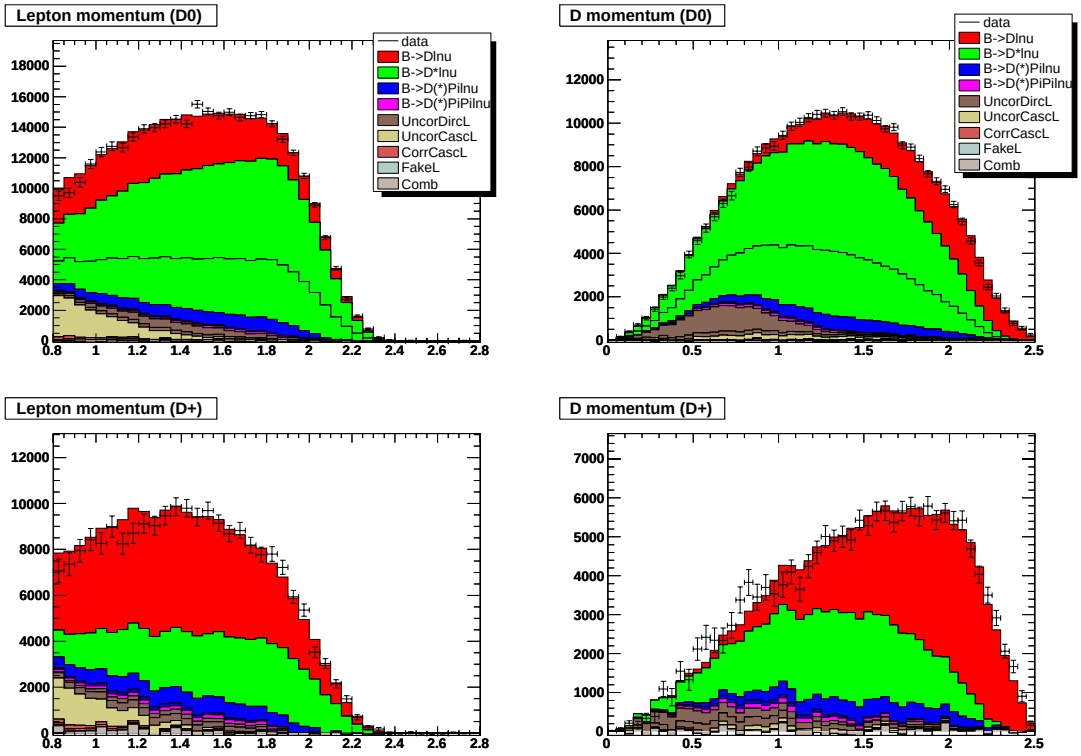

Figure 3.3: [p_ℓ **and** p_D **spectrum**] Lepton momentum (left) and D momentum (right) spectrum after D mass sideband subtraction. The top is D^0 and the bottom is D^+. Black points are OnPeak - OffPeak data. Red is $B \to D\ell\nu$, green is $B \to D^*\ell\nu$, blue is $B \to D^{(*)}\pi\ell\nu$, magenta is $B \to D^{(*)}\pi\pi\ell\nu$, and the rest is background. Dark brown is Uncorrelated Direct Lepton, light brown is Uncorrelated Cascade Lepton, dark red is Correlated Cascade Lepton, blue gray is Fake Lepton, and light gray is Combinatorial. Correlated Cascade Lepton, Fake Lepton and Combinatorial are tiny after event selection and D mass sideband subtraction.

- Momentum < 10 GeV
- Distance from beam line < 1.5 cm
- Distance from the collision point along the beam line < 10 cm
- Number of hits in DCH ≥ 12

D^0 candidates are reconstructed in 4 modes: $D^0 \to K^-\pi^+$, $D^0 \to K^-\pi^+\pi^+\pi^-$, $D^0 \to K^-\pi^+\pi^0$ and $D^0 \to \bar{K}^0\pi^+\pi^-$, and D^+ candidates are reconstructed in 2 modes: $D^+ \to K^-\pi^+\pi^+$ and $D^+ \to \bar{K}^0\pi^+$. Since statistical errors are not a limiting uncertainty in our analysis, we select the cleanest modes only; we use only $D^0 \to K^-\pi^+$ and $D^+ \to K^-\pi^+\pi^+$ modes.

For K^- tracks in the skim,

- The KLHNotPion selector is used to identify K^- to reconstruct D^+

  This LH stands for likelihood. A selection cut is applied based on the likelihood calculated by comparing measured dE/dx with expected values assuming the particle is a kaon. A very loose cut is chosen.

We apply the same KLHNotPion selector to identify the K^- to reconstruct D^0 as described in section 3.4.2.

Electrons and muons are selected using the following Particle Identification (PID) selectors :

- The PidLHElectron selector for electrons

  A selection cut is applied based on a likelihood. First, a likelihood function is constructed using the deposited energy and the shower shape in the EMC and the Cerenkov angle in the DIRC. Then the final likelihood is computed from the likelihood function and a likelihood of the measured dE/dx. A tight cut is adopted.

- The muNNTight selector for muons

  This NN stands for Neural Network. Instead of making simple cuts on variables, a neural network is used as a multi-variable discriminator. Input variables are the energy deposited in the EMC, the number of hit layers, the track χ^2 and the multiplicity of hit strips per layer in the IFR and the interaction length traversed in the BaBar detector. A tight cut is also adopted for muon.

The efficiency (fake rate) of the PidLHElectron selector is 94 % (1 %), and the efficiency (fake rate) of the muNNTight selector is 70 % (2 %) for tracks with momentum greater than 1.4 GeV.

The following cuts are also applied

- Lepton momentum cut

  $0.8 < p^*_\ell < 3.0$ GeV, where p^*_ℓ is the lepton momentum in the $\Upsilon(4S)$ rest frame.

- Lepton and kaon charge correlation cut

  The kaon and lepton must have the same sign of charge. See Appendix A.

3.4.2 Kaon Selection

As described above, in the BToDlnu skim, the KLHNotPion selector is used only in D^+ reconstruction. We apply the KLHNotPion selector to D^0 reconstruction as well to reduce kaon mis-identification. The uncertainties on the signal yields before and after the KLHNotPion requirement are given in Table 3.2. The uncertainty on the signal yield is reduced by 41 %. There is no change in D^+ mode because the KLHNotPion selector was already applied in the BToDlnu skim.

3.4.3 Vertexing

A vertex is the decay point of a particle. For example, in the decay $D^0 \to K^-\pi^+$, the K^- and π^+ originate from the D^0 decay point. Thus, the reconstructed trajectories of the K^- and π^+ are expected to intersect at a point corresponding to the D^0 decay

vertex. We calculate a χ^2 based on the assumption. No vertexing cut is made in the BToDlnu skim. We apply the TreeFitter algorithm [33] to calculate the χ^2 of the D and B decay vertices. By B vertex, we mean the vertex of the $D\ell$ combination. We cut on the probability value, $P(\chi^2, ndf)$, calculated by the χ^2 and the number of degrees of freedom (ndf) of the fitting. We chose :

$$P^D(\chi^2, ndf) > 0.001, \quad P^B(\chi^2, ndf) > 0.01, \tag{3.3}$$

These cuts reduce the uncertainties on the signal yields by 19 % for D^0 mode and by 22 % for D^+ mode, as listed in Table 3.2.

3.4.4 Thrust cut

$B\bar{B}$ events are isotropic, since they are produced just above threshold and are spinless, while other $q\bar{q}$ events, which are produced far above threshold, tend to result in back to back jets of particles in the center-of-mass (CM) frame. Thus, we can separate $q\bar{q}$ events from $B\bar{B}$ events using the event topology. A thrust axis is the axis that maximizes the sum of the momentum components of particles along the axis. We calculate two thrust axes : one for the $D\ell$ candidate and the other for the "non-$D\ell$" particles in each event. Here, "non-$D\ell$" particles means all charged tracks and calorimeter energy deposits other than the ones used to reconstruct the $D\ell$ candidate. For signal events, the $D\ell$ is presumed to come from one B in the event; thus, the non-$D\ell$ particles should correspond to the other B in the event. However, since we do not reconstruct D^* or D^{**}, pions from D^* or D^{**} on $D\ell$ side are included in non-$D\ell$ particles. Nevertheless we can achieve a good separation between $B\bar{B}$ events and $q\bar{q}$ events. We calculate $|\cos\theta_{Dl-nonDl}|$, which is the cosine of the angle between thrust axes of the $D\ell$ candidate and the non-$D\ell$ particles. The distribution is shown in Figure 3.4. It is almost flat for signal events but peaked at $|\cos\theta_{Dl-nonDl}| = 1$ for $q\bar{q}$ events, as expected.

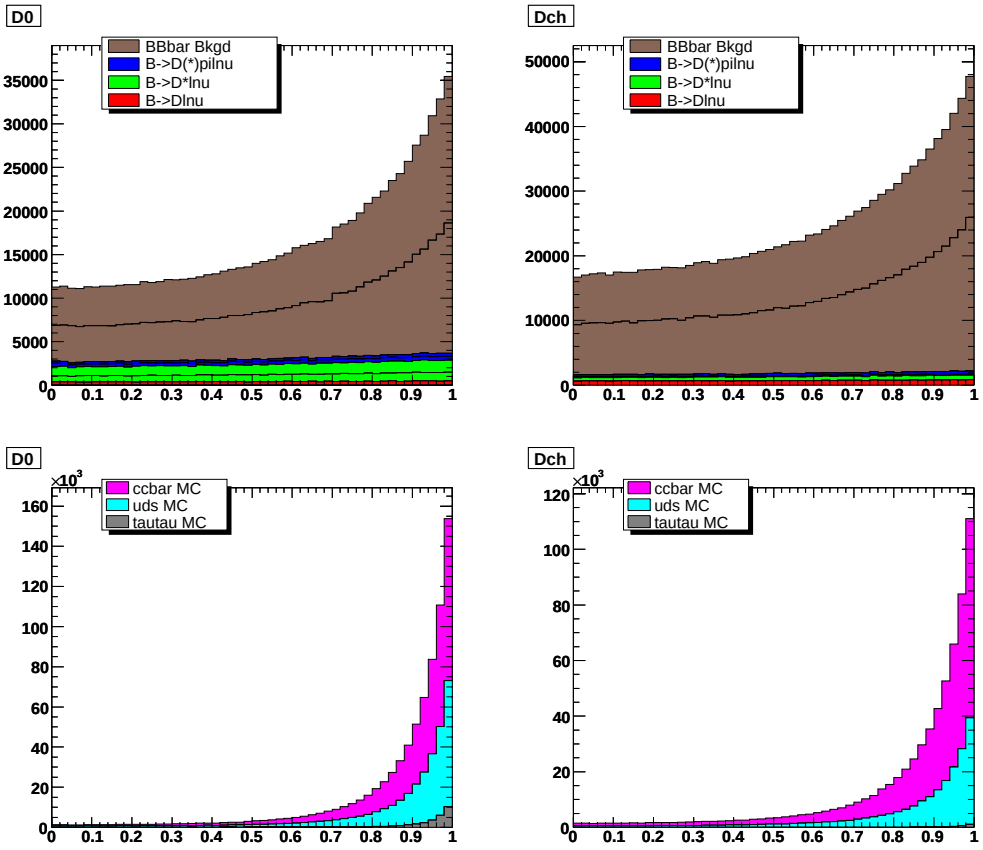

Figure 3.4: [$|\cos\theta_{Dl-nonDl}|$ **distribution**] $|\cos\theta_{Dl-nonDl}|$ plot for D^0 (left) and D^+ (right). In the top plot, red is $B \to D\ell\nu$, green is $B \to D^*\ell\nu$ and yellow is $B \to D^{(*)}\pi\ell\nu$ signals, and brown is $B\bar{B}$ backgrounds. In the bottom plot, magenta is $c\bar{c}$, light blue is $q\bar{q}$ ($q = u, d$ or s) and gray is $\tau^+\tau^-$. These plots are before event selection cuts and D mass sideband subtraction.

To optimize the cut, we calculate the uncertainty on signal. Our choice is

$$|\cos\theta_{Dl-nonDl}| < 0.92 \tag{3.4}$$

With this cut, we can reduce the uncertainties on the signal yields by 18 % for D^0 and by 15 % for D^+, as shown in Table 3.2.

3.4.5 Kinematic cuts to further reduce background.

Monte Carlo simulation did not describe the background distribution well. Trial fits were performed but they resulted in producing a poor fit quality. Further kine-

matic cuts were found to be necessary to reduce the uncertainties from backgrounds. Since most backgrounds are in the low lepton momentum and D momentum regions (Figure 3.3), we apply momentum cuts :

- $p^*_\ell > 1.2$ GeV
- $p^*_D > 0.8$ GeV

where p^*_ℓ is the lepton momentum and p^*_D is the D momentum in the CM frame. We also looked at $\cos\theta_{B-Dl}$, which is defined by

$$\cos\Theta_{B-Dl} = \frac{2E_B E_{Dl} - m_B^2 - m_{Dl}^2}{2|\boldsymbol{p}_B||\boldsymbol{p}_{Dl}|} \tag{3.5}$$

where E_B, m_B and $\boldsymbol{p}_B$ (E_{Dl}, m_{Dl} and $\boldsymbol{p}_{Dl}$) are the energy, mass and momentum of B ($D\ell$ pair), respectively. The B energy and momentum are calculated from the CM energy $\sqrt{s}$, as follows

$$E_B = \sqrt{s}/2, \quad |\boldsymbol{p}_B| = \sqrt{s/4 - m_B^2} \tag{3.6}$$

where B^0 mass is used for m_B (see Appendix D for more details). $\cos\theta_{B-Dl}$ is plotted in Figure 3.5. As can be seen from the plot, we cut on

- $-2 < \cos\theta_{B-Dl} < 1.1$

to reduce backgrounds. The upper bound is set to 1.1 to avoid the sharp edge at $\cos\theta_{B-Dl} = 1$ for $B \to D\ell\nu$ decays, which is smeared by the resolution. These three kinematic cuts are chosen to select a region dominated by signal decays and to reduce our sensitivity to uncertainties in the modeling of the background processes.

3.4.6 Summary of event selection cuts

Table 3.2 summarizes the cuts we applied, the uncertainty on signal, σ_S/S, and the number of selected signal candidates in the D mass peak region, N^{Sig}_{peak}. The selection

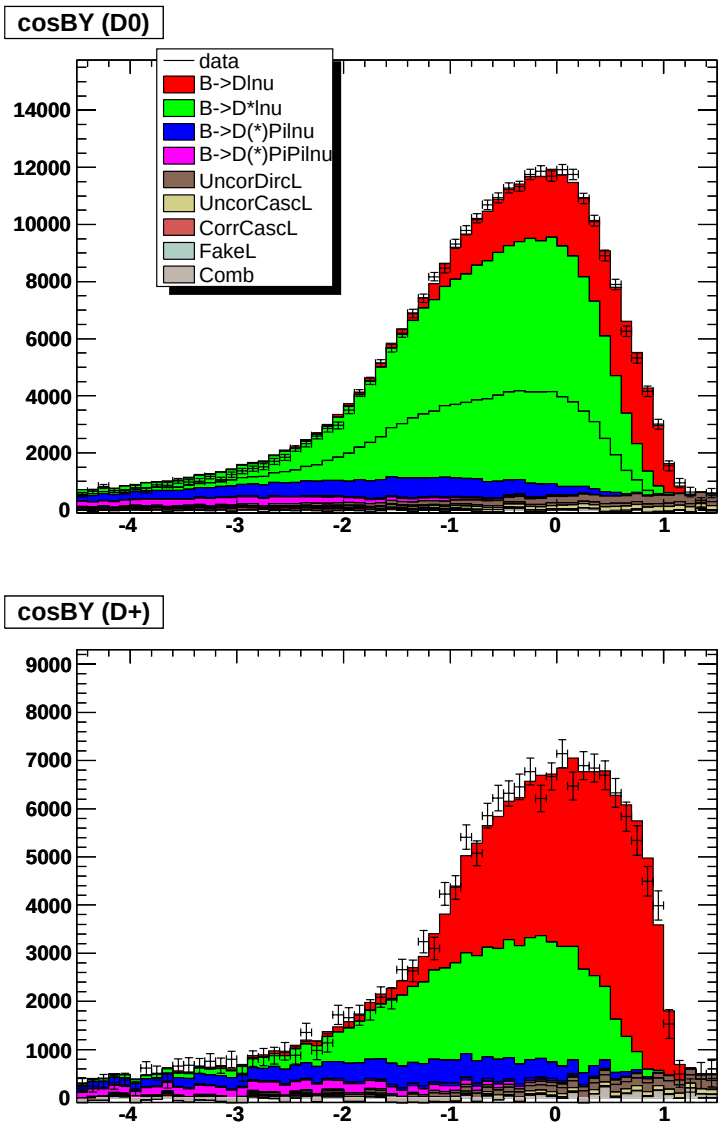

Figure 3.5: [$\cos\theta_{B-Dl}$ **spectrum**] $\cos\theta_{B-Dl}$ after D mass sideband subtraction. The top is D^0 and the bottom is D^+. Black points are OnPeak - OffPeak data. Red is $B \to D\ell\nu$, green is $B \to D^*\ell\nu$, blue is $B \to D^{(*)}\pi\ell\nu$, magenta is $B \to D^{(*)}\pi\pi\ell\nu$, and the rest is background. Dark brown is Uncorrelated Direct Lepton, light brown is Uncorrelated Cascade Lepton, dark red is Correlated Cascade Lepton, blue gray is Fake Lepton, and light gray is Combinatorial. Correlated Cascade Lepton, Fake Lepton and Combinatorial are tiny after event selection and D mass sideband subtraction.

cuts	D^0		D^+	
	$\frac{\sigma_S}{S}$	N_{peak}^{Sig}	$\frac{\sigma_S}{S}$	N_{peak}^{Sig}
BToDlnu skim	0.01152	1.0639×10^6	0.01538	628185
KLHNotPion selector	0.00657	1.0349×10^6	0.01538	628170
$P^D(\chi^2, ndf) > 0.001$				
$P^B(\chi^2, ndf) > 0.01$	0.00525	974632	0.01174	568799
$\lvert\cos\theta_{Dl-nonDl}\rvert < 0.92$	0.00428	882038	0.00992	515792
Kinematic cuts	0.00264	492955	0.00660	279686

Table 3.2: [**Event selection cuts**] Summary of event selection cuts.

reduces the uncertainties on the signal yields by 77 % for D^0 and by 57 % for D^+. We also lose 54 % and 55 % of signal candidates with these selection cuts. Tables 3.3 and 3.4 are cut-flow tables for D^0 and D^+ respectively. (OnPeak - OffPeak) data and $B\bar{B}$ MC are compared in these tables. The relative efficiencies show good agreement between data and MC. The efficiency corrections described in section 6.3.3 are not applied.

Figure 3.6 compares the D mass distributions before and after selection cuts. We can see significant improvement in data-MC agreement. After all selection cuts, there is still a small disagreement. However, since the data-MC difference for combinatorial background is flat throughout the D mass region, this difference disappears after D mass sideband subtraction. We also took wide enough peak regions to cover peak position differences.

OnPeak - OffPeak	Yield	Efficiency	Cumulative efficiency
BToDlnu skim	1.3388×10^6		
KLHNotPion selector	1.3410×10^6	1.00	1.00
$P^D(\chi^2, ndf) > 0.001$			
$P^B(\chi^2, ndf) > 0.01$	1.1961×10^6	0.89	0.89
$\lvert\cos\theta_{Dl-nonDl}\rvert < 0.92$	1.0651×10^6	0.89	0.78
Kinematic cuts	479296	0.45	0.36
BB MC	Yield	Efficiency	Cumulative efficiency
BToDlnu skim	1.4679×10^6		
KLHNotPion selector	1.4449×10^6	0.99	0.99
$P^D(\chi^2, ndf) > 0.001$			
$P^B(\chi^2, ndf) > 0.01$	1.3204×10^6	0.92	0.90
$\lvert\cos\theta_{Dl-nonDl}\rvert < 0.92$	1.1789×10^6	0.89	0.80
Kinematic cuts	502995	0.43	0.34

Table 3.3: [**Cut-flow Table,** D^0] The cut-flow table for D^0. The yield is the number of candidates after D mass sideband subtraction. The efficiency corrections described in section 6.3.3 are not applied.

OnPeak - OffPeak	Yield	Efficiency	Cumulative efficiency
BToDlnu skim	825616		
KLHNotPion selector	825625	1.00	1.00
$P^D(\chi^2, ndf) > 0.001$			
$P^B(\chi^2, ndf) > 0.01$	700745	0.85	0.85
$\lvert\cos\theta_{Dl-nonDl}\rvert < 0.92$	621453	0.89	0.75
Kinematic cuts	266127	0.43	0.32
BB MC	Yield	Efficiency	Cumulative efficiency
BToDlnu skim	1.0061×10^6		
KLHNotPion selector	1.0061×10^6	1.00	1.00
$P^D(\chi^2, ndf) > 0.001$			
$P^B(\chi^2, ndf) > 0.01$	870188	0.85	0.85
$\lvert\cos\theta_{Dl-nonDl}\rvert < 0.92$	766995	0.88	0.76
Kinematic cuts	294623	0.38	0.29

Table 3.4: [**Cut-flow Table,** D^+] The cut-flow table for D^+. The yield is the number of candidates after D mass sideband subtraction. The efficiency corrections described in section 6.3.3 are not applied.

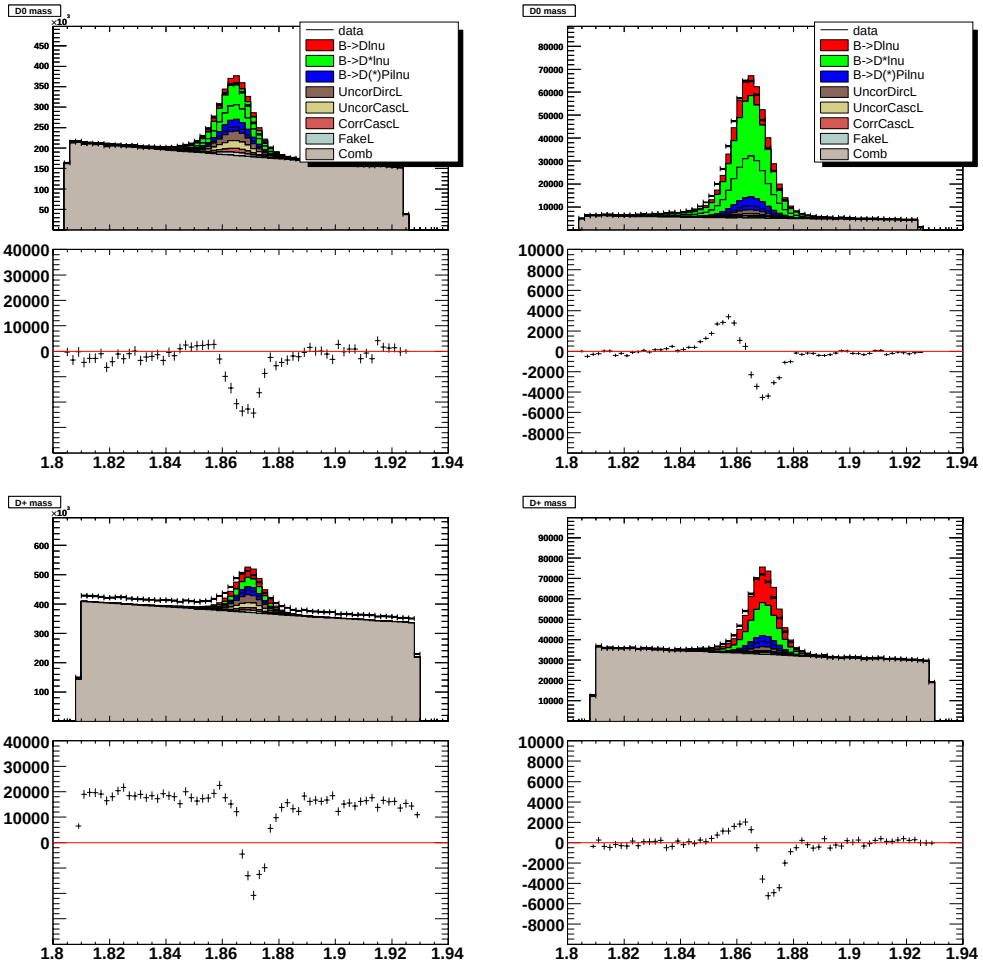

Figure 3.6: [D **mass distributions before and after event selection**] D mass distributions before (left) and after (right) applying selection cuts. The top two rows are for D^0 and the bottom two are for D^+. The colors of the histograms are same as others. Data - MC difference is also plotted at the bottom of each plot.

Chapter 4

Outline of the analysis method

Before going into the actual fitting procedure (section 6), we give a simplified example to illustrate the fundamentals of the fitting method. For the sake of the example we will suppose that semileptonic $B \to X_c \ell \nu$ decays have only two signal decay modes S1 and S2 with branching fractions BF_1 and BF_2, and there is only one type of $B\bar{B}$ background B1.

4.1 3-dimensional (3D) binned histogram making

First we make 3-dimensional (3D) binned histograms of OnPeak data, OffPeak data, S1, S2 and B1. The histograms of S1, S2 and B1 are made from $B\bar{B}$ MC using MC truth information. We denote the number of candidates in the i-th bin for OnPeak data by N_i^{OnPeak}, for OffPeak data by $N_i^{OffPeak}$, for the two signals by N_i^{S1} and N_i^{S2}, and for the one background by N_i^{B1}. These numbers are

- After event selection cuts.
- After D mass sideband subtraction.
- The OffPeak data and $B\bar{B}$ MC are scaled to the luminosity of the OnPeak data.

We then perform continuum (OffPeak) subtraction to get

- $N_i^{data} = N_i^{OnPeak} - N_i^{OffPeak}$

By 3D we mean that we use three kinematic variables to characterize each decay mode. We use the following three variables :

- lepton momentum in the CM frame p_ℓ^*
- D momentum in the CM frame p_D^*
- $\cos\theta_{B-Dl}$ (see section 3.4.5 and Appendix D)

The reason for this choice is the following. In the $B \to D\ell\nu$ decays, there are only three independent kinematic variables. For example, in Figure 2.3, supposing D^* is D and does not decay, the independent variables can be the magnitude of lepton momentum, the magnitude of D momentum and θ_ℓ because χ and θ_V are irrelevant. The same is true in other decay modes when we reconstruct only $D\ell$ pairs. We chose three variables, p_ℓ^*, p_D^* and $\cos\theta_{B-Dl}$, because this combination is simple, well known and useful to discriminate among signal decay modes and backgrounds. The shapes of the histograms for each MC mode are quite different. The projected plots of 3D histograms onto each variable axis are shown in Figures 3.3 and 3.5. Figure 4.1 shows the difference in the 3D distribution for each signal and background component in one bin of $\cos\theta_{B-Dl}$. We can clearly see the difference.

4.2 MC re-weighting

The input values used to create our fully-simulated MC samples differ from the most recent values available. There have been new measurements of, for example, the branching fractions (BF) for certain decays and some form factor parameters. Where new measurements are available, we updated the MC samples to the new values. This is done by assigning to each MC event a weight such that the weighted sample reflects the updated input parameter values. We call this MC re-weighting. Details

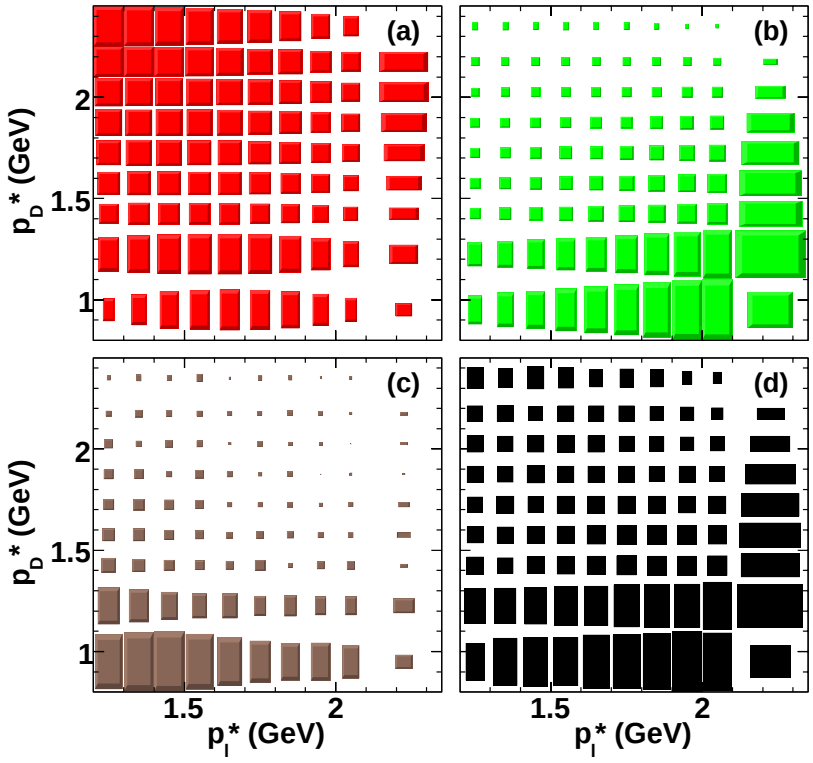

Figure 4.1: [**2D projection plots**] Projections onto p^*_D versus p^*_ℓ for $D\ell$ candidates that satisfy $0 < \cos\theta_{B-Dl} < 1.1$, after sideband subtraction. The shaded boxes have area proportional to the number of entries. The plots show, (a) $B \to D\ell\nu$, (b) $B \to D^*\ell\nu$, (c) sum of $B \to D^{(*)}\pi\ell\nu$, $B \to D^{(*)}\pi\pi\ell\nu$ and background, and (d) data after OffPeak subtraction.

of MC re-weighting are explained in chapter 5. Several aspects of the MC simulation are modified by re-weighting.

- Background BF

  Branching fractions of background processes are updated to new values.

- $D^{(*,**)}$ decay BF

  $D^{(*,**)}$ decay BFs are updated to new values.

- Form factor (FF)

  Form factor parameters are updated to new values and the FF models are replaced where necessary.

We also correct tracking and PID efficiencies as described in section 6.3.3. Most of the re-weighting is done during the 3D histogram making process because weights vary from candidate to candidate. However, some of these weights can be applied in the fitting process by splitting histograms as described below.

4.3 Fitting

Using the above histograms we form a χ^2

$$\chi^2 = \sum_i \frac{(N_i^{data} - N_i^{S1} - N_i^{S2} - N_i^{B1})^2}{(\sigma_i^{data})^2 + (\sigma_i^{S1})^2 + (\sigma_i^{S2})^2 + (\sigma_i^{B1})^2} \tag{4.1}$$

where $\sigma_i^{\rm xx}$ are the statistical uncertainties of i-th bin. If $B\bar{B}$ MC provides a perfect description of the data, we should have $\chi^2 \simeq$ (number of bins) because the fluctuation in a bin is the same size as the statistical uncertainty of the bin and each bin gives 1 as an average.

However, the MC is not perfect. The BF of S1 and S2 in the MC, BF_1^{MC} and BF_2^{MC}, are different from the true values. This difference makes the χ^2 larger than

the number of bins. We can adjust the BF difference using coefficients

$$C^{S1} = \frac{BF_1}{BF_1^{MC}}, \quad C^{S2} = \frac{BF_2}{BF_2^{MC}}, \tag{4.2}$$

to N_i^{S1} and N_i^{S2}. The BF_1^{MC} and BF_2^{MC} are fixed values, but BF_1 and BF_2 can be variables. Then χ^2 becomes

$$\chi^2 = \sum_i \frac{(N_i^{data} - C^{S1}N_i^{S1} - C^{S2}N_i^{S2} - N_i^{B1})^2}{(\sigma_i^{data})^2 + (C^{S1}\sigma_i^{S1})^2 + (C^{S2}\sigma_i^{S2})^2 + (\sigma_i^{B1})^2} \tag{4.3}$$

If we minimize this χ^2 by floating BF_1 and BF_2, we can determine the branching fractions BF_1 and BF_2 which the data favor.

This is how we determine branching fractions in the fit. Next, we explain how to access form factor (FF) parameters. One way is to remake MC histograms with a new set of FF parameters. This is what we call FF re-weighting. Suppose the decay rate of S1 is given by

$$\Gamma = a(w) + b(w)c \tag{4.4}$$

where a and b are functions of the velocity transfer w and c is the FF parameter we would like to measure. The weight is given by

$$W = \frac{a(w) + b(w)c}{a(w) + b(w)c^{MC}} \tag{4.5}$$

where c^{MC} is the value used in existing MC. This weight differs candidate by candidate because the velocity transfer w varies candidate by candidate. So, we apply this weight candidate by candidate and count the weighted number of candidates to make a new histogram. This means, for example, new N_i^{S1} is given by

$$N_i^{S1} = \sum_k W_{ik} \tag{4.6}$$

where k is the k-th candidate in i-th bin. But this is computationally expensive when c is a free parameter because the fit code needs to remake the histogram for each iteration in the minimization of χ^2. There is a better way to do the fitting. Instead of making one histogram for S1 with one weight, we can separate the weight into two :

$$W = \frac{a(w)}{a(w) + b(w)c^{MC}} + \frac{b(w)}{a(w) + b(w)c^{MC}}\, c \equiv W^a + W^b\, c \tag{4.7}$$

to separate out the c, which is what we fit for. Then we make two histograms :

$$N_i^{S1a} = \sum_k W_{ik}^a, \qquad N_i^{S1b} = \sum_k W_{ik}^b \tag{4.8}$$

We can recover full histogram of S1 by

$$N_i^{S1} = N_i^{S1a} + cN_i^{S1b} \tag{4.9}$$

with a different value of c. With this approach, the χ^2 is given by

$$\chi^2 = \sum_i \frac{(N_i^{data} - C^{S1}(N_i^{S1a} + cN_i^{S1b}) - C^{S2}N_i^{S2} - N_i^{B1})^2}{(\sigma_i^{data})^2 + (C^{S1}\sigma_i^{S1})^2 + (C^{S2}\sigma_i^{S2})^2 + (\sigma_i^{B1})^2} \tag{4.10}$$

where σ_i^{S1} can be determined by the similar method as shown in section 6.8. Now, we can fit for the FF parameter c by minimizing this χ^2 without remaking histograms N_i^{S1a} and N_i^{S1b} at each iteration of the minimization. The actual χ^2 we use is a more complex version of this and is fully described in chapter 6.

4.4 Calculation of $\mathcal{G}(1)|V_{cb}|$ and $\mathcal{F}(1)|V_{cb}|$

After determining the branching fractions $\mathcal{B}(B \to D\ell\nu)$ and $\mathcal{B}(B \to D^*\ell\nu)$, and form factor parameters ρ_D^2, ρ^2, R_1, and R_2 from the fit, we can calculate $\mathcal{G}(1)|V_{cb}|$ and $\mathcal{F}(1)|V_{cb}|$. Here we show an outline of the calculation; details are given in Appendix F.

4.4.1 $\mathcal{G}(1)|V_{cb}|$

The differential decay rate for $B \to D\ell\nu$ decays is given in Equation (2.10). Combined with the CLN parametrization given in Equation (2.17), the differential decay rate is given by

$$\begin{aligned}&\frac{d\Gamma(B \to D\ell\nu)}{dw}\\ &= \frac{G_F^2 m_B^5}{48\pi^3} r^3 (w^2-1)^{3/2} (1+r)^2 [1 - 8\rho_D^2 z + (51\rho_D^2 - 10)z^2 - (252\rho_D^2 - 84)z^3]^2\\ &\quad \times (\mathcal{G}(1)|V_{cb}|)^2 \end{aligned} \tag{4.11}$$

Note that $\mathcal{G}(1) = h_+(1)$. By integrating over w, we get

$$\begin{aligned}&\frac{\mathcal{B}(B \to D\ell\nu)}{\tau_B}\\ &= \frac{G_F^2 m_B^5}{48\pi^3} r^3 (1+r)^2 \int (w^2-1)^{3/2} [1 - 8\rho_D^2 z + (51\rho_D^2 - 10)z^2 - (252\rho_D^2 - 84)z^3]^2 dw\\ &\quad \times (\mathcal{G}(1)|V_{cb}|)^2 \end{aligned} \tag{4.12}$$

where τ_B is the lifetime of the B meson. Note that z is a function of w (Equation (2.18)) and is going to be integrated out. Thus, using fit results, $\mathcal{B}(B \to D\ell\nu)$ and ρ_D^2, we can calculate $\mathcal{G}(1)|V_{cb}|$.

4.4.2 $\mathcal{F}(1)|V_{cb}|$

The differential decay rate for $B \to D^*\ell\nu$ decays is given in Equation (2.26). Combined with the CLN parametrization given in Equation (2.25), the differential decay rate is given by

$$\begin{aligned}&\frac{d\Gamma(B \to D^*\ell\nu)}{dw}\\ &= \frac{G_F^2 |V_{cb}|^2 m_B^5}{48\pi^3} r^3 (w^2-1)^{1/2} (w+1)^2\\ &\quad \times [\mathcal{F}(1)]^2 [1 - 8\rho^2 z + (53\rho^2 - 15)z^2 - (231\rho^2 - 91)z^3]^2 (\tilde{h}_+^2 + \tilde{h}_-^2 + \tilde{h}_0^2) \end{aligned} \tag{4.13}$$

Note that $\mathcal{F}(1) = h_{A_1}(1)$. By integrating over w, we get

$$\frac{\mathcal{B}(B \to D^* \ell \nu)}{\tau_B} = \frac{G_F^2 m_B^5}{48\pi^3} r^3 \left(\mathcal{F}(1)|V_{cb}|\right)^2 \int (w^2-1)^{1/2}(w+1)^2(\tilde{h}_+^2 + \tilde{h}_-^2 + \tilde{h}_0^2) \times [1 - 8\rho^2 z + (53\rho^2 - 15)z^2 - (231\rho^2 - 91)z^3]^2 dw \quad (4.14)$$

Thus, using fit results $\mathcal{B}(B \to D^* \ell \nu)$, R_1, R_2 and ρ^2, we can calculate $\mathcal{F}(1)|V_{cb}|$.

4.5 Extraction of $|V_{cb}|$

To extract $|V_{cb}|$, we use theoretical calculations of $\mathcal{G}(1)$ and $\mathcal{F}(1)$. For $\mathcal{G}(1)$, we use [23]

$$\mathcal{G}(1) = 1.074 \pm 0.018 \pm 0.016 \quad (4.15)$$

and for $\mathcal{F}(1)$ [34],

$$\mathcal{F}(1) = 0.921 \pm 0.013 \pm 0.020 \quad (4.16)$$

These need to be multiplied by the QED radiative correction factor of 1.007 [35].

Chapter 5

Details of MC re-weighting

Because of theoretical and experimental improvements, some numbers and formulas used in existing MC are obsolete. In order to take new results into account, we re-weight existing MC. In our analysis, we re-weight decay branching fractions and form factors. In this chapter, the details of MC re-weighting are presented.

5.1 Background BF re-weighting

We need to update some of decay branching fractions in background processes to get a better description of data.

5.1.1 Semileptonic $D(D_s)$ decay branching fractions

For uncorrelated and correlated cascade lepton backgrounds, we correct the branching fractions of semileptonic $D(D_s)$ decays. The decay modes updated in our analysis are listed in Table 9.3.

5.1.2 Inclusive $B \to X\ell\nu$ decay branching fractions

For uncorrelated direct lepton and combinatorial backgrounds, we correct the branching fraction of inclusive $B \to X\ell\nu$ decays. Weights are given by the ratios of new and old branching fractions as summarized in the table below. New branching fractions are taken from Refs. [10,36] and averaged assuming isospin symmetry. These weights are only applied to the B decay that produces the lepton in the $D\ell$ candidate.

Decay mode	MC	New BF [10, 36]	Weight
$B^+ \to \bar{X}^0 \ell^+ \nu$	0.106088	0.1112 ± 0.0019	1.048 ± 0.018
$B^0 \to X^- \ell^+ \nu$	0.106100	0.1038 ± 0.0018	0.979 ± 0.017

5.1.3 Inclusive $B \to D(D_s)$ decay branching fractions

For uncorrelated direct lepton, uncorrelated cascade lepton, correlated cascade lepton and fake lepton backgrounds, we correct the branching fraction of inclusive $B \to D(D_s)$ decays using measured branching fractions from Refs. [37, 38]. The $D(D_s)$ momentum dependent weights are given in Figures 5.1 - 5.3. These weights fluctuate due to poor statistics of the measurements. Thus, we fit the weight distributions with a 4-th (3-rd) order polynomial, and use the fit function to apply weights. If we apply these weights to, for example, uncorrelated direct lepton background, we get the D momentum distribution shown in Figure 5.4.

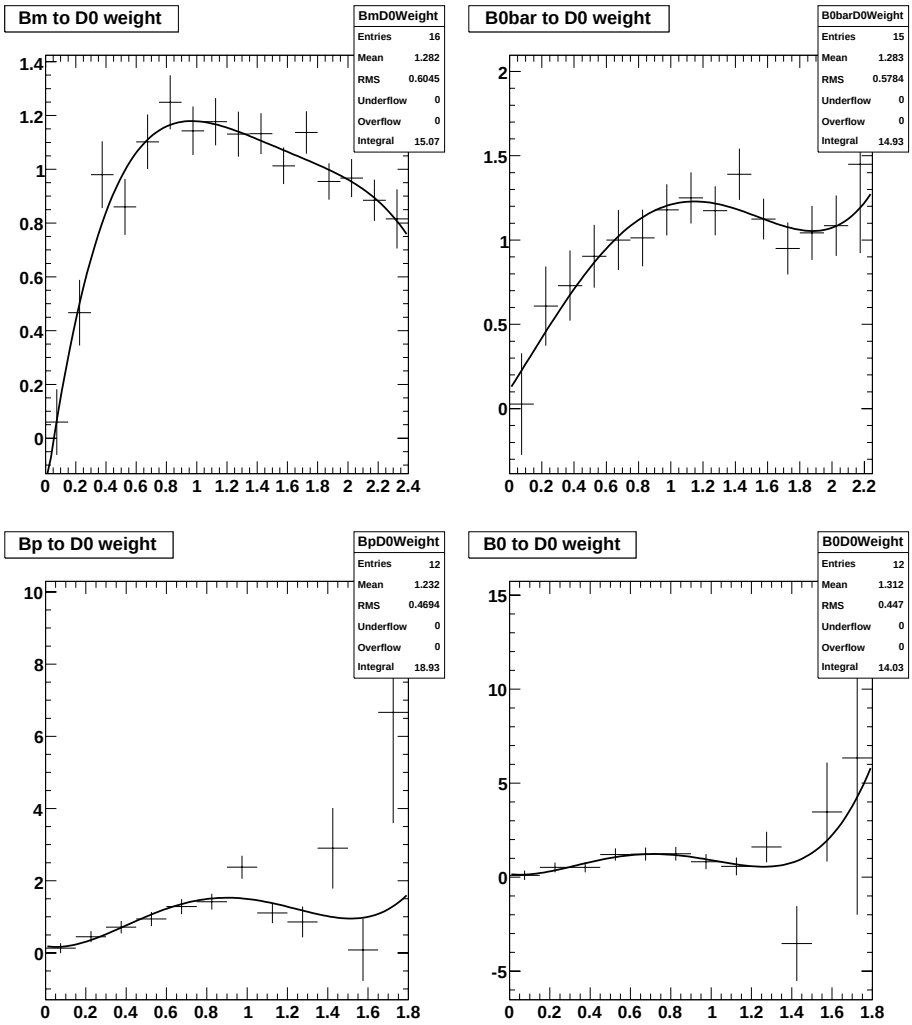

Figure 5.1: [$B \to D^0$ **weights**] 4th order polynomial fit for $B \to D^0$ weight. Top-left : $B^- \to D^0$, top-right : $\bar{B}^0 \to D^0$, bottom-left : $B^+ \to D^0$ and bottom-right : $B^0 \to D^0$

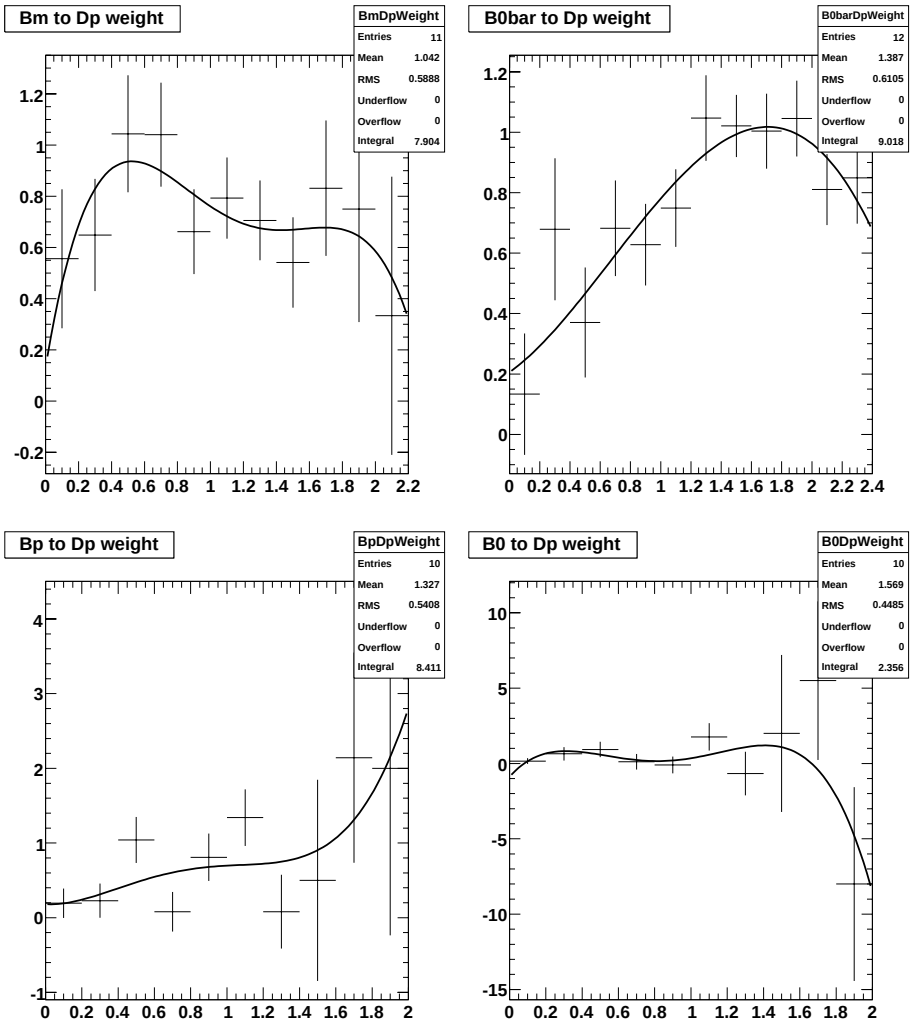

Figure 5.2: [$B \to D^+$ **weights**] 4th order polynomial fit for $B \to D^+$ weight. Top-left : $B^- \to D^+$, top-right : $\bar{B}^0 \to D^+$, bottom-left : $B^+ \to D^+$ and bottom-right : $B^0 \to D^+$

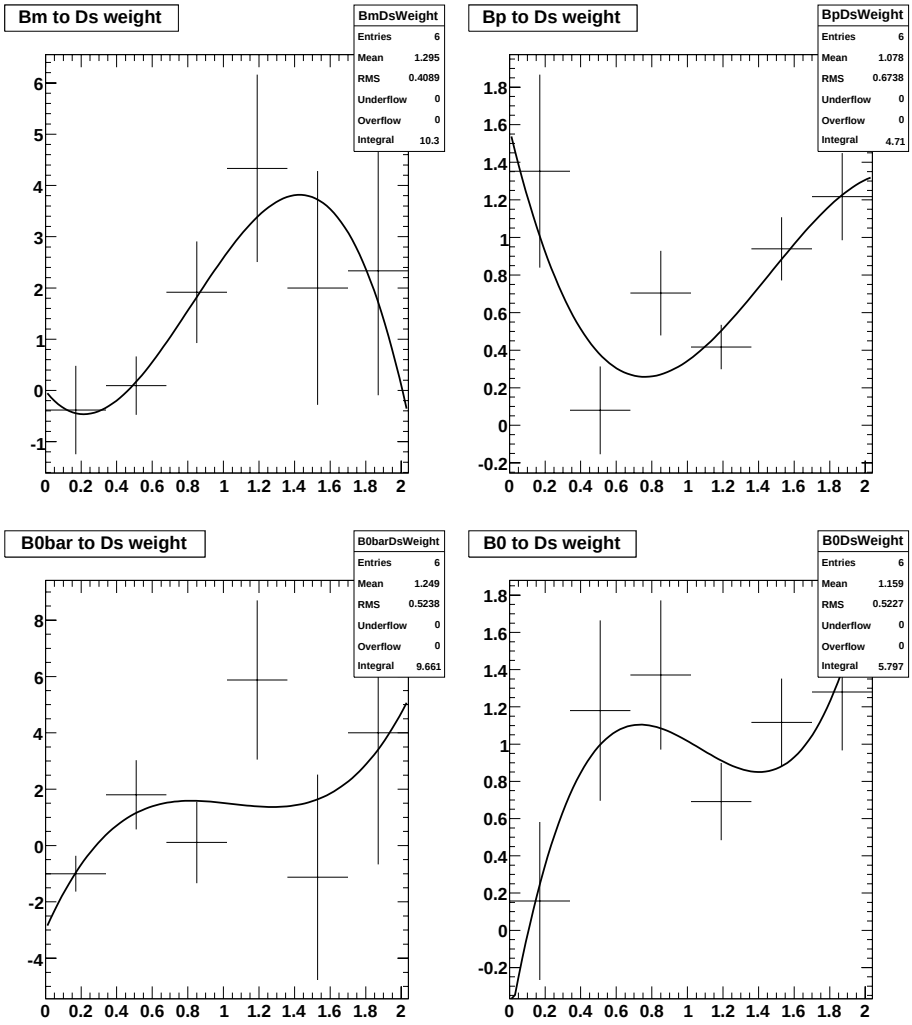

Figure 5.3: [$B \to D_s^+$ **weights**] 3rd order polynomial fit for $B \to D_s^+$ weight. Top-left : $B^- \to D_s^+$, top-right : $B^+ \to D_s^+$, bottom-left : $\bar{B}^0 \to D_s^+$ and bottom-right : $B^0 \to D_s^+$

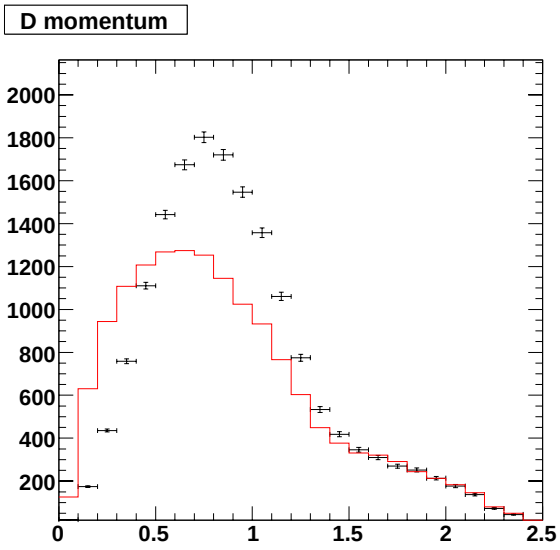

Figure 5.4: [**Effect of $B \rightarrow D$ BF correction**] Effect of $B \rightarrow D$ BF correction on uncorrelated direct lepton background. The black points with error bars are after correction, red histogram is before correction.

5.2 Charm decay BF re-weighting

For charm decay BFs, we adopt the following new values in our fit. These are not applied at the candidate level in order to allow them, if desired, to be determined in the fit. Thus, these values go into the coefficients in the fit. See details in section 6.4. Subsequently, it was decided to hold these BFs fixed.

5.2.1 D^{**} decay branching fractions

For D_0^*, D_1 and D_1', based on isospin symmetry, we use

$$\begin{aligned}&\mathcal{B}(D_0^{*+} \to D^0\pi^+) = \mathcal{B}(D_0^{*0} \to D^+\pi^-) = \mathcal{B}(D_1^+ \to D^{*0}\pi^+) = \mathcal{B}(D_1^0 \to D^{*+}\pi^-)\\ &= \mathcal{B}(D_1'^+ \to D^{*0}\pi^+) = \mathcal{B}(D_1'^0 \to D^{*+}\pi^-) = 0.6667\end{aligned} \tag{5.1}$$

and

$$\begin{aligned}&\mathcal{B}(D_0^{*+} \to D^+\pi^0) = \mathcal{B}(D_0^{*0} \to D^0\pi^0) = \mathcal{B}(D_1^+ \to D^{*+}\pi^0) = \mathcal{B}(D_1^0 \to D^{*0}\pi^0)\\ &= \mathcal{B}(D_1'^+ \to D^{*+}\pi^0) = \mathcal{B}(D_1'^0 \to D^{*0}\pi^0) = 0.3333\end{aligned} \tag{5.2}$$

Here we assume that D^{**} decays 100 % into $D^{(*)}\pi$. However there is an observation of $D_1 \to D\pi^+\pi^-$ decays [39]. We consider this in the systematic study in chapter 9. For D_2^*, from two measurements in Ref. [10],

$$\frac{\mathcal{B}(D_2^{*+} \to D^0\pi^+)}{\mathcal{B}(D_2^{*+} \to D^{*0}\pi^+)} = 1.9 \pm 1.1 \pm 0.3 \tag{5.3}$$

$$\frac{\mathcal{B}(D_2^{*0} \to D^+\pi^-)}{\mathcal{B}(D_2^{*0} \to D^{*+}\pi^-)} = 2.3 \pm 0.6 \tag{5.4}$$

BaBar measure [47]

$$\frac{\mathcal{B}(D_2^{*+} \to D^0\pi^+) + \mathcal{B}(D_2^{*0} \to D^-\pi^+)}{\mathcal{B}(D_2^{*+} \to D^{(*)0}\pi^+) + \mathcal{B}(D_2^{*0} \to D^{(*)+}\pi^-)} = 0.62 \pm 0.03 \pm 0.02 \tag{5.5}$$

Assuming isospin symmetry, we take an average over these three results to get

$$f_{D_2^*} \equiv \frac{\mathcal{B}(D_2^{*+} \to D^0\pi^+)}{\mathcal{B}(D_2^{*+} \to D^{*0}\pi^+)} = \frac{\mathcal{B}(D_2^{*0} \to D^+\pi^-)}{\mathcal{B}(D_2^{*0} \to D^{*+}\pi^-)} = 1.7 \pm 0.4 \tag{5.6}$$

Individual branching fractions are given by following formulae

$$\mathcal{B}(D_2^{*+} \to D^0\pi^+) = \mathcal{B}(D_2^{*0} \to D^+\pi^-) = \frac{2f_{D_2^*}}{3(1+f_{D_2^*})} \tag{5.7}$$

$$\mathcal{B}(D_2^{*+} \to D^+\pi^0) = \mathcal{B}(D_2^{*0} \to D^0\pi^0) = \frac{f_{D_2^*}}{3(1+f_{D_2^*})} \tag{5.8}$$

$$\mathcal{B}(D_2^{*+} \to D^{*0}\pi^+) = \mathcal{B}(D_2^{*0} \to D^{*+}\pi^-) = \frac{2}{3(1+f_{D_2^*})} \tag{5.9}$$

$$\mathcal{B}(D_2^{*+} \to D^{*+}\pi^0) = \mathcal{B}(D_2^{*0} \to D^{*0}\pi^0) = \frac{1}{3(1+f_{D_2^*})} \tag{5.10}$$

5.2.2 $D^{(*)}$ decay branching fractions

We use PDG values [10]

$$\begin{aligned}
&\mathcal{B}(D^0 \to K^-\pi^+) = 0.0389 \pm 0.0005 \\
&\mathcal{B}(D^+ \to K^-\pi^+\pi^+) = 0.0922 \pm 0.0021 \\
&\mathcal{B}(D^{*+} \to D^0\pi^+) = 0.677 \pm 0.005 \\
&\mathcal{B}(D^{*+} \to D^+\pi^0) = 0.307 \pm 0.005 \\
&\mathcal{B}(D^{*+} \to D^+\gamma) = 0.016 \pm 0.004
\end{aligned} \tag{5.11}$$

For D^{*0} decay BF, we keep existing MC values because there are no new results.

5.3 An example of BF re-weighting

Here we give a specific example to illustrate BF re-weighting. In the case of a correlated cascade lepton background :

- $B^+ \to D^{*-}D^+K^+$

  with $D^{*-} \to \bar{D}^0\pi^-$ and $D^+ \to \bar{K}^0e^+\nu$

and these $\bar{D}^0$ and e^+ form a Dl candidate as if $B^+ \to \bar{D}^0 e^+ \nu$

The number of this background is given by

$$\begin{aligned} &N = (\text{number of produced } B^+B^- \text{ pairs}) \times \\ &\mathcal{B}(B^+ \to D^{*-}D^+K^+)\mathcal{B}(D^{*-} \to \bar{D}^0\pi^-)\mathcal{B}(D^+ \to \bar{K}^0 e^+\nu)\mathcal{B}(\bar{D}^0 \to K^+\pi^-) \end{aligned} \tag{5.12}$$

Thus, it is proportional to a product of branching fractions. This means that the weight is given by the ratio of new and old branching fractions. This also means that if we know, for example, $D^+ \to \bar{K}^0 e^+ \nu$ is included in the chain, we can apply a weight only for the known part. We do not have to know the details of the entire decay chain to apply a weight.

In the above example, for the lepton side, we apply

- Inclusive $B^+ \to D^+$ BF weight (section 5.1.3)
- Semileptonic $D^+ \to \bar{K}^0 e^+ \nu$ BF weight (section 5.1.1)

and for the D side, we apply

- $D^{*-} \to \bar{D}^0 \pi^-$ decay BF weight (section 5.2.2)
- $D^0 \to K^-\pi^+$ decay BF weight (section 5.2.2)

Total weight is given by the product of these 4 weights. The former two weights are applied in the histogram making process and the latter two weights are applied in the fitting process.

5.4 Beam energy re-weighting

The beam energy distribution in data is not well simulated in the MC. There is a dedicated study of data beam energy using fully reconstructed B decays. We use the result to make the MC beam energy distribution match that of the data. Table 5.1

shows the mean and width of the beam energy distributions of data and MC averaged over each run period of data taking.

Beam energies of data and MC, as a function of energy E, are parametrized by Gaussians. We take ratios of these two Gaussians to get a weight

$$W^{\rm beam}(E) = \xi \exp\left[-\frac{(E_{\rm data}-E)^2}{2\sigma^2_{\rm data}}\right] \Big/ \exp\left[-\frac{(E_{\rm MC}-E)^2}{2\sigma^2_{\rm MC}}\right] \tag{5.13}$$

where ξ is the normalization factor to make the integrals of original and weighted distributions equal.

The weight $W^{\rm beam}(E)$ can be read as the ratio of numbers of data and MC events at beam energy E. Thus, for example, if the weight is larger than 1, it means we need to increase the number of MC events by the factor $W^{\rm beam}(E)$. This is exactly what we did in above BF re-weighting. This $W^{\rm beam}(E)$ needs to be multiplied by other weights to be integrated into total weight. $W^{\rm beam}(E)$ depends on the event because the beam energy E differs event by event. Thus, this weight goes into the histogram making process.

5.4.1 OffPeak data beam energy re-weighting

OffPeak data is taken at the energy 39 MeV below the OnPeak data energy. Thus, we need to scale lepton energy and D energy by a factor to match OnPeak data. The factor $r_{\rm beam}$ is given by

$$r_{\rm beam} = \frac{E^{OnPeak}_{\rm data}}{E^{OffPeak}_{\rm data}} = \frac{E_{\rm data}}{E_{\rm data} - 0.039\,{\rm GeV}} \tag{5.14}$$

where $E_{\rm data}$ is given in Table 5.1.

Run	data		MC		Normalization factor (ξ)
	mean ($E_{\rm data}$)	width ($\sigma_{\rm data}$)	mean ($E_{\rm MC}$)	width ($\sigma_{\rm MC}$)	
Run1	10.577618	0.00499	10.5778	0.00481	0.963934
Run2	10.578668	0.00501	10.5778	0.00481	0.960076
Run3	10.578393	0.00487	10.5778	0.00481	0.987636
Run4	10.577699	0.00492	10.5778	0.00481	0.977638

Table 5.1: [**Beam energy**] Average beam energy and width of each Run. Normalization factor ξ is also shown.

5.5 FF re-weighting

There have been some improvements to form factors (FF) parameterization since our MC were generated. To take those improvements into account, form factor re-weighting is necessary. Moreover, as described in chapter 4, FF re-weighting is also required to fit for FF parameters.

5.5.1 Normalization

When we change parameters in form factor (FF) parameterizations, we need to make sure that total decay rates stay the same. Thus, we need a normalization factor, R_N, such that

$$\Gamma = \int \frac{d\Gamma(\text{old FF})}{dw} dw = R_N \int \frac{d\Gamma(\text{new FF})}{dw} dw \tag{5.15}$$

In the actual integration we use a numerical integration method : Gaussian quadrature.

5.5.2 $B \to D\ell\nu$ decays

In this mode, the ISGW2 model [27, 28] was used in existing MC. ISGW2 is a constituent quark model. We need to replace it by the HQET (Heavy Quark Effective Theory) model [21, 22]. The ISGW2 model gives form factors $f_+(q^2)$ and $f_-(q^2)$, where q^2 is the momentum transfer from the hadronic system (B and D mesons) to lepton pairs (ℓ and ν). The HQET model gives form factors $h_+(w)$ and $h_-(w)$, where w is the velocity transfer (see section 2.4.1 and Appendix E). These form factors are related by

$$h_+ = \frac{1}{R}\left(f_+ + \frac{1-r}{1+r} f_-\right), \;\; h_- = \frac{1}{R}\left(\frac{1-r}{1+r} f_+ + f_-\right) \tag{5.16}$$

The differential decay rate is proportional to $\mathcal{J}_D(w)$ (Equation (2.11)). Here

$$\begin{aligned}
&(1+r)h_+ - (1-r)h_- \\
&\quad = (1+r)\frac{1}{R}\left(f_+ + \frac{1-r}{1+r}f_-\right) - (1-r)\frac{1}{R}\left(\frac{1-r}{1+r}f_+ + f_-\right) \\
&\quad = \frac{1+r}{R}\frac{(1+r)^2-(1-r)^2}{(1+r)^2}f_+ = \frac{1+r}{R}\frac{4r}{(1+r)^2}f_+ = \frac{1+r}{R}R^2 f_+ \\
&\quad = (1+r)Rf_+
\end{aligned} \tag{5.17}$$

Thus

$$\mathcal{J}_D^{ISGW2} = [(1+r)Rf_+]^2 \tag{5.18}$$

In the HQET model, from Equations (2.15) and (2.17)

$$\mathcal{J}_D^{HQET} = (1+r)^2[h_+(1)]^2[1 - 8\rho_D^2 z + (51\rho_D^2 - 10)z^2 - (252\rho_D^2 - 84)z^3]^2 \tag{5.19}$$

We can express f_+ as a function of w. Then, the weight is given by

$$W(w) = \frac{\mathcal{J}_D^{HQET}}{\mathcal{J}_D^{ISGW2}}R_N = \frac{[h_+(1)]^2[1 - 8\rho_D^2 z + (51\rho_D^2 - 10)z^2 - (252\rho_D^2 - 84)z^3]^2}{[Rf_+]^2}R_N \tag{5.20}$$

where, the normalization factor, R_N, is given by

$$\begin{aligned}
&\int_0^{1.590} dw\ \ (w^2-1)^{3/2}\,[Rf_+]^2 \\
&\quad = R_N \int_1^{1.590} dw\ \ (w^2-1)^{3/2}[h_+(1)]^2 \times \\
&\qquad\qquad \left[1 - 8\rho_D^2 z + (51\rho_D^2 - 10)z^2 - (252\rho_D^2 - 84)z^3\right]^2
\end{aligned} \tag{5.21}$$

Figure 5.5 shows the distribution of the weight in the case of $\rho_D^2 = 1.17$ [36], corresponding to the normalization factor $R_N = 1.686$. The change in the spectra of lepton momentum and D momentum are given in Figure 5.6.

In the decay rate formula (Equation (2.10)), lepton mass is set to zero; however,

muon mass may not be neglected [40–42]. If we include lepton mass terms, an additional phase space factor

$$f_{ps} = \left(1 - \frac{m_\ell^2}{m_B^2 + m_D^2 - 2m_B m_D w}\right)^2 = \left(1 - \frac{1}{1 + r^2 - 2rw}\frac{m_\ell^2}{m_B^2}\right)^2 \tag{5.22}$$

needs to be inserted in the decay rate formula. Moreover, the form factor contribution to the differential decay rate is given by [41]

$$\mathcal{J}_D(w) = (1+r)^2 |h_+(w)|^2 \left[1 + \mathcal{K}_D(w)\frac{m_\ell^2}{m_B^2}\right] \tag{5.23}$$

where

$$\mathcal{K}_D(w) \equiv \left[1 + 3\left(\frac{1-r}{1+r}\right)^2 \left(\frac{w+1}{w-1}\right)\right] \frac{1}{2(1 + r^2 - 2rw)} \tag{5.24}$$

Hence, we need an additional weight for muons :

$$W_D = \left(1 - \frac{1}{1 + r^2 - 2rw}\frac{m_\ell^2}{m_B^2}\right)^2 \left[1 + \mathcal{K}_D(w)\frac{m_\ell^2}{m_B^2}\right] \tag{5.25}$$

5.5.3 $B \to D^* \ell\nu$ decays

The differential decay rate is given in Equation (2.19). To make the notation simple, we define

$$c_L \equiv \cos\theta_\ell, \quad c_V \equiv \cos\theta_V, \quad c_\chi \equiv \cos\chi \tag{5.26}$$

These definitions along with the notations in Equation (2.28) simplify the differential decay rate to

$$\frac{d\Gamma(B \to D^* \ell\nu)}{dw dc_V dc_L d\chi} = \frac{G_F^2 |V_{cb}|^2 m_B^5}{48\pi^3} r^3 (w^2-1)^{1/2} \times \frac{9}{64\pi}(w+1)^2 \ \mathcal{J}_{FF} \tag{5.27}$$

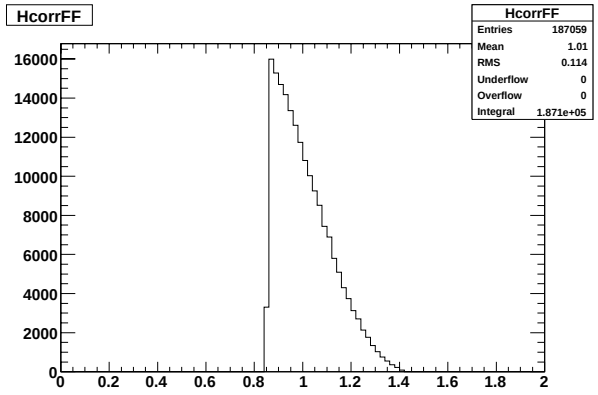

Figure 5.5: [$B \to D\ell\nu$ **FF weight**] The distribution of weights for $B \to D\ell\nu$ decays.

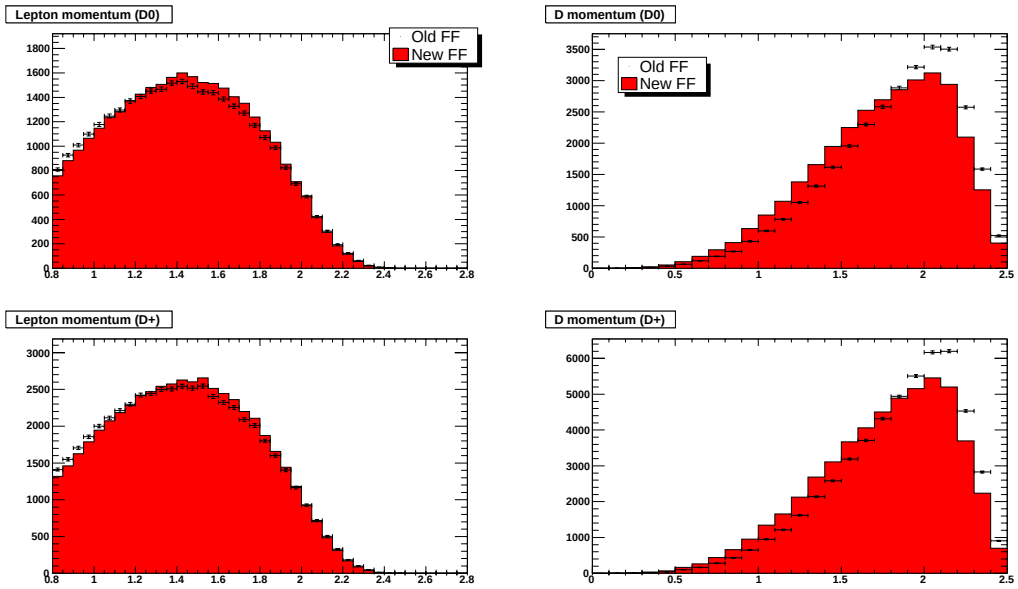

Figure 5.6: [p_ℓ **and** p_D **after** $B \to D\ell\nu$ **re-weighting**] Lepton momentum (left) and D momentum (right) spectrum of $B^+ \to \bar{D}^0\ell\nu$ decays (top) and $B^0 \to D^-\ell\nu$ decays (bottom). Black points are ISGW2 model and red histogram is HQET model with CLN slope $\rho_D^2 = 1.17$

where

$$\begin{aligned}\mathcal{J}_{FF}(R_1,R_2,\rho^2) &= [h_{A_1}(w)]^2 \times \\ &[(1-c_L)^2(1-c_V^2)\tilde{h}_+^2+(1+c_L)^2(1-c_V^2)\tilde{h}_-^2 \\ &+4(1-c_L^2)c_V^2\tilde{h}_0^2-2(1-c_L^2)(1-c_V^2)(2c_\chi^2-1)\tilde{h}_+\tilde{h}_- \\ &-4\sqrt{1-c_L^2}(1-c_L)\sqrt{1-c_V^2}c_Vc_\chi\tilde{h}_+\tilde{h}_0 \\ &+4\sqrt{1-c_L^2}(1+c_L)\sqrt{1-c_V^2}c_Vc_\chi\tilde{h}_-\tilde{h}_0]\end{aligned} \tag{5.28}$$

In existing MC, the values of parameters are

$$R_1^{MC}=1.18, \quad R_2^{MC}=0.72, \quad (\rho^2)^{MC}=0.92 \tag{5.29}$$

with the parametrization

$$\begin{aligned}R_1(w) &= R_1^{MC} \\ R_2(w) &= R_2^{MC} \\ h_{A_1}(w) &= h_{A_1}(1)\left[1-(\rho^2)^{MC}(w-1)\right]\end{aligned} \tag{5.30}$$

We use the CLN parametrization given in Equation (2.25). Thus, the weight is given by

$$W(w)=\frac{\mathcal{J}_{FF}(R_1,R_2,\rho^2)}{\mathcal{J}_{FF}(R_1^{MC},R_2^{MC},\rho_0^{MC})} \tag{5.31}$$

To calculate the normalization factor R_N, we need to integrate over c_V, c_L and χ. Thus, it is easier to use $d\Gamma/dw$ form given in Equation (2.26) which is proportional to $\mathcal{J}_{WD}(R_1,R_2,\rho^2)$ (Equation(2.27)). Thus, the normalization factor is given by

$$\begin{aligned}&\int_1^{1.504} dw\ (w^2-1)^{1/2}\mathcal{J}_{WD}(R_1^0,R_2^0,\rho_0^2) \\ &= R_N\int_1^{1.504} dw\ (w^2-1)^{1/2}\mathcal{J}_{WD}(R_1,R_2,\rho^2)\end{aligned} \tag{5.32}$$

Figure 5.7 shows the distribution of the weight in the case of the CLN parametrization with [43, 44]

$$\rho^2 = 1.179, \quad R_1 = 1.417, \quad R_2 = 0.836 \tag{5.33}$$

corresponding to the normalization factor $R_N = 1.033$. The change in the spectra of lepton momentum and D momentum, which is different from D^* momentum, are given in Figure 5.8.

If we include muon mass terms, $\mathcal{J}_{WD}(R_1, R_2, \rho^2)$ needs to be replaced by [41]

$$\mathcal{J}_{WD}(R_1, R_2, \rho^2) = (w+1)^2 [h_{A_1}]^2 (\tilde{h}_+^2 + \tilde{h}_-^2 + \tilde{h}_0^2) \left[1 + \mathcal{K}_{D^*}(w) \frac{m_\ell^2}{m_B^2}\right] \tag{5.34}$$

where

$$\mathcal{K}_{D^*}(w) \equiv \left[1 + \frac{3}{2} \frac{\tilde{h}_t^2}{\tilde{h}_+^2 + \tilde{h}_-^2 + \tilde{h}_0^2}\right] \frac{1}{2(1 + r^2 - 2rw)} \tag{5.35}$$

Hence, we need an additional weight for muons :

$$W_{D^*} = \left(1 - \frac{1}{1 + r^2 - 2rw} \frac{m_\ell^2}{m_B^2}\right)^2 \left[1 + \mathcal{K}_{D^*}(w) \frac{m_\ell^2}{m_B^2}\right] \tag{5.36}$$

The $\tilde{h}_t(w)$ in the above equations is defined by

$$\tilde{h}_t(w) \equiv (1 - r) \tilde{H}_t(w) \tag{5.37}$$

Here, $\widetilde{H}_t(w)$ is related to H_t by a relation similar to Equation (2.19). If we define a new form factor ratio R_3 similar to the ones given in Equation (2.21)

$$R_3(w) \equiv \frac{h_{A_3} - r h_{A_2}}{h_{A_1}} \tag{5.38}$$

then,

$$\tilde{h}_t(w) = \sqrt{w^2-1}\left(1 + \frac{r-w}{w+1}R_3 - \frac{1-2rw+r^2}{r(w+1)}R_2\right) \tag{5.39}$$

Since the contribution of the $\mathcal{K}_{D^*}(w)$ term is small, we approximate $R_3(w) \simeq 1$. This approximation has a negligible effect on our final results.

5.5.4 $B \to D^{**}\ell\nu$ decays

In our MC, the ISGW2 model was used. We would like to use the HQET-based LLSW model [45, 46]. Details of the LLSW model are given in Appendix G. We use the Approximation B_1 with FF slope $\hat{\tau}' = -1.5$ to calculate the form factors and the Approximation B_2 to estimate systematic uncertainties. The differential decay rates are given as functions of w and θ. This θ is the angle between the charged lepton and the charmed meson in the rest frame of the virtual W boson. Thus $\theta = \pi - \theta_\ell$, e.g.,

$$\cos\theta = \cos(\pi - \theta_\ell) = -\cos\theta_\ell \tag{5.40}$$

$B \to D_0^*\ell\nu$

The ISGW2 form factors $u_+(q^2)$ and $u_-(q^2)$ are related to the LLSW form factors $g_+(w)$ and $g_-(w)$

$$g_+ = \frac{1}{R}\left(u_+ + \frac{1-r}{1+r}u_-\right), \;\; g_- = \frac{1}{R}\left(\frac{1-r}{1+r}u_+ + u_-\right) \tag{5.41}$$

where

$$R = \frac{2\sqrt{m_B m_{D_0^*}}}{m_B + m_{D_0^*}}, \;\; r = \frac{m_{D_0^*}}{m_B} \tag{5.42}$$

The differential decay rate is given by

$$\frac{d^2\Gamma_{D_0^*}}{dw\,d\cos\theta} = \frac{G_F^2|V_{cb}|^2 m_B^5}{64\pi^3} r^3 (w^2-1)^{3/2}\,\mathcal{I}_{D_0^*}(w,\theta) \tag{5.43}$$

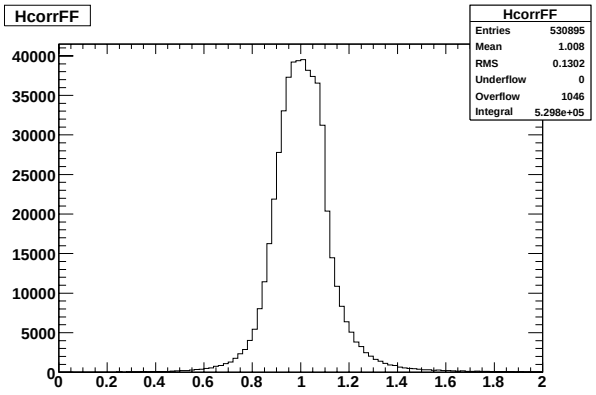

Figure 5.7: [$B \to D^*\ell\nu$ **FF weight**] The distribution of weights for $B \to D^*\ell\nu$ decays.

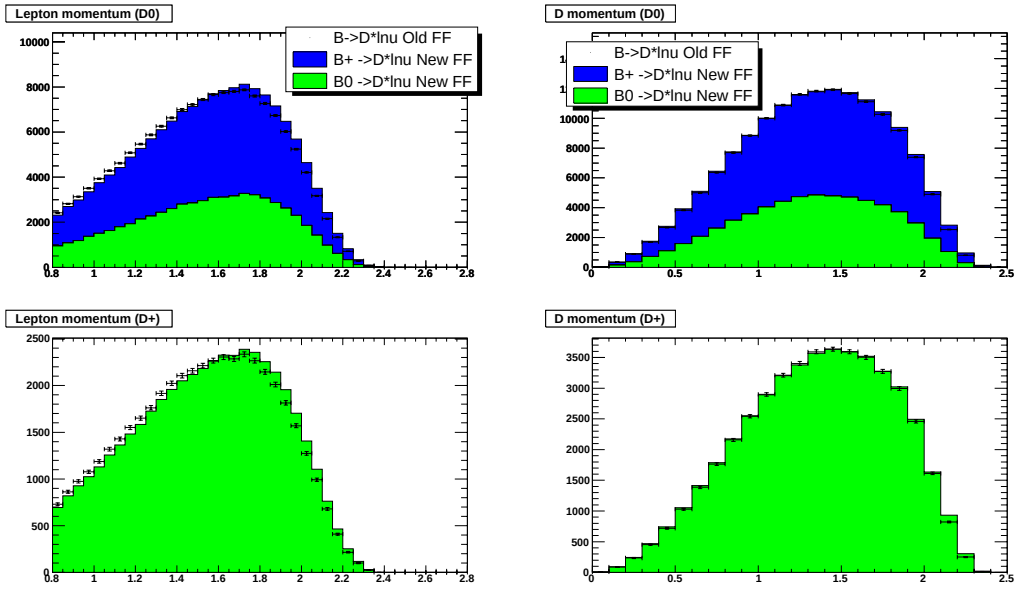

Figure 5.8: [p_ℓ **and** p_D **after** $B \to D^*\ell\nu$ **re-weighting**] Lepton momentum (left) and D momentum (right) spectrum of $B \to D^*\ell\nu$ decays. The top is D^0 and the bottom is D^+. Black points are with old FF parameters and histogram is with new FF parameters. Green is the contribution from B^+ and blue is from B^0.

where

$$\mathcal{I}_{D_0^*}(w,\theta) = (1-\cos^2\theta)[(1+r)g_+ - (1-r)g_-]^2 \tag{5.44}$$

The weight is given by the ratio of the $\mathcal{I}_{D_0^*}$ terms :

$$W(w) = \frac{\mathcal{I}_{D_0^*}^{LLSW}}{\mathcal{I}_{D_0^*}^{ISGW2}} R_N \tag{5.45}$$

Integrated over θ, the differential decay rate is

$$\frac{d\Gamma(B \to D_0^* \ell\nu)}{dw} = \frac{G_F^2 |V_{cb}|^2 m_B^5}{48\pi^3} r^3 (w^2-1)^{3/2}\, \mathcal{J}_{D_0^*}(w) \tag{5.46}$$

where

$$\mathcal{J}_{D_0^*}(w) = [(1+r)g_+ - (1-r)g_-]^2 \tag{5.47}$$

Thus, the normalization factor, R_N, is given by

$$\int_0^{1.327} (w^2-1)^{3/2} \mathcal{J}_{D_0^*}^{ISGW2} dw = R_N \int_1^{1.327} (w^2-1)^{3/2} \mathcal{J}_{D_0^*}^{LLSW} dw \tag{5.48}$$

Figure 5.9 shows the distribution of the weight in the case of the Approximation B_1, corresponding to the normalization factor $R_N = 0.1624$.

$B \to D_1' \ell\nu$

The ISGW2 form factors q, l and c_+ are related to the LLSW form factors g_A, g_{V_1}, g_{V_2} and g_{V_3}.

$$g_A = R m_B (1+r) q \tag{5.49}$$

$$g_{V_1} = \frac{2}{R m_B (1+r)} l \tag{5.50}$$

$$g_{V_3} + r g_{V_2} = R m_B (1+r) c_+ \tag{5.51}$$

where

$$R = \frac{2\sqrt{m_B m_{D_1'}}}{m_B + m_{D_1'}}, \quad r = \frac{m_{D_1'}}{m_B} \tag{5.52}$$

The differential decay rate is given by

$$\frac{d^2\Gamma_{D_1'}}{dw\, d\cos\theta} = \frac{G_F^2 |V_{cb}|^2 m_B^5}{64\pi^3} r^3 (w^2-1)^{1/2}\, \mathcal{I}_{D_1'}(w,\theta) \tag{5.53}$$

where

$$\begin{aligned}\mathcal{I}_{D_1'}(w,\theta) &= (1-\cos^2\theta)[(w-r)g_{V_1} + (w^2-1)(g_{V_3} + r g_{V_2})]^2 \\ &+(1-2rw+r^2)[(1+\cos^2\theta)(g_{V_1}^2 + (w^2-1)g_A^2) - 4\cos\theta\sqrt{w^2-1}\, g_{V_1} g_A]\end{aligned} \tag{5.54}$$

The weight is given by the ratio of the $\mathcal{I}_{D_1'}$ terms :

$$W(w) = \frac{\mathcal{I}_{D_1'}^{LLSW}}{\mathcal{I}_{D_1'}^{ISGW2}} R_N \tag{5.55}$$

Integrated over θ, the differential decay rate is

$$\frac{d\Gamma(B \to D_1 \ell\nu)}{dw} = \frac{G_F^2 |V_{cb}|^2 m_B^5}{48\pi^3} r^3 (w^2-1)^{1/2}\, \mathcal{J}_{D_1'}(w) \tag{5.56}$$

where

$$\begin{aligned}\mathcal{J}_{D_1'}(w) &= \left[(w-r)g_{V_1} + (w^2-1)(g_{V_3} + r g_{V_2})\right]^2 \\ &+2(1-2rw+r^2)[g_{V_1}^2 + (w^2-1)g_A^2]\end{aligned} \tag{5.57}$$

Thus, the normalization factor, R_N, is given by

$$\int_0^{1.316} dw (w^2-1)^{1/2} \mathcal{J}_{D_1'}^{ISGW2} = R_N \int_1^{1.316} dw (w^2-1)^{1/2} \mathcal{J}_{D_1'}^{LLSW} \tag{5.58}$$

Figure 5.9 shows the distribution of the weight in the case of the Approximation B_1, corresponding to the normalization factor $R_N = 0.5488$.

$B \to D_1 \ell \nu$

The ISGW2 form factors v, r and s_+ are related to the LLSW form factor f_A, f_{V_1}, f_{V_2} and f_{V_3}.

$$f_A = R m_B (1+r) v \tag{5.59}$$

$$f_{V_1} = \frac{2}{R m_B (1+r)} r \tag{5.60}$$

$$f_{V_3} + r f_{V_2} = R m_B (1+r) s_+ \tag{5.61}$$

where

$$R = \frac{2\sqrt{m_B m_{D_1}}}{m_B + m_{D_1}}, \quad r = \frac{m_{D_1}}{m_B} \tag{5.62}$$

The differential decay rate is given by

$$\frac{d^2\Gamma_{D_1}}{dw\, d\cos\theta} = \frac{G_F^2 |V_{cb}|^2 m_B^5}{64\pi^3} r^3 (w^2-1)^{1/2}\, \mathcal{I}_{D_1}(w,\theta) \tag{5.63}$$

where

$$\begin{aligned} \mathcal{I}_{D_1}(w,\theta) &= (1-\cos^2\theta)[(w-r) f_{V_1} + (w^2-1)(f_{V_3} + r f_{V_2})]^2 \\ &+ (1-2rw+r^2)[(1+\cos^2\theta)(f_{V_1}^2 + (w^2-1) f_A^2) - 4\cos\theta \sqrt{w^2-1} f_{V_1} f_A] \end{aligned} \tag{5.64}$$

The weight is given by the ratio of the $\mathcal{I}_{D_1}$ terms :

$$W(w) = \frac{\mathcal{I}_{D_1}^{LLSW}}{\mathcal{I}_{D_1}^{ISGW2}} R_N \tag{5.65}$$

Integrated over θ, the differential decay rate is

$$\frac{d\Gamma(B \to D_1 \ell\nu)}{dw} = \frac{G_F^2 |V_{cb}|^2 m_B^5}{48\pi^3} r^3 (w^2-1)^{1/2}\, \mathcal{J}_{D_1}(w) \tag{5.66}$$

where

$$\begin{aligned}\mathcal{J}_{D_1}(w) = &\left[(w-r) f_{V_1} + (w^2-1)(f_{V_3} + r f_{V_2})\right]^2 \\ &+2(1-2rw+r^2)[f_{V_1}^2 + (w^2-1) f_A^2]\end{aligned} \tag{5.67}$$

Thus, the normalization factor, R_N, is given by

$$\int_0^{1.320} dw (w^2-1)^{1/2} \mathcal{J}_{D_1}^{ISGW2} = R_N \int_1^{1.320} dw (w^2-1)^{1/2} \mathcal{J}_{D_1}^{LLSW} \tag{5.68}$$

Figure 5.9 shows the distribution of the weight in the case of the Approximation B_1, corresponding to the normalization factor $R_N = 0.7330$.

$B \to D_2^* \ell\nu$

The ISGW2 form factors h, k and b_+ are related to the LLSW form factor k_V, k_{A_1}, k_{A_2} and k_{A_3}.

$$k_V = R m_B^2 (1-r) h \tag{5.69}$$

$$k_{A_1} = \frac{2}{R(1-r)} k \tag{5.70}$$

$$k_{A_3} + r k_{A_2} = R m_B^2 (1-r) b_+ \tag{5.71}$$

where

$$R = \frac{2\sqrt{m_B m_{D_2^*}}}{m_B + m_{D_2^*}}, \quad r = \frac{m_{D_2^*}}{m_B} \tag{5.72}$$

The differential decay rate is given by

$$\frac{d^2\Gamma_{D_2^*}}{dw\,d\cos\theta} = \frac{G_F^2|V_{cb}|^2 m_B^5}{64\pi^3} r^3 (w^2-1)^{3/2}\,\frac{1}{2}\,\mathcal{I}_{D_2^*}(w,\theta) \tag{5.73}$$

where

$$\begin{aligned}\mathcal{I}_{D_2^*}(w,\theta) = \frac{4}{3}(1-\cos^2\theta)[(w-r)k_{A_1} + (w^2-1)(k_{A_3} + rk_{A_2})]^2 \\ +(1-2rw+r^2)[(1+\cos^2\theta)(k_{A_1}^2 + (w^2-1)k_V^2) - 4\cos\theta\sqrt{w^2-1}k_{A_1}k_V]\end{aligned} \tag{5.74}$$

The weight is given by the ratio of the $\mathcal{I}_{D_2^*}$ terms :

$$W(w) = \frac{\mathcal{I}_{D_2^*}^{LLSW}}{\mathcal{I}_{D_2^*}^{ISGW2}} R_N \tag{5.75}$$

Integrated over θ, decay rate is

$$\frac{d\Gamma(B\to D_2^*\ell\nu)}{dw} = \frac{G_F^2|V_{cb}|^2 m_B^5}{48\pi^3} r^3 (w^2-1)^{3/2}\,\mathcal{J}_{D_2^*}(w) \tag{5.76}$$

where

$$\begin{aligned}\mathcal{J}_{D_2^*}(w) = \frac{2}{3}\left[(w-r)k_{A_1} + (w^2-1)(k_{A_3} + rk_{A_2})\right]^2 \\ +2(1-2rw+r^2)[k_{A_1}^2 + (w^2-1)k_V^2]\end{aligned} \tag{5.77}$$

Thus, the normalization factor, R_N, is given by

$$\int_0^{1.306} dw(w^2-1)^{3/2}\mathcal{J}_{D_2^*}^{ISGW2} = R_N \int_1^{1.306} dw(w^2-1)^{3/2}\mathcal{J}_{D_2^*}^{LLSW} \tag{5.78}$$

Figure 5.9 shows the distribution of the weight in the case of the Approximation B_1, corresponding to the normalization factor $R_N = 0.7490$.

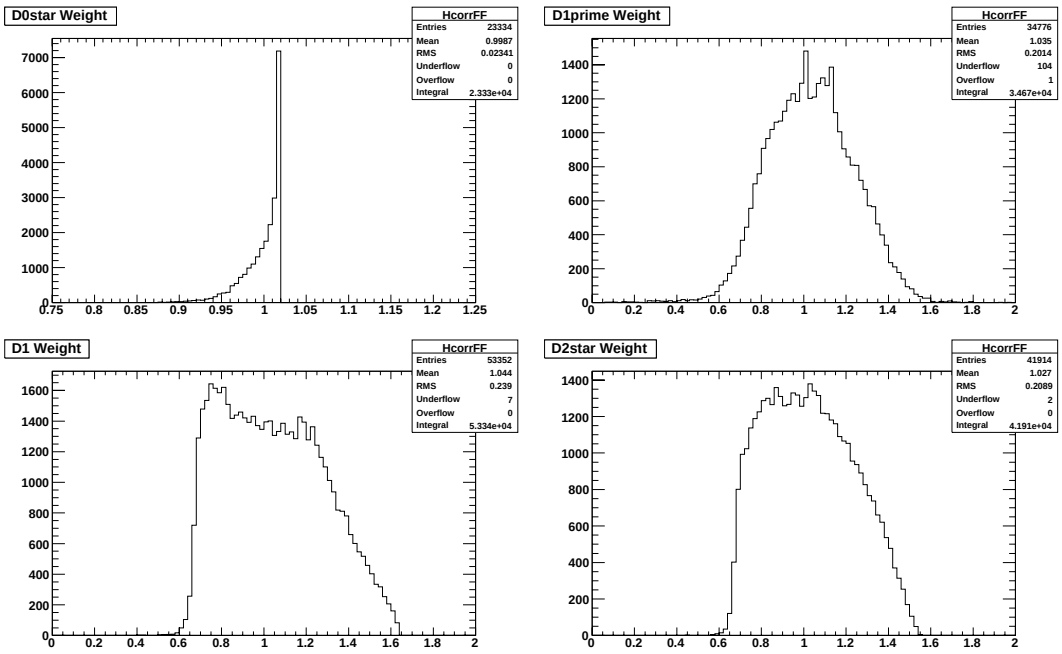

Figure 5.9: [$B \to D^{**}\ell\nu$ **FF weight**] The distribution of weights for $B \to D_0^*\ell\nu$ decays (top-left), $B \to D_1'\ell\nu$ decays (top-right), $B \to D_1\ell\nu$ decays (bottom-left) and $B \to D_2^*\ell\nu$ decays (bottom-right).

Effect on kinematic variables

The changes in the spectra of lepton momentum, D momentum, which is different from D^{**} momentum, and $\cos\theta_{B-Dl}$ are given in Figures 5.10 and 5.11.

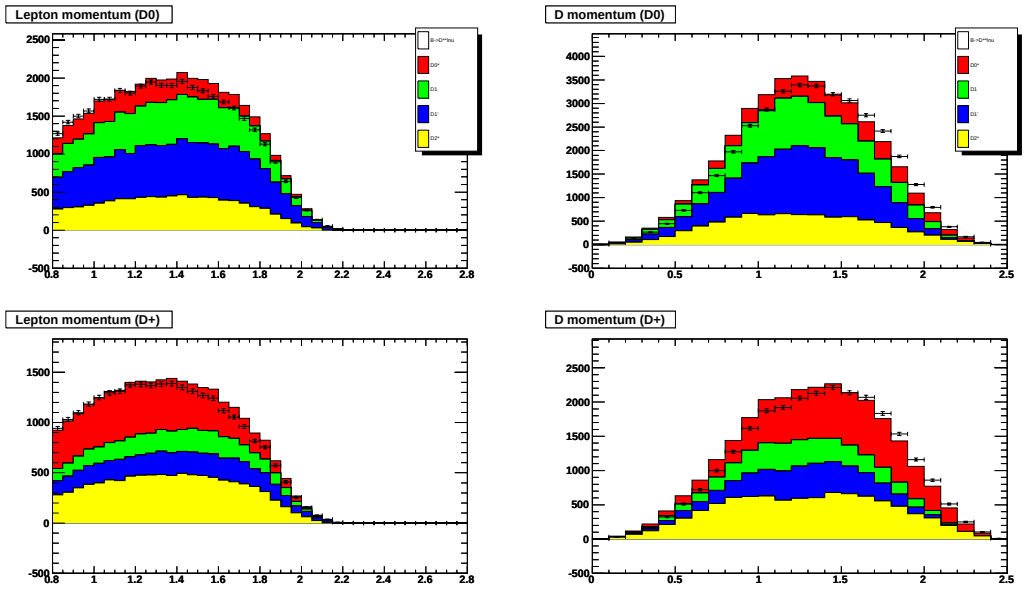

Figure 5.10: [p_ℓ **and** p_D **after** $B \to D^{**}\ell\nu$ **re-weighting**] Lepton momentum (left) and D momentum (right) spectrum of $B \to D^{**}\ell\nu$ decays. Black points are ISGW2 model and colored histogram is LLSW model. Red is D_0^*, green is D_1, blue is D_1' and yellow is D_2^*.

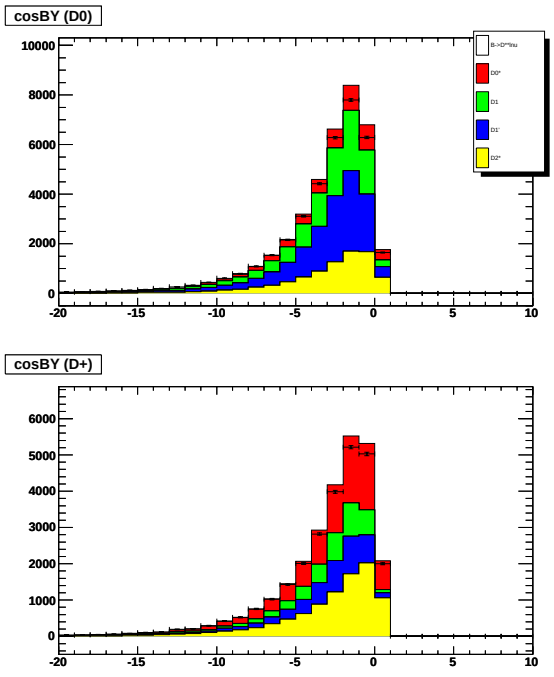

Figure 5.11: [$\cos\theta_{B-Dl}$ **after** $B \to D^{**}\ell\nu$ **re-weighting**] $\cos\theta_{B-Dl}$ of $B \to D^{**}\ell\nu$ decays. Black points are ISGW2 model and colored histogram is LLSW model. Red is D_0^*, green is D_1, blue is D_1' and yellow is D_2^*.

Chapter 6

Details of the fitting method

6.1 The χ^2

Since we reconstruct $D^0\ell$ and $D^+\ell$, the χ^2 consists of two parts as given in the following equation

$$\chi^2 = \sum_i^{D^0\ell} \frac{(N_i^{data} - \sum_j C_j^{MC} N_{ij}^{MC})^2}{(\sigma_i^{data})^2 + \sum_j (C_j^{MC}\sigma_{ij}^{MC})^2} + \sum_i^{D^+\ell} \frac{(N_i^{data} - \sum_j C_j^{MC} N_{ij}^{MC})^2}{(\sigma_i^{data})^2 + \sum_j (C_j^{MC}\sigma_{ij}^{MC})^2} \qquad (6.1)$$

where

- i represents each bin
- j represents each MC mode.

MC modes are listed in section 6.4 separately for the D^0 and D^+ samples. See also Appendix A.

Quantities in the χ^2 are:

- N_i^{data} = The number of continuum subtracted data candidates in the i-th bin. (see section 6.3.2)
- N_{ij}^{MC} = The number of candidates in the i-th bin in MC mode j, luminosity normalized to OnPeak data. Details are in section 6.3.1. The effect of data

MC differences from tracking and PID are corrected (see section 6.3.3). MC re-weighting is also done.

- C_j^{MC} = The coefficient of each MC mode (j). These include branching fractions to be determined in the fit. Details are in section 6.4.

- σ_i^{data} = The statistical uncertainty of N_i^{data}. Details are in section 6.3.4.

- σ_{ij}^{MC} = The statistical uncertainty of N_{ij}^{MC}. Details are in section 6.3.4.

We use bins which have more than 10 expected candidates ($\sum_j C_j^{MC} N_{ij}^{MC} > 10$) and neglect other bins to avoid non-Gaussian effects. The number 10 is changed for cross checks.

6.2 Binning (i)

We use the following binning to accommodate the kinematic cuts described in section 3.4.5

- lepton momentum in the CM frame p_ℓ^*

  (10 bins (GeV)) : 1.2, 1.3, 1.4, 1.5, 1.6, 1.7, 1.8, 1.9, 2.0, 2.1, 2.35

- D momentum in the CM frame p_D^*

  (9 bins (GeV)) : 0.8, 1.1, 1.35, 1.5, 1.65, 1.8, 1.95, 2.1, 2.25, 2.45

- $\cos\theta_{B-Dl}$

  (3 bins) : -2, -1, 0, 1.1

The binning is decided by balancing two opposing requirements :

- It needs to be as fine as possible to preserve the sensitivity to the fitted parameters.

- It needs to be as coarse as necessary to have adequate statistics per bin to allow the use of a χ^2 fit.

The projection plots with this binning are given in chapter 8.

6.3 Histogram making

6.3.1 Number of MC Candidates N_{ij}^{MC}

We calculate the number of candidates from $B\bar{B}$ MC. The number of MC candidates N_{ij}^{MC} is given by

$$N_{ij}^{MC} = r_{MC}^{Lumi} \sum_{k} r_k^{Trk} r_k^{KPID} r_k^{LPID} W_{jk}^{MC} \tag{6.2}$$

where

- k represents the k-th candidate in the i-th bin.

  The sum of k is taken only over the candidates in the i-th bin.

and

- r_{MC}^{Lumi} is the luminosity normalization factor (⇒ section 6.3.2)
- r_k^{Trk} is the tracking efficiency correction factor (⇒ section 6.3.3)
- r_k^{KPID} is the kaon PID correction factor (⇒ section 6.3.3)
- r_k^{LPID} is the lepton PID correction factor (⇒ section 6.3.3)
- W_{jk}^{MC} is the MC weight (⇒ chapter 5)

6.3.2 Luminosity normalization r^{Lumi}

All MC and OffPeak data are normalized to OnPeak data by luminosity. Supposing OnPeak luminosity is $\mathcal{L}^{OnPeak}$ and MC luminosity is $\mathcal{L}^{MC}$, the normalization factor r_{MC}^{Lumi} is given by

$$r_{MC}^{Lumi} = \frac{\mathcal{L}^{OnPeak}}{\mathcal{L}^{MC}} \tag{6.3}$$

The $\mathcal{L}^{MC}$ can be determined as follows. First the number of $B\bar{B}$ events is counted by applying hadronic event selection to OffPeak subtracted data. Then the number

is compared with the number of simulated events to determine $\mathcal{L}^{MC}$. The relative numbers of B^+B^- and $B^0\bar{B}^0$ events are explained in section 6.4.

To normalize the OffPeak data, since OffPeak data is taken at 39 MeV lower energy than OnPeak data, we need to correct for $1/s$ dependence of $e^+e^- \to f\bar{f}$ cross section, where s is the square of CM beam energy :

$$\begin{aligned} s_{OnPeak} &= 10.58^2 \ \text{GeV}^2 \\ s_{OffPeak} &= (10.58 - 0.039)^2 \ \text{GeV}^2 \end{aligned} \tag{6.4}$$

Thus, correction factor is given by

$$r^{Lumi}_{OffPeak} = \frac{\mathcal{L}^{OnPeak} s_{OffPeak}}{\mathcal{L}^{OffPeak} s_{OnPeak}} \tag{6.5}$$

The N_i^{data} is calculated with this luminosity factor

$$N_i^{data} = N_i^{OnPeak} - N_i^{OffPeak} = N_i^{OnPeak} - r^{Lumi}_{OffPeak} N_i^0 \tag{6.6}$$

where N_i^0 is the number of OffPeak candidates in i-th bin before normalization. Statistical uncertainties are explained in section 6.3.4

6.3.3 PID and Tracking efficiency correction

Tracking efficiency and PID efficiency are not completely equal in both data and MC. There is always a difference no matter how sophisticated the codes to reconstruct charged tracks and to identify particles are. Tracking efficiency and PID corrections are to account for the residual differences between data and MC. Correction factors or weights are determined by comparing data and MC on specific control samples.

Tracking efficiency correction : r_k^{Trk}

Tracking efficiency correction factors are given for each charged track, depending on its transverse momentum, direction in the laboratory frame and the multiplicity of

the event. These correction factors are determined by comparing data and MC on multi-hadron events.

Three charged tracks are used to reconstruct a $D^0(K\pi)l$ candidate, and 4 charged tracks to reconstruct a $D^+(K\pi\pi)l$ candidate. The correction factor r_k^{Trk} is given by the product of the correction factors for each charged track in the k-th candidate.

PID correction : r_k^{LPID} and r_k^{KPID}

PID correction factors (called weights) are given one for each PID selector. Thus, we have one factor r_k^{LPID} for lepton (PidLHElectron for electrons and muNNTight for muons) and another factor r_k^{KPID} for kaon (KLHNotPion) for each candidate (k). These weights are determined by comparing data and MC on specific control samples such as $e^+e^- \to e^+e^-\gamma$, $e^+e^- \to \mu^+\mu^-\gamma$ and $D^{*+} \to D^0\pi^+ \to (K^-\pi^+)\pi^+$.

When the particles are correctly identified, r_k^{LPID} and r_k^{KPID} are the factors to correct for the identification efficiency differences. When the particles are mis-identified, r_k^{LPID} and r_k^{KPID} give the factors to correct fake rate differences.

6.3.4 Statistical uncertainty σ_i

After the D mass sideband subtraction, the number and statistical uncertainty of OnPeak data are given by

$$\begin{aligned} N_i^{OnPeak} &= N_{peak}^{OnPeak}{}_i - r_{side} N_{side}^{OnPeak}{}_i \\ \sigma_i^{OnPeak} &= \sqrt{N_{peak}^{OnPeak}{}_i + r_{side}^2 N_{side}^{OnPeak}{}_i} \end{aligned} \tag{6.7}$$

where r_{side} is the scale factor to account for the differences between peak and sideband mass ranges. Statistical uncertainties of OffPeak data and MC are a bit more complicated because they are luminosity normalized and re-weighted. In this section, we explain how the statistical uncertainty of OffPeak data and MCs are calculated.

Luminosity normalization and statistical uncertainty

OffPeak and MC are luminosity normalized to OnPeak data. We take OffPeak data as an example. If the number of OffPeak candidates in the i-th bin is $N_i^0 = N_{peak_i}^0 - r_{side} N_{sidei}^0$, the number of luminosity normalized candidates in the bin is given by

$$N_i^{OffPeak} = r_{OffPeak}^{Lumi} N_i^0 = r_{OffPeak}^{Lumi} \left(N_{peak_i}^0 - r_{side} N_{sidei}^0 \right) \tag{6.8}$$

and the statistical uncertainty of the bin is given by

$$\sigma_i^{OffPeak} = r_{OffPeak}^{Lumi} \sqrt{N_{peak_i}^0 + r_{side}^2 N_{sidei}^0} \tag{6.9}$$

MC re-weighting and statistical uncertainty

Supposing the total weight of the k-th candidate of MC mode j is

$$w_{jk}^T \equiv r_k^{Trk} r_k^{KPID} r_k^{LPID} W_{jk}^{MC} \tag{6.10}$$

The number of candidates in the i-th bin is given by

$$N_{ij}^{MC} = r_{MC}^{Lumi} \left(\sum_k^{peak} w_{jk}^T - r_{side} \sum_k^{side} w_{jk}^T \right) \tag{6.11}$$

We add the statistical uncertainties quadratically. Thus,

$$\sigma_{ij}^{MC} = r_{MC}^{Lumi} \sqrt{\sum_k^{peak} \left(w_{jk}^T \right)^2 + r_{side}^2 \sum_k^{side} \left(w_{jk}^T \right)^2} \tag{6.12}$$

6.4 Coefficients in the fitting C_j^{MC}

Coefficients consist of branching fractions, some of which are to be determined by the fit. Coefficients are given by taking ratios between new branching fractions and

the ones used in MC (the ones with superscript MC in the following subsections). The decays contributing to each MC mode are shown in Appendix A and B.

The luminosity of $B\bar{B}$ MC is calculated by the generated number of events and the counted number of B in OnPeak data as described in section 6.3.2. The luminosity calculation was done based on the assumption that produced number of B^+B^- and $B^0\bar{B}^0$ pairs are equal. The difference in $\Upsilon(4S) \to B^+B^-$ and $\Upsilon(4S) \to B^0\bar{B}^0$ branching fractions is taken into account in the coefficients.

6.4.1 Number of produced B

Branching fractions of B^+B^- and $B^0\bar{B}^0$ of $\Upsilon(4S)$ resonance are denoted by

$$\begin{aligned} f_{+-} &= \mathcal{B}(\Upsilon(4S) \to B^+B^-) \\ f_{00} &= \mathcal{B}(\Upsilon(4S) \to B^0\bar{B}^0) \end{aligned} \tag{6.13}$$

We define the ratio of these two branching fractions

$$f_{+0} \equiv \frac{f_{+-}}{f_{00}} \tag{6.14}$$

In existing MC, $f_{+0}^{MC} = 1$. We also assume that $\Upsilon(4S)$ decays only $B\bar{B}$ pairs, *i.e.*

$$f_{+-} + f_{00} = 1 \tag{6.15}$$

The number of produced B is related to the ratio f_{+0}. Supposing the number of $B\bar{B}$-pairs produced is given by $N_{B\bar{B}}$, the number of produced neutral B is

$$N_{neut}^{prod} = 2f_{00}N_{B\bar{B}} \tag{6.16}$$

and the number of produced charged B is

$$N_{chrg}^{prod} = 2f_{+-}N_{B\bar{B}} = f_{+0}N_{neut}^{prod} \tag{6.17}$$

Thus,

$$N^{prod}_{neut} = \frac{2}{1+f_{+0}} N_{B\bar{B}}, \qquad N^{prod}_{chrg} = \frac{2f_{+0}}{1+f_{+0}} N_{B\bar{B}} \tag{6.18}$$

6.4.2 $B\bar{B}$ luminosity correction

As explained above, we assumed $f_{+0} = 1$ in the luminosity normalization. We need to correct these. The correction factors are given by

$$\begin{aligned} C_{B^+} &= \frac{2f_{+0}}{1+f_{+0}} \qquad \text{for } B^+B^- \text{ MC} \\ C_{B^0} &= \frac{2}{1+f_{+0}} \qquad \text{for } B^0\bar{B}^0 \text{ MC} \end{aligned} \tag{6.19}$$

The coefficients C_j^{MC} include the factor C_{B^+} if those are of B^+B^- MC and C_{B^0} if those are of $B^0\bar{B}^0$ MC.

6.4.3 Examples of coefficients

Coefficients are given by taking a ratio between new values and the values used in our MC. We give a few examples to illustrate how coefficients are calculated.

1. $B^0 \to D^{*-}\ell^+\nu$ with $D^{*-} \to \bar{D}^0\pi^-$

   The number of produced events is given by

$$N = N_{B\bar{B}} C_{B^0} \mathcal{B}(B^0 \to D^{*-}\ell^+\nu)\mathcal{B}(D^{*+} \to D^0\pi^+)\mathcal{B}(D^0 \to K^-\pi^+) \tag{6.20}$$

   Thus, the coefficient is given by

$$C_3^{MC} = \frac{C_{B^0}\mathcal{B}(B^0 \to D^{*-}\ell^+\nu)\mathcal{B}(D^{*+} \to D^0\pi^+)\mathcal{B}(D^0 \to K^-\pi^+)}{\mathcal{B}^{MC}(B^0 \to D^{*-}\ell^+\nu)\mathcal{B}^{MC}(D^{*+} \to D^0\pi^+)\mathcal{B}^{MC}(D^0 \to K^-\pi^+)} \tag{6.21}$$

2. Uncorrelated direct lepton background ($B^+B^- \to D^0\ell$ case)

$$C_{16}^{MC} = \frac{C_{B^+}\mathcal{B}(D^0 \to K^-\pi^+)}{\mathcal{B}^{MC}(D^0 \to K^-\pi^+)} \tag{6.22}$$

3. Correlated cascade lepton background ($B^0\bar{B}^0 \to D^+\ell$ case)

$$C_{20}^{MC} = \frac{C_{B^0}\mathcal{B}(D^+ \to K^-\pi^+\pi^+)}{\mathcal{B}^{MC}(D^+ \to K^-\pi^+\pi^+)} \tag{6.23}$$

6.5 MC modes for D^0

The following MC modes eventually produce $D^0\ell$ candidates.

6.5.1 Signals : $j = 1 - 15$

- $j = 1 :\ B^+ \to \bar{D}^0\ell^+\nu$
- $j = 2 :\ B^+ \to \bar{D}^{*0}\ell^+\nu$ with $\bar{D}^{*0} \to \bar{D}^0 + \gamma/\pi^0$
- $j = 3 :\ B^0 \to D^{*-}\ell^+\nu$ with $D^{*-} \to \bar{D}^0\pi^-$
- $j = 4 :\ B^+ \to \bar{D}_0^{*0}\ell^+\nu$ with $\bar{D}_0^{*0} \to \bar{D}^0\pi^0$
- $j = 5 :\ B^0 \to D_0^{*-}\ell^+\nu$ with $D_0^{*-} \to \bar{D}^0\pi^+$
- $j = 6 :\ B^+ \to \bar{D}_1^0\ell^+\nu$

  The decays contribute to this mode are

  $B^+ \to \bar{D}_1^0\ell^+\nu$ with $\bar{D}_1^0 \to D^{*-}\pi^+$ and $D^{*-} \to \bar{D}^0\pi^-$

  $B^+ \to \bar{D}_1^0\ell^+\nu$ with $\bar{D}_1^0 \to \bar{D}^{*0}\pi^0$ and $\bar{D}^{*0} \to \bar{D}^0 + \gamma/\pi^0$
- $j = 7 :\ B^0 \to D_1^-\ell^+\nu$

  The decays contribute to this mode are

  $B^0 \to D_1^-\ell^+\nu$ with $D_1^- \to D^{*-}\pi^0$ and $D^{*-} \to \bar{D}^0\pi^-$

  $B^0 \to D_1^-\ell^+\nu$ with $D_1^- \to \bar{D}^{*0}\pi^-$ and $\bar{D}^{*0} \to \bar{D}^0 + \gamma/\pi^0$
- $j = 8 :\ B^+ \to \bar{D}_1^{\prime 0}\ell^+\nu$

  The decays contribute to this mode are

  $B^+ \to \bar{D}_1^{\prime 0}\ell^+\nu$ with $\bar{D}_1^{\prime 0} \to D^{*-}\pi^+$ and $D^{*-} \to \bar{D}^0\pi^-$

  $B^+ \to \bar{D}_1^{\prime 0}\ell^+\nu$ with $\bar{D}_1^{\prime 0} \to \bar{D}^{*0}\pi^0$ and $\bar{D}^{*0} \to \bar{D}^0 + \gamma/\pi^0$

- $j = 9 :\ B^0 \to D_1'^- \ell^+ \nu$

  The decays contribute to this mode are

  $B^0 \to D_1'^- \ell^+ \nu$ with $D_1'^- \to D^{*-} \pi^0$ and $D^{*-} \to \bar{D}^0 \pi^-$

  $B^0 \to D_1'^- \ell^+ \nu$ with $D_1'^- \to \bar{D}^{*0} \pi^-$ and $\bar{D}^{*0} \to \bar{D}^0 + \gamma/\pi^0$

- $j = 10 :\ B^+ \to \bar{D}_2^{*0} \ell^+ \nu$

  The decays contribute to this mode are

  $B^+ \to \bar{D}_2^{*0} \ell^+ \nu$ with $\bar{D}_2^{*0} \to D^{*-} \pi^+$ and $D^{*-} \to \bar{D}^0 \pi^-$

  $B^+ \to \bar{D}_2^{*0} \ell^+ \nu$ with $\bar{D}_2^{*0} \to \bar{D}^{*0} \pi^0$ and $\bar{D}^{*0} \to \bar{D}^0 + \gamma/\pi^0$

  $B^+ \to \bar{D}_2^{*0} \ell^+ \nu$ with $\bar{D}_2^{*0} \to \bar{D}^0 \pi^0$

- $j = 11 :\ B^0 \to D_2^{*-} \ell^+ \nu$

  The decays contribute to this mode are

  $B^0 \to D_2^{*-} \ell^+ \nu$ with $D_2^{*-} \to D^{*-} \pi^0$ and $D^{*-} \to \bar{D}^0 \pi^-$

  $B^0 \to D_2^{*-} \ell^+ \nu$ with $D_2^{*-} \to \bar{D}^{*0} \pi^-$ and $\bar{D}^{*0} \to \bar{D}^0 + \gamma/\pi^0$

  $B^0 \to D_2^{*-} \ell^+ \nu$ with $D_2^{*-} \to \bar{D}^0 \pi^-$

- $j = 12 :\ B^+ \to \bar{D}^0 \pi^0 \ell^+ \nu$

- $j = 13 :\ B^0 \to \bar{D}^0 \pi^- \ell^+ \nu$

- $j = 14 :\ B^+ \to D^* \pi \ell^+ \nu$

  The decays contribute to this mode are

  $B^+ \to D^{*-} \pi^+ \ell^+ \nu$ with $D^{*-} \to \bar{D}^0 + \pi^-$

  $B^+ \to \bar{D}^{*0} \pi^0 \ell^+ \nu$ with $\bar{D}^{*0} \to \bar{D}^0 + \gamma/\pi^0$

- $j = 15 :\ B^0 \to D^* \pi \ell^+ \nu$

  The decays contribute to this mode are

  $B^0 \to D^{*-} \pi^0 \ell^+ \nu$ with $D^{*-} \to \bar{D}^0 + \pi^-$

  $B^0 \to \bar{D}^{*0} \pi^- \ell^+ \nu$ with $\bar{D}^{*0} \to \bar{D}^0 + \gamma/\pi^0$

6.5.2 Backgrounds : $j = 16 - 27$

- $j = 16$, Uncorrelated Direct Lepton from B^+B^-
- $j = 17$, Uncorrelated Direct Lepton from $B^0\bar{B}^0$
- $j = 18$, Uncorrelated Cascade Lepton from B^+B^-
- $j = 19$, Uncorrelated Cascade Lepton from $B^0\bar{B}^0$
- $j = 20$, Correlated Cascade Lepton from B^+B^-
- $j = 21$, Correlated Cascade Lepton from $B^0\bar{B}^0$
- $j = 22$, Fake Lepton from B^+B^-
- $j = 23$, Fake Lepton from $B^0\bar{B}^0$
- $j = 24$, Combinatorial with True Lepton from B^+B^-
- $j = 25$, Combinatorial with True Lepton from $B^0\bar{B}^0$
- $j = 26$, Combinatorial with Fake Lepton from B^+B^-
- $j = 27$, Combinatorial with Fake Lepton from $B^0\bar{B}^0$

6.6 MC modes for D^+

The following MC modes eventually produce $D^+\ell$ candidates.

6.6.1 Signals : $j = 1 - 14$

- $j = 1 : B^0 \to D^-\ell^+\nu$
- $j = 2 : B^0 \to D^{*-}\ell^+\nu$ with $D^{*-} \to D^- + \gamma/\pi^0$
- $j = 3 : B^+ \to \bar{D}_0^{*0}\ell^+\nu$ with $\bar{D}_0^{*0} \to D^- + \pi^+$
- $j = 4 : B^0 \to D_0^{*-}\ell^+\nu$ with $D_0^{*-} \to D^-\pi^0$

- $j = 5:\ B^+ \to \bar{D}_1^0 \ell^+ \nu$ with $\bar{D}_1^0 \to D^{*-} + \pi^+$ and $D^{*-} \to D^- + \pi^0/\gamma$
- $j = 6:\ B^0 \to D_1^- \ell^+ \nu$ with $D_1^- \to D^{*-}\pi^0$ and $D^{*-} \to D^- + \pi^0/\gamma$
- $j = 7:\ B^+ \to \bar{D}_1'^0 \ell^+ \nu$ with $\bar{D}_1'^0 \to D^{*-} + \pi^+$ and $D^{*-} \to D^- + \pi^0/\gamma$
- $j = 8:\ B^0 \to D_1'^- \ell^+ \nu$ with $D_1'^- \to D^{*-}\pi^0$ and $D^{*-} \to D^- + \pi^0/\gamma$
- $j = 9:\ B^+ \to \bar{D}_2^{*0} \ell^+ \nu$

  The decays contribute to this mode are

  $B^+ \to \bar{D}_2^{*0} \ell^+ \nu$ with $\bar{D}_2^{*0} \to D^{*-} + \pi^+$ and $D^{*-} \to D^- + \pi^0/\gamma$

  $B^+ \to \bar{D}_2^{*0} \ell^+ \nu$ with $\bar{D}_2^{*0} \to D^- + \pi^+$
- $j = 10:\ B^0 \to D_2^{*-} \ell^+ \nu$

  The decays contribute to this mode are

  $B^0 \to D_2^{*-} \ell^+ \nu$ with $D_2^{*-} \to D^{*-}\pi^0$ and $D^{*-} \to D^- + \pi^0/\gamma$

  $B^0 \to D_2^{*-} \ell^+ \nu$ with $D_2^{*-} \to D^-\pi^0$
- $j = 11:\ B^+ \to D^-\pi^+\ell^+\nu$
- $j = 12:\ B^0 \to D^-\pi^0\ell^+\nu$
- $j = 13:\ B^+ \to D^{*-}\pi^+\ell^+\nu$ with $D^{*-} \to D^- + \gamma/\pi^0$
- $j = 14:\ B^0 \to D^{*-}\pi^0\ell^+\nu$ with $D^{*-} \to D^- + \gamma/\pi^0$

6.6.2 Backgrounds : $j = 15 - 26$

- $j = 15$, Uncorrelated Direct Lepton from B^+B^-
- $j = 16$, Uncorrelated Direct Lepton from $B^0\bar{B}^0$
- $j = 17$, Uncorrelated Cascade Lepton from B^+B^-
- $j = 18$, Uncorrelated Cascade Lepton from $B^0\bar{B}^0$

- $j = 19$, Correlated Cascade Lepton from B^+B^-
- $j = 20$, Correlated Cascade Lepton from $B^0\bar{B}^0$
- $j = 21$, Fake Lepton from B^+B^-
- $j = 22$, Fake Lepton from $B^0\bar{B}^0$
- $j = 23$, Combinatorial with True Lepton from B^+B^-
- $j = 24$, Combinatorial with True Lepton from $B^0\bar{B}^0$
- $j = 25$, Combinatorial with Fake Lepton from B^+B^-
- $j = 26$, Combinatorial with Fake Lepton from $B^0\bar{B}^0$

6.7 Parametrization of $B \to D^{(*)}\pi\ell\nu$ decay branching fractions

We parameterize $B \to D^{(*)}\pi\ell\nu$ decay branching fractions with one total branching fraction and five branching fraction ratios. First, we define a total branching fraction

$$\begin{aligned}
&\mathcal{B}(B^+ \to D^{(*)}\pi\ell\nu) \\
&\qquad \equiv \mathcal{B}(B^+ \to \bar{D}_1^0\ell^+\nu) + \mathcal{B}(B^+ \to \bar{D}_2^{*0}\ell^+\nu) \\
&\qquad +\mathcal{B}(B^+ \to \bar{D}_0^{*0}\ell^+\nu) + \mathcal{B}(B^+ \to \bar{D}_1'^0\ell^+\nu) \\
&\qquad +\mathcal{B}^{NR}(B^+ \to D^-\pi^+\ell^+\nu) + \mathcal{B}^{NR}(B^+ \to \bar{D}^0\pi^0\ell^+\nu) \\
&\qquad +\mathcal{B}^{NR}(B^+ \to D^{*-}\pi^+\ell^+\nu) + \mathcal{B}^{NR}(B^+ \to \bar{D}^{*0}\pi^0\ell^+\nu)
\end{aligned} \tag{6.24}$$

and five branching fraction ratios

$$f_{D_2^*/D_1} \equiv \frac{\mathcal{B}(B^+ \to \bar{D}_2^{*0}\ell^+\nu)}{\mathcal{B}(B^+ \to \bar{D}_1^0\ell^+\nu)} \tag{6.25}$$

$$f_{D\pi/D_0^*} \equiv \frac{\mathcal{B}^{NR}(B^+ \to D^-\pi^+\ell^+\nu)}{\mathcal{B}(B^+ \to \bar{D}_0^{*0}\ell^+\nu)} \tag{6.26}$$

$$f_{D^*\pi/D_1'} \equiv \frac{\mathcal{B}^{NR}(B^+ \to D^{*-}\pi^+\ell^+\nu)}{\mathcal{B}(B^+ \to \bar{D}_1'^0\ell^+\nu)} \tag{6.27}$$

$$f_{D_0^* D\pi/D_1 D_2^*} \equiv \frac{\mathcal{B}(B^+ \to \bar{D}_0^{*0}\ell^+\nu) + \mathcal{B}^{NR}(B^+ \to D^-\pi^+\ell^+\nu) + \mathcal{B}^{NR}(B^+ \to \bar{D}^0\pi^0\ell^+\nu)}{\mathcal{B}(B^+ \to \bar{D}_1^0\ell^+\nu) + \mathcal{B}(B^+ \to \bar{D}_2^{*0}\ell^+\nu)} \tag{6.28}$$

$$f_{D_1' D^*\pi/D_1 D_2^*} \equiv \frac{\mathcal{B}(B^+ \to \bar{D}_1'^0\ell^+\nu) + \mathcal{B}^{NR}(B^+ \to D^{*-}\pi^+\ell^+\nu) + \mathcal{B}^{NR}(B^+ \to \bar{D}^{*0}\pi^0\ell^+\nu)}{\mathcal{B}(B^+ \to \bar{D}_1^0\ell^+\nu) + \mathcal{B}(B^+ \to \bar{D}_2^{*0}\ell^+\nu)} \tag{6.29}$$

The quantity $f_{D_2^*/D_1}$ is the ratio between two narrow states (see Appendix B), $f_{D\pi/D_0^*}$ ($f_{D^*\pi/D_1'}$) is between two broad states decaying to $D\pi$ ($D^*\pi$) and the other two ratios are between broad and narrow states. Individual branching fractions are given by these six parameters as follows

$$\mathcal{B}(B^+ \to \bar{D}_1^0\ell^+\nu) = \frac{\mathcal{B}(B^+ \to D^{(*)}\pi\ell\nu)}{(1+f_{D_2^*/D_1})(1+f_{D_0^*D\pi/D_1D_2^*}+f_{D_1'D^*\pi/D_1D_2^*})} \tag{6.30}$$

$$\mathcal{B}(B^+ \to \bar{D}_2^{*0}\ell^+\nu) = f_{D_2^*/D_1}\mathcal{B}(B^+ \to \bar{D}_1^0\ell^+\nu) \tag{6.31}$$

$$\mathcal{B}(B^+ \to \bar{D}_0^{*0}\ell^+\nu) = \frac{2f_{D_0^*D\pi/D_1D_2^*}\mathcal{B}(B^+ \to D^{(*)}\pi\ell\nu)}{(2+3f_{D\pi/D_0^*})(1+f_{D_0^*D\pi/D_1D_2^*}+f_{D_1'D^*\pi/D_1D_2^*})} \tag{6.32}$$

$$\mathcal{B}(B^+ \to \bar{D}_1'^0\ell^+\nu) = \frac{2f_{D_1'D^*\pi/D_1D_2^*}\mathcal{B}(B^+ \to D^{(*)}\pi\ell\nu)}{(2+3f_{D^*\pi/D_1'})(1+f_{D_0^*D\pi/D_1D_2^*}+f_{D_1'D^*\pi/D_1D_2^*})} \tag{6.33}$$

$$\mathcal{B}(B^+ \to D^-\pi^+\ell^+\nu) = f_{D\pi/D_0^*}\mathcal{B}(B^+ \to \bar{D}_0^{*0}\ell^+\nu) \tag{6.34}$$

$$\mathcal{B}(B^+ \to D^{*-}\pi^+\ell^+\nu) = f_{D^*\pi/D_1'}\mathcal{B}(B^+ \to \bar{D}_1'^0\ell^+\nu) \tag{6.35}$$

The corresponding $\mathcal{B}(B^+ \to \bar{D}^0\pi^0\ell^+\nu)$, $\mathcal{B}(B^+ \to \bar{D}^{*0}\pi^0\ell^+\nu)$ and B^0 branching fractions can be obtained by isospin symmetry. For example

$$\begin{aligned}\mathcal{B}(B^+ \to \bar{D}^{*0}\pi^0\ell^+\nu) &= \mathcal{B}(B^+ \to D^{*-}\pi^+\ell^+\nu)/2 \\ \mathcal{B}(B^0 \to D_1^-\ell^+\nu) &= \mathcal{B}(B^+ \to \bar{D}_1^0\ell^+\nu)/t_{+0}\end{aligned} \tag{6.36}$$

where $t_{+0} \equiv \tau_{B^+}/\tau_{B^0}$ is the lifetime ratio of B^+ and B^0.

This parameterization allows us to fit for $\mathcal{B}(B^+ \to D^{(*)}\pi\ell\nu)$. However, this branching fraction is eventually held fixed due to large systematic uncertainties from

$B^+ \to D^{(*)}\pi\pi\ell\nu$ and backgrounds.

6.8 FF parameter fitting technique

6.8.1 $B \to D\ell\nu$ slope fitting

As explained in section 4.3, we create additional histograms to fit for $B \to D\ell\nu$ slope. We may rewrite the weight (Equation (5.20))

$$W^{MC}(w) = \left[(1-10z^2+84z^3)\frac{[h_+(1)]^2}{[Rf_+]^2} - \frac{2(1-10z^2+84z^3)(8z-51z^2+252z^3)[h_+(1)]^2}{[Rf_+]^2}\rho_D^2 + \frac{(8z-51z^2+252z^3)^2[h_+(1)]^2}{[Rf_+]^2}\left(\rho_D^2\right)^2\right] R_N \quad (6.37)$$

Hence, if we define three weights $W^0(w)$, $W^1(w)$ and $W^2(w)$ by

$$W^{MC}(w) \equiv \left[W^0(w) - W^1(w)\rho_D^2 + W^2(w)\left(\rho_D^2\right)^2\right] R_N \quad (6.38)$$

then, the number of events is given by

$$N_{ij}^{MC} = \left[\sum_l \left(r_l^{Lumi}\sum_k r_k^{Trk} r_k^{KPID} r_k^{LPID} W_{jk}^0\right) - \sum_l \left(r_l^{Lumi}\sum_k r_k^{Trk} r_k^{KPID} r_k^{LPID} W_{jk}^1\right)\rho_D^2 + \sum_l \left(r_l^{Lumi}\sum_k r_k^{Trk} r_k^{KPID} r_k^{LPID} W_{jk}^2\right)\left(\rho_D^2\right)^2\right] R_N \quad (6.39)$$

Here the sum of k is taken over peak and sideband separately and sideband is subtracted. This can be expressed by

$$N_{ij}^{MC} \equiv \left[N_{ij}^0 - N_{ij}^1\rho_D^2 + N_{ij}^2\left(\rho_D^2\right)^2\right] R_N \quad (6.40)$$

Instead of using $B \to D\ell\nu$ histogram N_{ij}^{MC}, we can use these three histograms, N_{ij}^{0}, N_{ij}^{1} and N_{ij}^{2}, in our fit. Then we do not have to re-create histograms during the fitting process. We can create the $B \to D\ell\nu$ histogram with a new slope ρ_D^2 from the three existing histograms N_{ij}^{0}, N_{ij}^{1} and N_{ij}^{2}.

6.8.2 Statistical uncertainty

Since our events are weighted, the variance is given by the sum of the squares of the weights.

$$\sum_k \left[W_k^{MC}(w)\right]^2 \tag{6.41}$$

Hence, by taking a square of Equation (6.38), we need 5 histograms to calculate the variance

$$\sigma^2 = \left[N_1 - N_2\rho_D^2 + N_3\left(\rho_D^2\right)^2 - N_4\left(\rho_D^2\right)^3 + N_5\left(\rho_D^2\right)^4\right] R_N^2 \tag{6.42}$$

6.8.3 $B \to D^*\ell\nu$ parameter fitting

A similar method can be adopted for $B \to D^*\ell\nu$ decay FF parameter fitting. Since we have three parameters ρ^2, R_1 and R_2, we need 18 histograms for the $B \to D^*\ell\nu$ distribution and 75 histograms to calculate its statistical uncertainty.

Chapter 7

Validation of the fitting method

We validate our fit as described in the following sections. $B\bar{B}$ MC was used for the validation. We fit electron and muon samples separately because they have different systematic uncertainties (see chapter 9). Since the electron sample has higher statistics and smaller PID uncertainties, we use only electrons for this validation study. As can be seen in chapter 10, the two samples give compatible results.

7.1 Fit configuration for validation study

Before starting the full validation study using MC, we performed a variety of test fits to data to determine the fit configurations which give us an acceptable χ^2 and good stability against changes of input parameters. We tried to determine which parameters should be held fixed, what constraints needed to be imposed and so on. Based on test fits, we picked up the following configuration to do full validation study : we fit four form factor parameters

- $B \to D\ell\nu$ decay FF slope : ρ_D^2
- $B \to D^*\ell\nu$ decay FF slope : ρ^2
- $B \to D^*\ell\nu$ decay FF ratio : R_1
- $B \to D^*\ell\nu$ decay FF ratio : R_2

and two branching fractions

- $\mathcal{B}(B^+ \to \bar{D}^0 \ell^+ \nu)$
- $\mathcal{B}(B^+ \to \bar{D}^{*0} \ell^+ \nu)$

with isospin constraints on B decays. Input parameters are

$$\begin{aligned}
&\mathcal{B}(B^+ \to \bar{D}^{(*)} \pi \ell^+ \nu) = 0.0158 \\
&f_{D_2^*/D_1} = 0.66 \\
&f_{D_0^* D\pi / D_1 D_2^*} = 0.87 \\
&f_{D_1' D^*\pi / D_1 D_2^*} = 0.67 \\
&f_{D\pi / D_0^*} = 0.19 \\
&f_{D^*\pi / D_1'} = 0.06 \\
&\mathcal{B}(B^+ \to \bar{D}^{(*)} \pi\pi \ell^+ \nu) = 0.011 \\
&f_{+0} = 1.065 \\
&t_{+0} = 1.071
\end{aligned} \tag{7.1}$$

7.2 Toy MC study

7.2.1 Method of toy MC study

To validate our fitting method, we perform a toy MC study. The following procedure is used :

1. Construct fake OnPeak - OffPeak data using fully simulated $B\bar{B}$ MC, with input values as shown in Table 7.1.
2. Fluctuate the population of each bin of the fake data using Gaussian random numbers based on the statistical uncertainty of the bin.
3. Fit the fluctuated fake data.

Parameters	Set a	Set b	Set c
ρ_D^2	1.17	1.3	1.17
ρ^2	1.191	1.3	1.191
R_1	1.429	1.6	1.429
R_2	0.827	0.6	0.827
$\mathcal{B}(B^+ \to D^0 \ell^+ \nu)$	0.0233	0.0233	0.025
$\mathcal{B}(B^+ \to \bar{D}^{*0} \ell^+ \nu)$	0.0583	0.0583	0.056

Table 7.1: [**Parameters of fake data**] The parameter values used to create fake data. Set b has different FF parameters than set a and set c has different BF values.

4. Iterate steps 2 and 3 approximately 1,000 times.

5. Plot the pull distributions of the 1,000 fits and record the mean and standard deviation of each distribution.

In Table 7.1, three sets of input parameters are listed; set b has different FF parameters than set a, and set c has different B decay BF values. We perform 1,000 toy fits each for each parameter set.

7.2.2 Pull results

Pulls are calculated by

$$\text{pull} = \frac{\text{fitted value} - \text{true value}}{\text{fitted uncertainty}} \tag{7.2}$$

The mean and standard deviation (r.m.s.) for each pull distribution are listed in Table 7.2. At the bottom line of the Table the statistical uncertainty on the mean and standard deviation are listed. The uncertainty on the mean is given by

$$\frac{\sigma}{\sqrt{N}} = \frac{1}{\sqrt{1000}} = 0.0316 \tag{7.3}$$

Parameters	Set a		Set b		Set c	
	Mean	r.m.s.	Mean	r.m.s.	Mean	r.m.s.
ρ_D^2	+0.0253	1.014	-0.0112	1.017	+0.0329	1.016
ρ^2	-0.0755	1.028	-0.0195	1.017	-0.0671	1.023
R_1	+0.0303	0.993	-0.1166	0.996	+0.0366	0.995
R_2	+0.1079	1.005	+0.0234	0.997	+0.0998	1.004
$\mathcal{B}(B^+ \to \bar{D}^0 \ell^+ \nu)$	+0.1477	1.000	+0.1378	1.000	+0.1608	1.006
$\mathcal{B}(B^+ \to \bar{D}^{*0} \ell^+ \nu)$	-0.0940	0.977	-0.0263	1.012	-0.1030	1.017
Uncertainty	0.0316	0.0224	0.0316	0.0224	0.0316	0.0224

Table 7.2: [**Toy MC pulls : Mean and Standard Deviation**] Mean and standard deviation (r.m.s.) of pull distributions of toy MC. The uncertainty on mean and standard deviation are also listed in the bottom line. Pulls are calculated from the difference to input values.

and the uncertainty on the standard deviation is calculated by

$$\frac{\sigma}{\sqrt{2N}} = \frac{1}{\sqrt{2 \times 1000}} = 0.0224 \tag{7.4}$$

The χ^2 and the pull distributions are shown in Figures 7.1 and 7.2 only for the parameter Set a. Results show very small biases. We do not correct for these because they are negligible in comparison with the total uncertainties on these quantities.

7.3 Validation fits using fully simulated MC

7.3.1 Validation fit method

For another validation of our fitting method, we split the MC into two halves. We use one half to construct fake data. We then create component histograms from the other half, and fit the fake data using the component histograms. Again, we use the three different parameter sets given in Table 7.1 to create fake data. We split the MC four different ways

- Split A : Separate even number events and odd number events.

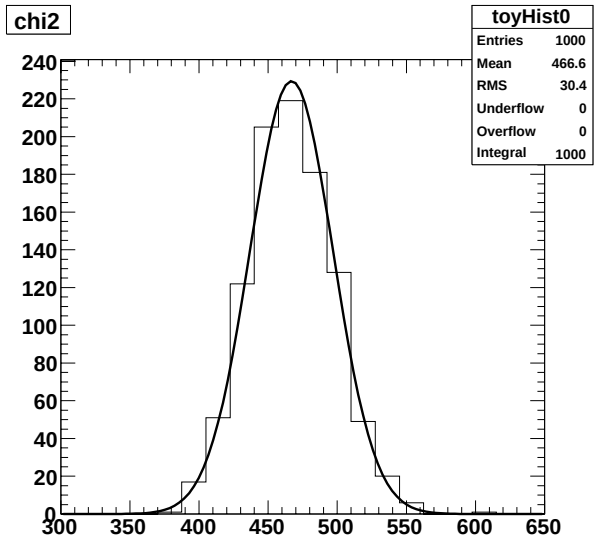

Figure 7.1: [**Toy MC χ^2 (Set a)**] Toy MC χ^2 for parameter set a. The number of degrees of freedom is 468.

- Splits B, C and D : Separate events using three independent sets of random numbers.

7.3.2 Validation fit results

Fit results are given in Tables 7.3 - 7.5. For each fit, we calculate pulls as defined in Equation (7.2). We also calculate an overall χ^2 between the input and fitted parameter values, namely

$$\chi^2_{Val} = (\Delta_1, \Delta_2, ..., \Delta_k) \begin{pmatrix} \text{Inverse} \\ \text{covariance} \\ \text{matrix} \end{pmatrix} \begin{pmatrix} \Delta_1 \\ \Delta_2 \\ . \\ . \\ . \\ \Delta_k \end{pmatrix} \tag{7.5}$$

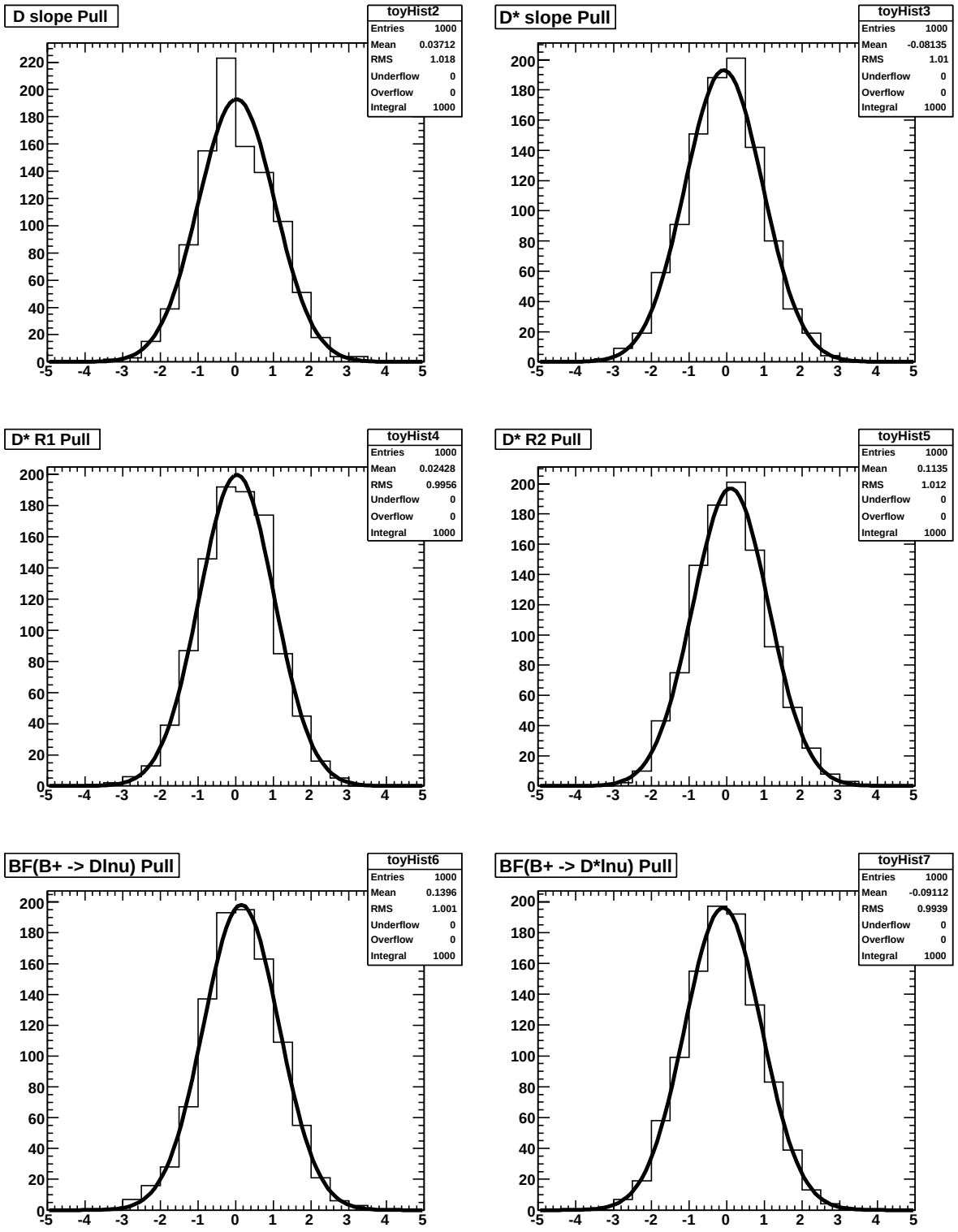

Figure 7.2: [**Toy MC Pulls (Set a)**] Toy MC pull distributions for parameter Set a. Pulls are plotted from top left to bottom right for ρ_D^2, ρ^2, R_1, R_2, $\mathcal{B}(B^+ \to \bar{D}^0 \ell^+ \nu)$ and $\mathcal{B}(B^+ \to \bar{D}^{*0} \ell^+ \nu)$.

where Δ_i is the difference between fitted and input values of i-th parameter :

$$\Delta_i = \text{fitted value} - \text{true value} \tag{7.6}$$

The results do not show any significant bias.

	Input	Split A		Split B		Split C		Split D	
	(Set a)	fit result	pulls	fit result	pulls	fit result	pulls	fit result	pulls
ρ_D^2	1.17	1.107 ± 0.036	-1.77	1.149 ± 0.034	-0.63	1.154 ± 0.034	-0.46	1.115 ± 00035	-1.58
ρ^2	1.191	1.238 ± 0.032	+1.47	1.203 ± 0.032	+0.38	1.154 ± 0.032	-1.16	1.222 ± 0.030	+1.02
R_1	1.429	1.476 ± 0.047	+1.02	1.405 ± 0.043	-0.54	1.382 ± 0.041	-1.15	1.412 ± 0.042	-0.39
R_2	0827	0.754 ± 0.038	-1.93	0.829 ± 0.036	+0.05	0.852 ± 0.034	+0.74	0.836 ± 0.034	+0.27
$\mathcal{B}(B^+ \to D^0 \ell^+ \nu)$	0.0233	0.02304 ± 0.00024	-1.10	0.02338 ± 0.00024	+0.33	0.02316 ± 0.00024	-0.57	0.02334 ± 0.00024	+0.15
$\mathcal{B}(B^+ \to \bar{D}^{*0} \ell^+ \nu)$	0.0583	0.05885 ± 0.00034	+1.62	0.05819 ± 0.00034	-0.31	0.05854 ± 0.00034	+0.17	0.05806 ± 0.00034	-0.71
χ^2/ndof (P-value)		466/456 (0.36)		498/458 (0.10)		437/459 (0.76)		498/457 (0.09)	
χ^2_{Val}			7.4		4.8		3.1		12.1

Table 7.3: [**MC vs MC (Parameter set a)**] Validation fit results using parameter set a.

	Input	Split A		Split B		Split C		Split D	
	(Set b)	fit result	pulls	fit result	pulls	fit result	pulls	fit result	pulls
ρ_D^2	1.3	1.243 ± 0.031	-1.83	1.278 ± 0.034	-0.76	1.289 ± 0.029	-0.38	1.253 ± 0.030	-1.56
ρ^2	1.3	1.363 ± 0.034	+1.84	1.320 ± 0.034	+0.60	1.267 ± 0.032	-1.00	1.328 ± 0.032	+0.87
R_1	1.6	1.674 ± 0.059	+1.26	1.587 ± 0.055	-0.23	1.546 ± 0.050	-1.07	1.580 ± 0.051	-0.40
R_2	0.6	0.501 ± 0.048	-2.09	0.589 ± 0.044	-0.24	0.628 ± 0.041	+0.69	0.610 ± 0.042	+0.25
$\mathcal{B}(B^+ \to D^0 \ell^+ \nu)$	0.0233	0.02305 ± 0.00024	-1.05	0.02336 ± 0.00024	+0.29	0.02316 ± 0.00024	-0.58	0.02333 ± 0.00024	+0.14
$\mathcal{B}(B^+ \to \bar{D}^{*0} \ell^+ \nu)$	0.0583	0.05881 ± 0.00033	+1.55	0.05820 ± 0.00033	-0.29	0.05836 ± 0.00033	+0.19	0.05804 ± 0.00034	-0.76
χ^2/ndof (P-value)		464/456 (0.39)		504/458 (0.07)		443/459 (0.70)		498/457 (0.09)	
χ^2_{Val}			7.9		4.9		2.8		11.9

Table 7.4: [**MC vs MC (Parameter set b)**] Validation fit results using parameter set b.

	Input	Split A		Split B		Split C		Split D	
	(Set c)	fit result	pulls	fit result	pulls	fit result	pulls	fit result	pulls
ρ_D^2	1.17	1.110 ± 0.033	-1.80	1.149 ± 0.032	-0.68	1.156 ± 0.032	-0.46	1.119 ± 0.033	-1.56
ρ^2	1.191	1.241 ± 0.033	+1.49	1.203 ± 0.033	+0.37	1.151 ± 0.033	-1.22	1.222 ± 0.031	+0.99
R_1	1.429	1.477 ± 0.049	+0.99	1.405 ± 0.045	-0.53	1.378 ± 0.043	-1.19	1.412 ± 0.044	-0.38
R_2	0827	0.752 ± 0.039	-1.92	0.830 ± 0.037	+0.07	0.855 ± 0.035	+0.79	0.837 ± 0.035	+0.28
$\mathcal{B}(B^+ \to \bar{D}^0 \ell^+ \nu)$	0.025	0.02474 ± 0.00024	-1.08	0.02508 ± 0.00024	+0.32	0.02486 ± 0.00024	-0.59	0.02503 ± 0.00024	+0.13
$\mathcal{B}(B^+ \to \bar{D}^{*0} \ell^+ \nu)$	0.056	0.05655 ± 0.00034	+1.65	0.05589 ± 0.00034	-0.34	0.05605 ± 0.00034	+0.13	0.05576 ± 0.00034	-0.71
χ^2/ndof (P-value)		469/458 (0.35)		495/460 (0.13)		438/459 (0.75)		498/457 (0.09)	
χ^2_{Val}			7.5		5.0		3.3		11.8

Table 7.5: [**MC vs MC (Parameter set c)**] Validation fit results using parameter set c.

parameter	fit result
ρ_D^2	1.240 ± 0.049
ρ^2	1.300 ± 0.052
R_1	1.530 ± 0.084
R_2	0.730 ± 0.067
$\mathcal{B}(D^0\ell^+\nu)(\%)$	2.399 ± 0.037
$\mathcal{B}(\bar{D}^{*0}\ell^+\nu)(\%)$	5.444 ± 0.049
χ^2/ndof (P-value)	422/468 (0.94)

Table 7.6: [**Test fit results**] Test fit results on the electron sample.

7.4 Cross Checks

We fit data with the configuration given in section 7.1. The results are given in Table 7.6. Based on these fit results we perform the following cross check fits to data as a further validation of the fit. In cross check fits, as an indication of agreement to test fit results, we calculate normalized residuals (NR) for each variable

$$\mathrm{NR} = \frac{(\text{Cross check fit value}) - (\text{Test fit value})}{\sigma_{\text{CrossCheck}}} \tag{7.7}$$

7.4.1 Binning

We change the binning and see how the fit results change. The nominal binning is given in section 6.2.

For alternative lepton momentum binning :

- p_ℓ^* Binning 1

  (10 bins (GeV)) : 1.2, 1.35, 1.45, 1.55, 1.65, 1.75, 1.85, 1.95, 2.05, 2.15, 2.35)

- p_ℓ^* Binning 2

  (5 bins (GeV)) : 1.2, 1.4, 1.6, 1.8, 2.0, 2.35

D momentum binning :

- p^*_D Binning 1

  (9 bins (GeV)) : 0.8, 1.05, 1.3, 1.45, 1.6, 1.75, 1.9, 2.05, 2.2, 2.45

- p^*_D Binning 2

  (4 bins (GeV)) : 0.8, 1.2, 1.6, 2.0, 2.45

and $\cos\theta_{B-Dl}$ binning :

- $\cos\theta_{B-Dl}$ Binning 1 (3 bins) : -2, -0.5, 0.5, 1.1

- $\cos\theta_{B-Dl}$ Binning 2 (2 bins) : -2, 0, 1.1

Results are given in Tables 7.7-7.9. The results are consistent with the test fit.

7.4.2 Minimum entries per bin

We change the requirement on the minimum entries per bin to 25, 50, 75 and 100. In nominal fit it is set to 10. Results are shown in Tables 7.10 and 7.11. The results show good agreement with the test fit. When we change the requirement, the number of bins going into χ^2 changes as follows

- Minimum entry per bin > 10 : number of bins going into $\chi^2 = 475$

- Minimum entry per bin > 25 : number of bins going into $\chi^2 = 464$

- Minimum entry per bin > 50 : number of bins going into $\chi^2 = 449$

- Minimum entry per bin > 75 : number of bins going into $\chi^2 = 446$

- Minimum entry per bin > 100 : number of bins going into $\chi^2 = 439$

7.4.3 D mass peak region

We take a wider or narrower D mass peak region by adding or subtracting 2 MeV at both ends of the region. The results in Table 7.12 show good agreement with the test fit.

p_ℓ^* binning	binning 1		binning 2	
	Fit result	NR	Fit result	NR
ρ_D^2	1.230 ± 0.049	-0.20	1.241 ± 0.049	+0.02
ρ^2	1.307 ± 0.052	+0.14	1.318 ± 0.054	+0.34
R_1	1.526 ± 0.082	-0.05	1.539 ± 0.086	+0.11
R_2	0.693 ± 0.067	-0.16	0.678 ± 0.070	-0.36
$\mathcal{B}(B^+ \to \bar{D}^0 \ell^+ \nu)$	0.02396 ± 0.00037	-0.09	0.02397 ± 0.00037	-0.04
$\mathcal{B}(B^+ \to \bar{D}^{*0} \ell^+ \nu)$	0.05465 ± 0.00049	+0.41	0.05462 ± 0.00049	+0.36
χ^2/ndof (P-value)	469/453 (0.29)		237/241 (0.57)	

Table 7.7: [**Effect of p_ℓ^* binning**] Fit results with NR (Normalized Residual) for binning 1 (left) and binning 2 (right).

p_D^* binning	binning 1		binning 2	
	Fit result	NR	Fit result	NR
ρ_D^2	1.224 ± 0.049	-0.33	1.246 ± 0.051	+0.12
ρ^2	1.326 ± 0.051	+0.52	1.288 ± 0.057	-0.21
R_1	1.548 ± 0.083	+0.22	1.499 ± 0.088	-0.35
R_2	0.679 ± 0.066	-0.37	0.732 ± 0.073	+0.39
$\mathcal{B}(B^+ \to \bar{D}^0 \ell^+ \nu)$	0.02399 ± 0.00037	+0.01	0.02410 ± 0.00037	+0.30
$\mathcal{B}(B^+ \to \bar{D}^{*0} \ell^+ \nu)$	0.05457 ± 0.00049	+0.27	0.05434 ± 0.00050	-0.22
χ^2/ndof (P-value)	467/483 (0.69)		252/220 (0.07)	

Table 7.8: [**Effect of p_D^* binning**] Fit results with NR (Normalized Residual) for binning 1 (left) and binning 2 (right).

$\cos\theta_{B-Dl}$ binning	binning 1		binning 2	
	Fit result	NR	Fit result	NR
ρ_D^2	1.207 ± 0.051	-0.65	1.214 ± 0.052	-0.50
ρ^2	1.290 ± 0.051	-0.20	1.316 ± 0.053	+0.32
R_1	1.516 ± 0.077	-0.18	1.574 ± 0.087	+0.50
R_2	0.707 ± 0.063	+0.06	0.674 ± 0.070	-0.42
$\mathcal{B}(B^+ \to \bar{D}^0 \ell^+ \nu)$	0.02367 ± 0.00037	-0.85	0.02381 ± 0.00039	-0.46
$\mathcal{B}(B^+ \to \bar{D}^{*0} \ell^+ \nu)$	0.05482 ± 0.00047	+0.79	0.05453 ± 0.00050	+0.18
χ^2/ndof (P-value)	500/498 (0.47)		314/336 (0.81)	

Table 7.9: [**Effect of $\cos\theta_{B-Dl}$ binning**] Fit results with NR (Normalized Residual) for binning 1 (left) and binning 2 (right).

	> 25		> 50	
	Fit result	NR	Fit result	NR
ρ_D^2	1.240 ± 0.049	+0.01	1.238 ± 0.049	-0.04
ρ^2	1.299 ± 0.052	-0.01	1.292 ± 0.052	-0.14
R_1	1.529 ± 0.084	-0.01	1.519 ± 0.083	-0.14
R_2	0.704 ± 0.067	+0.01	0.712 ± 0.067	+0.13
$\mathcal{B}(B^+ \to \bar{D}^0 \ell^+ \nu)$	0.02399 ± 0.00037	-0.01	0.02398 ± 0.00037	-0.04
$\mathcal{B}(B^+ \to \bar{D}^{*0} \ell^+ \nu)$	0.05444 ± 0.00049	+0.00	0.05445 ± 0.00049	+0.01
χ^2/ndof (P-value)	415/457 (0.92)		402/442 (0.92)	

Table 7.10: [**Effect of minimum candidates per bin > 25 and 50**] Fit results with NR (Normalized Residual).

	> 75		> 100	
	Fit result	NR	Fit result	NR
ρ_D^2	1.238 ± 0.049	-0.05	1.243 ± 0.049	+0.06
ρ^2	1.294 ± 0.0520	-0.11	1.287 ± 0.053	-0.24
R_1	1.520 ± 0.083	-0.12	1.515 ± 0.083	-0.18
R_2	0.710 ± 0.067	+0.10	0.716 ± 0.066	+0.19
$\mathcal{B}(B^+ \to \bar{D}^0 \ell^+ \nu)$	0.02398 ± 0.00037	-0.03	0.02396 ± 0.00037	-0.07
$\mathcal{B}(B^+ \to \bar{D}^{*0} \ell^+ \nu)$	0.05446 ± 0.00049	+0.04	0.05444 ± 0.00049	-0.02
χ^2/ndof (P-value)	401/439 (0.90)		395/432 (0.90)	

Table 7.11: [**Effect of minimum candidates per bin > 75 and 100**] Fit results with NR (Normalized Residual).

	wider		narrower	
	Fit result	NR	Fit result	NR
ρ_D^2	1.201 ± 0.055	-0.71	1.230 ± 0.048	-0.20
ρ^2	1.320 ± 0.055	+0.37	1.310 ± 0.052	+0.20
R_1	1.562 ± 0.091	+0.35	1.553 ± 0.084	+0.28
R_2	0.664 ± 0.073	-0.54	0.670 ± 0.068	-0.49
$\mathcal{B}(B^+ \to \bar{D}^0 \ell^+ \nu)$	0.02392 ± 0.00040	-0.17	0.02389 ± 0.00035	-0.29
$\mathcal{B}(B^+ \to \bar{D}^{*0} \ell^+ \nu)$	0.05465 ± 0.00052	+0.40	0.05448 ± 0.00048	+0.07
χ^2/ndof (P-value)	446/468 (0.76)	1.01	462/468 (0.57)	1.21

Table 7.12: [D **mass peak region**] Fit results with NR (Normalized Residual).

Parameters	Run1-3 result	Run4 result	NR
ρ_D^2	1.174 ± 0.073	1.286 ± 0.066	+1.14
ρ^2	1.264 ± 0.070	1.328 ± 0.075	+0.62
R_1	1.488 ± 0.108	1.558 ± 0.123	+0.43
R_2	0.741 ± 0.087	0.676 ± 0.099	-0.50
$\mathcal{B}(B \to D\ell\nu)$	0.02364 ± 0.00051	0.02441 ± 0.00052	+1.05
$\mathcal{B}(B \to D^*\ell\nu)$	0.05495 ± 0.00068	0.05380 ± 0.00070	-1.18
χ^2/ndof (P-value)	427/457 (0.84)	487/458 (0.17)	4.6/6 (0.59)

Table 7.13: [**Run1-3 and Run4 fits**] Fit results with NR (Normalized Residual).

7.4.4 Run1-3 vs Run4

Our data were taken in 4 different running periods over the years 2000 to 2004 : Run1, Run2, Run3 and Run4. We compare the results with the data taken in earlier time (Run1-3) and later time (Run4). These two data sets have comparable statistics. The results are give in Table 7.13. The normalized residual (NR) in the Table is defined by

$$\mathrm{NR} = \frac{(\text{Run4 fitted value}) - (\text{Run1-3 fitted value})}{\sqrt{\sigma^2_{\text{Run4}} + \sigma^2_{\text{Run1-3}}}} \tag{7.8}$$

χ^2 for NR is defined by the sum of NR^2. Run1-3 and Run4 agree well.

Chapter 8

Fit results

We perform separate fits to the electron and muon samples. This allows the two samples to be combined in an optimal way when including both statistical and systematic errors. This is of the practical importance due to the differences in some systematic uncertainties such as PID efficiency and radiative corrections. We also fix R_1 and R_2. One reason is the precision of these parameters, including systematic uncertainties, is significantly poorer than the previous BaBar measurement [44]. Another reason is to facilitate the combination of results on branching fractions and form factor slopes with previous measurements, all of which are scaled to common values of R_1 and R_2.

8.1 Nominal fit configuration

In the nominal fit, we determine two form factor slopes

- $B \to D\ell\nu$ decay FF slope : ρ_D^2
- $B \to D^*\ell\nu$ decay FF slope : ρ^2

and two branching fractions

- $\mathcal{B}(B^+ \to \bar{D}^0\ell^+\nu)$
- $\mathcal{B}(B^+ \to \bar{D}^{*0}\ell^+\nu)$

Isospin symmetry is imposed on semileptonic B decays in the fit.

The input parameters are

$$
\begin{aligned}
&R_1 = 1.429 \pm 0.061 \pm 0.044 \\
&R_2 = 0.827 \pm 0.038 \pm 0.022 \\
&\mathcal{B}(B^+ \to \bar{D}^{(*)}\pi\ell^+\nu) = 0.0151 \pm 0.0015 \\
&f_{D_2^*/D_1} = 0.74 \pm 0.20 \\
&f_{D_0^* D\pi/D_1 D_2^*} = 0.87 \pm 0.43 \\
&f_{D_1' D^*\pi/D_1 D_2^*} = 0.68 \pm 0.25 \\
&f_{D\pi/D_0^*} = 0.21 \pm 0.21 \\
&f_{D^*\pi/D_1'} = 0.07 \pm 0.07 \\
&\mathcal{B}(B^+ \to \bar{D}^{(*)}\pi\pi\ell^+\nu) = 0.011 \pm 0.011 \\
&f_{+0} = 1.065 \pm 0.026 \\
&t_{+0} = 1.071 \pm 0.009
\end{aligned}
\tag{8.1}
$$

The R_1 and R_2 values are taken from a previous BaBar measurement [44]. f_{+0} and t_{+0} values are adopted from the PDG [10]. $\mathcal{B}(B^+ \to \bar{D}^{(*)}\pi\ell^+\nu)$ is given also from PDG [10] with isospin constraints. Calculations of other input parameters are explained in the following sub-section.

8.1.1 Calculation of input parameters

In this sub-section, we explain the calculation of some of the input parameters listed above.

$B \to D^{**}\ell\nu$ decay branching fractions

From HFAG [36]

$$
\begin{aligned}
&\mathcal{B}(B^+ \to \bar{D}_1^0\ell^+\nu)\mathcal{B}(D_1^0 \to D^{*+}\pi^-) = 0.0024 \pm 0.0004 \\
&\mathcal{B}(B^+ \to \bar{D}_2^{*0}\ell^+\nu)\mathcal{B}(D_2^{*0} \to D^{*+}\pi^-) = 0.0009 \pm 0.00025
\end{aligned}
\tag{8.2}
$$

BaBar measures [47]

$$\begin{aligned}
&\mathcal{B}(B^+ \to \bar{D}_1^0 \ell^+ \nu)\mathcal{B}(D_1^0 \to D^{*+}\pi^-) = 0.00297 \pm 0.00017 \pm 0.00017 \\
&\mathcal{B}(B^+ \to \bar{D}_2^{*0} \ell^+ \nu)\mathcal{B}(D_2^{*0} \to D^{(*)+}\pi^-) = 0.00229 \pm 0.00023 \pm 0.00021 \\
&\mathcal{B}(B^0 \to D_1^- \ell^+ \nu)\mathcal{B}(D_1^- \to D^{*0}\pi^-) = 0.00278 \pm 0.00024 \pm 0.00025 \\
&\mathcal{B}(B^0 \to D_2^{*-} \ell^+ \nu)\mathcal{B}(D_2^{*-} \to D^{(*)0}\pi^-) = 0.00177 \pm 0.00026 \pm 0.00011
\end{aligned} \tag{8.3}$$

We take the isospin average of these results assuming maximum correlation between total errors. BaBar also measures [48]

$$\begin{aligned}
&\mathcal{B}(B^+ \to \bar{D}_1^0 \ell^+ \nu)\mathcal{B}(D_1^0 \to D^{*+}\pi^-) = 0.0029 \pm 0.0003 \pm 0.0003 \\
&\mathcal{B}(B^+ \to \bar{D}_2^{*0} \ell^+ \nu)\mathcal{B}(D_2^{*0} \to D^{+}\pi^-) = 0.0012 \pm 0.0002 \pm 0.0001 \\
&\mathcal{B}(B^+ \to \bar{D}_1^{\prime 0} \ell^+ \nu)\mathcal{B}(D_1^{\prime 0} \to D^{*+}\pi^-) = 0.0030 \pm 0.0003 \pm 0.0004 \\
&\mathcal{B}(B^+ \to \bar{D}_0^{*0} \ell^+ \nu)\mathcal{B}(D_0^{*0} \to D^{+}\pi^-) = 0.0032 \pm 0.0004 \pm 0.0004
\end{aligned} \tag{8.4}$$

Using $f_{D_2^*}$ given in Equation (5.6), we combine the results given in the previous three equations to obtain

$$\begin{aligned}
&\mathcal{B}(B^+ \to \bar{D}_1^0 \ell^+ \nu) = 0.0042 \pm 0.00044 \\
&\mathcal{B}(B^+ \to \bar{D}_2^{*0} \ell^+ \nu) = 0.0031 \pm 0.0005 \\
&\mathcal{B}(B^+ \to \bar{D}_1^{\prime 0} \ell^+ \nu) = 0.0045 \pm 0.00075 \\
&\mathcal{B}(B^+ \to \bar{D}_0^{*0} \ell^+ \nu) = 0.0048 \pm 0.00085
\end{aligned} \tag{8.5}$$

The sum of these 4 branching fractions is

$$\mathcal{B}(B^+ \to \bar{D}^{**0} \ell^+ \nu) = 0.0166 \pm 0.0022 \tag{8.6}$$

Non-resonant $B \to D^{(*)}\pi\ell\nu$ decay branching fractions

The comparison of Equation (8.6) with the $B \to D^{(*)}\pi\ell\nu$ BF quoted in Equation (8.1) provides an estimate of the non-resonant $\mathcal{B}^{NR}(B^+ \to \bar{D}^{(*)}\pi\ell^+\nu)$ component :

$$\mathcal{B}(B^+ \to D^{(*)}\pi\ell^+\nu) - \mathcal{B}(B^+ \to \bar{D}^{**0}\ell^+\nu) = -0.0020 \pm 0.0043 \tag{8.7}$$

The non-resonant branching fractions have never been measured. The values usually assumed in BaBar are

$$\begin{aligned}
&\mathcal{B}^{NR}(B^+ \to D^-\pi^+\ell^+\nu) = 0.0040 \pm 0.0024 \\
&\mathcal{B}^{NR}(B^+ \to \bar{D}^0\pi^0\ell^+\nu) = 0.0020 \pm 0.0012 \\
&\mathcal{B}^{NR}(B^+ \to D^{*-}\pi^+\ell^+\nu) = 0.0012 \pm 0.0008 \\
&\mathcal{B}^{NR}(B^+ \to \bar{D}^{*0}\pi^0\ell^+\nu) = 0.0006 \pm 0.0004
\end{aligned} \tag{8.8}$$

However these sum to 0.0078. Thus we shrink them keeping the same D^*/D ratio

$$\begin{aligned}
&\mathcal{B}^{NR}(B^+ \to D^-\pi^+\ell^+\nu) = 0.0010 \pm 0.0010 \\
&\mathcal{B}^{NR}(B^+ \to \bar{D}^0\pi^0\ell^+\nu) = 0.0005 \pm 0.0005 \\
&\mathcal{B}^{NR}(B^+ \to D^{*-}\pi^+\ell^+\nu) = 0.0003 \pm 0.0003 \\
&\mathcal{B}^{NR}(B^+ \to \bar{D}^{*0}\pi^0\ell^+\nu) = 0.00015 \pm 0.00015
\end{aligned} \tag{8.9}$$

We assign 100 % uncertainties since these branching fractions have never been measured. We vary the D^*/D ratio when evaluating systematic errors.

Branching fraction ratios

We calculate the branching fraction ratios, discussed in section 6.7, by assuming the errors on the branching fractions given above are 100 % correlated. Results are given in Equation (8.1)

$B \to D^{(*)}\pi\pi\ell\nu$ decay branching fraction

From the PDG [10], the inclusive semileptonic BF is

$$\mathcal{B}(B^+ \to X_c\ell^+\nu) = 0.108 \pm 0.004 \tag{8.10}$$

BaBar measure [11]

$$\begin{aligned}
\mathcal{B}(B^+ \to \bar{D}^0\ell^+\nu) &= 0.0233 \pm 0.0009 \pm 0.0009 \\
\mathcal{B}(B^+ \to \bar{D}^{*0}\ell^+\nu) &= 0.0583 \pm 0.0015 \pm 0.0030 \\
\mathcal{B}(B^+ \to D^{(*)}\pi\ell^+\nu) &= 0.0152 \pm 0.0012 \pm 0.0010
\end{aligned} \tag{8.11}$$

Thus 0.108 - 0.0233 - 0.0583 - 0.0152 = 0.0112 is missing. We set

$$\mathcal{B}(B^+ \to D^{(*)}\pi\pi\ell^+\nu) = 0.011 \pm 0.011 \tag{8.12}$$

As we assign 100 % uncertainty, this covers systematic uncertainty from this unmeasured decay BF.

8.2 Fit results

The fit results are shown in Table 8.1. The fits to the electron and muon samples both give good χ^2 probabilities. The comparison of the parameter values from the two fits is made in chapter 10 after systematic uncertainties are considered. Correlations are given in Table 8.2. There are no dangerously large correlations. Projection plots onto the lepton momentum, D momentum and $\cos\theta_{B-Dl}$ after fitting are given in Figures 8.1 - 8.3. The ratio plots show good agreement between data and fit results. Figure 8.4 shows all bins for the electron sample. The binning is given in section 6.2.

Parameters	Electron fit	Muon fit
ρ^2_D	1.259 ± 0.046	1.155 ± 0.063
$\rho^2_{D^*}$	1.219 ± 0.025	1.229 ± 0.029
$\mathcal{B}(\bar{D}^0\ell^+\nu)(\%)$	2.411 ± 0.033	2.285 ± 0.038
$\mathcal{B}(\bar{D}^{*0}\ell^+\nu)(\%)$	5.417 ± 0.033	5.227 ± 0.037
χ^2/ndof (P-value)	424/470 (0.94)	496/466 (0.16)

Table 8.1: [**Nominal fit results**] Fit results on the electron and muon samples.

	Electron sample				Muon sample			
	ρ^2_D	$\rho^2_{D^*}$	$\mathcal{B}(D)$	$\mathcal{B}(D^*)$	ρ^2_D	$\rho^2_{D^*}$	$\mathcal{B}(D)$	$\mathcal{B}(D^*)$
ρ^2_D	1				1			
$\rho^2_{D^*}$	-0.304	1			-0.308	1		
$\mathcal{B}(D)$	$+0.303$	$+0.177$	1		$+0.274$	$+0.195$	1	
$\mathcal{B}(D^*)$	-0.386	$+0.077$	-0.527	1	-0.394	$+0.073$	-0.519	1

Table 8.2: [**Statistical correlation coefficients**] Correlations between parameters.

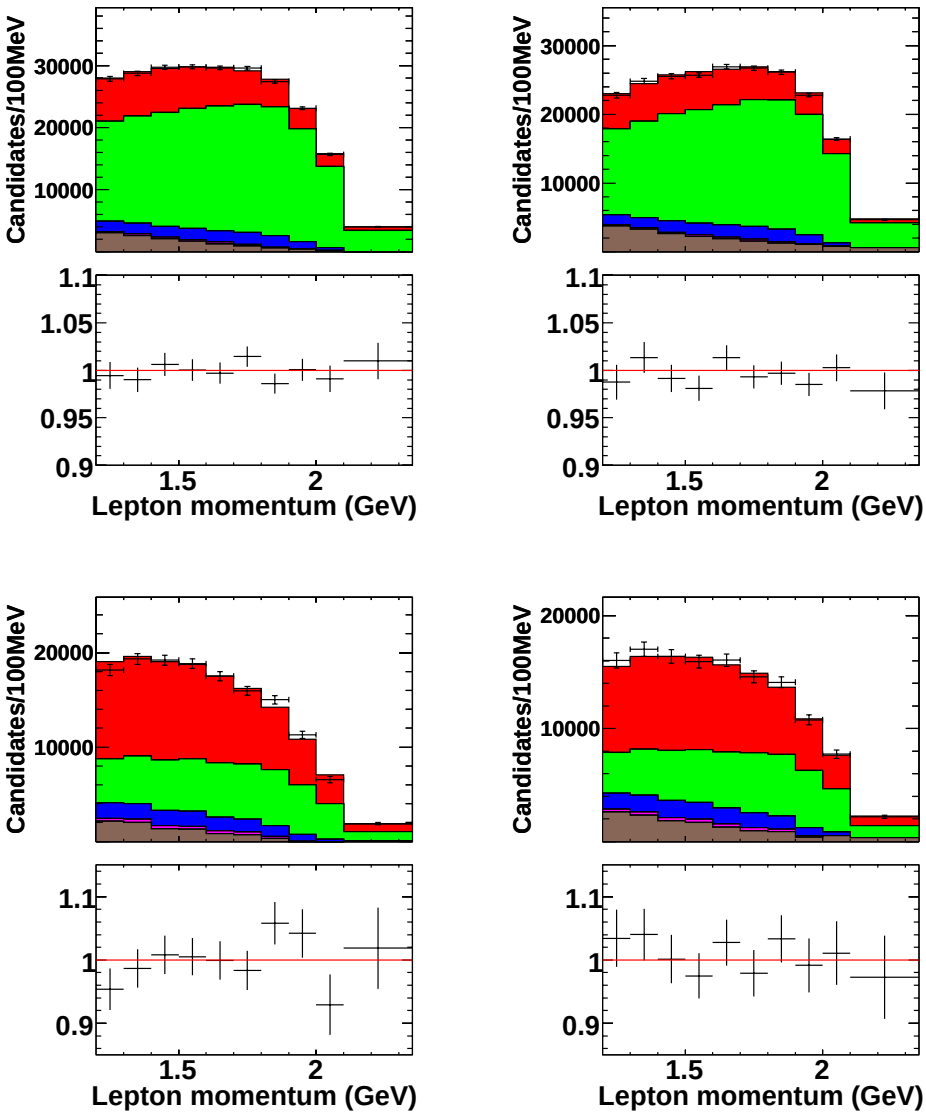

Figure 8.1: [p_ℓ **(Nominal fit)**] Data and fit results onto the lepton momentum. The left column is for the electron sample and the right column is for the muon sample. The top row is $D^0\ell$ and the bottom row is $D^+\ell$. Black points are OnPeak - OffPeak data. The red histogram is $B \to D\ell\nu$, green is $B \to D^*\ell\nu$, blue is $B \to D^{(*)}\pi\ell\nu$, magenta is $B \to D^{(*)}\pi\pi\ell\nu$, and brown is background.

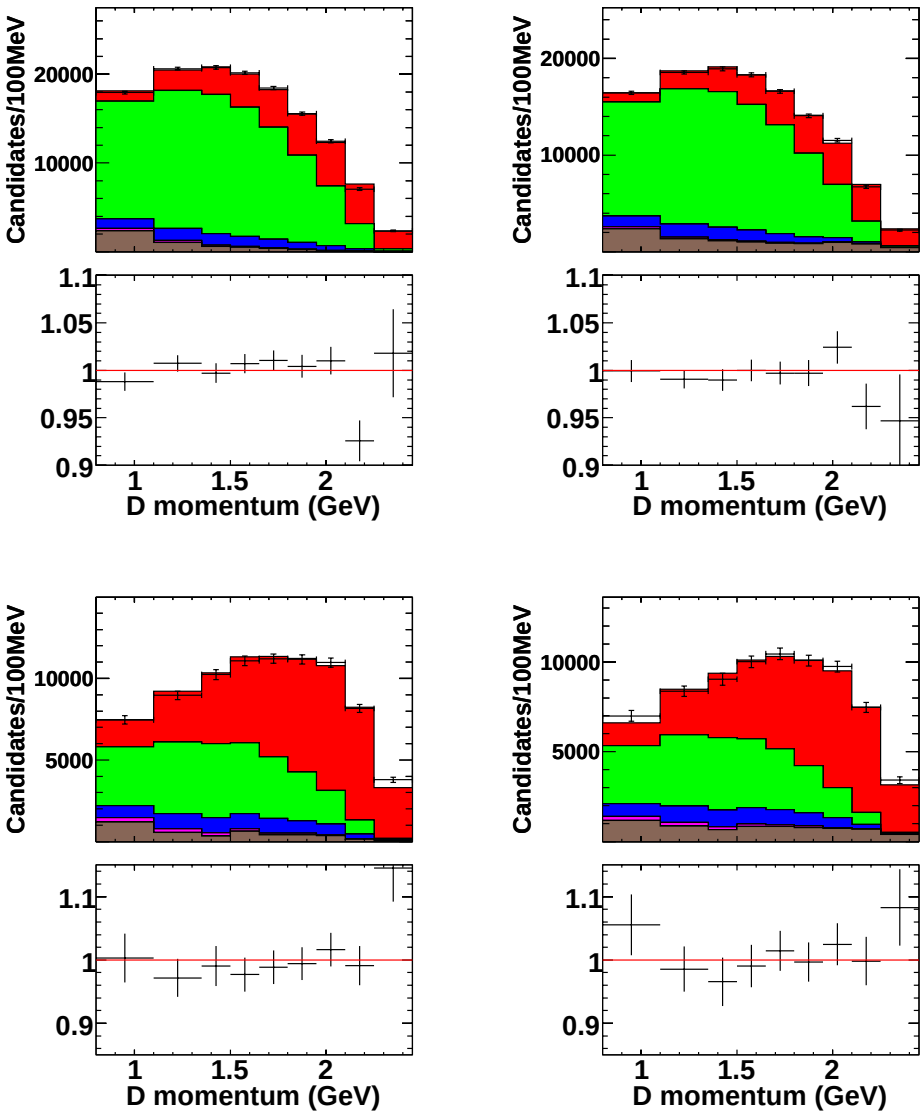

Figure 8.2: [p_D **(Nominal fit)**] Data and fit results onto the D momentum. The left column is for the electron sample and the right column is for the muon sample. The top row is $D^0\ell$ and the bottom row is $D^+\ell$. Black points are OnPeak - OffPeak data. The red histogram is $B \to D\ell\nu$, green is $B \to D^*\ell\nu$, blue is $B \to D^{(*)}\pi\ell\nu$, magenta is $B \to D^{(*)}\pi\pi\ell\nu$, and brown is background.

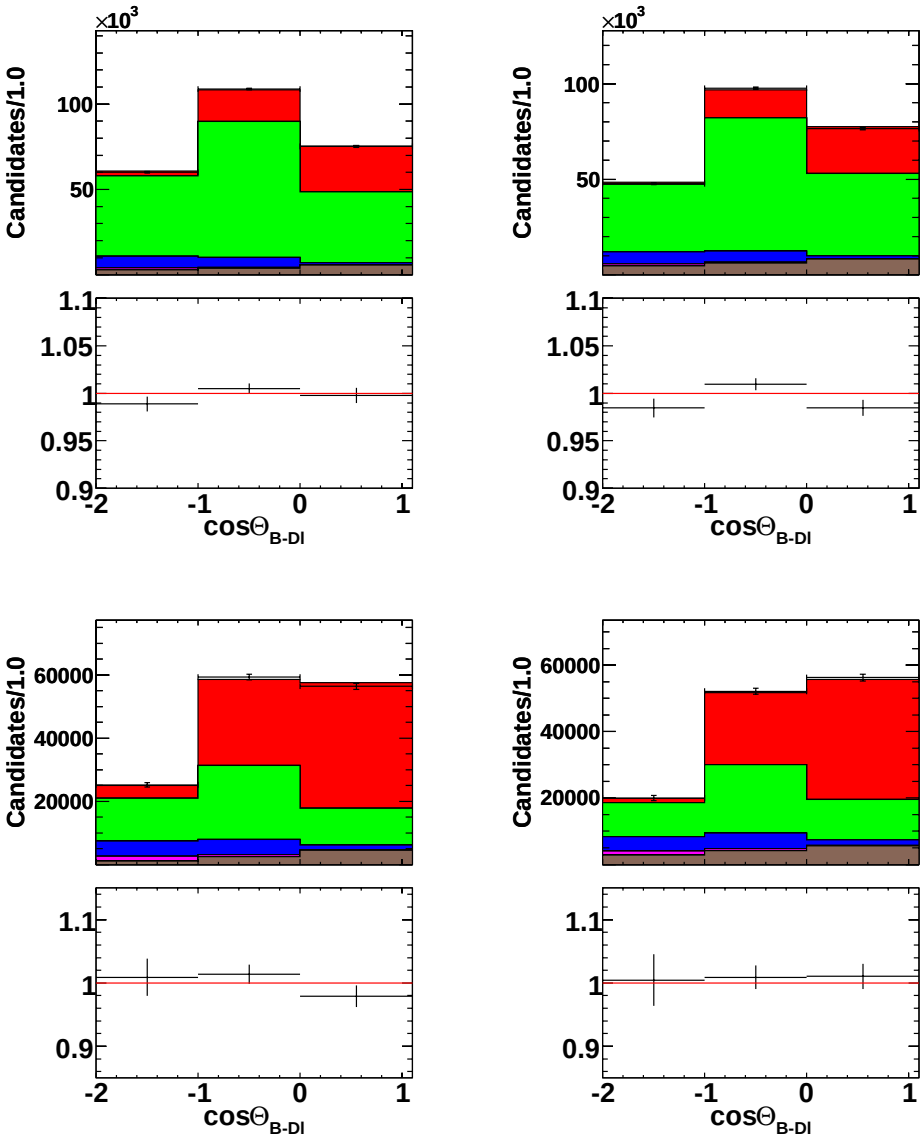

Figure 8.3: [$\cos\theta_{B-Dl}$ **(Nominal fit)**] Data and fit results onto the $\cos\theta_{B-Dl}$. The left column is for the electron sample and the right column is for the muon sample. The top row is $D^0\ell$ and the bottom row is $D^+\ell$. Black points are OnPeak - OffPeak data. The red histogram is $B \to D\ell\nu$, green is $B \to D^*\ell\nu$, blue is $B \to D^{(*)}\pi\ell\nu$, magenta is $B \to D^{(*)}\pi\pi\ell\nu$, and brown is background.

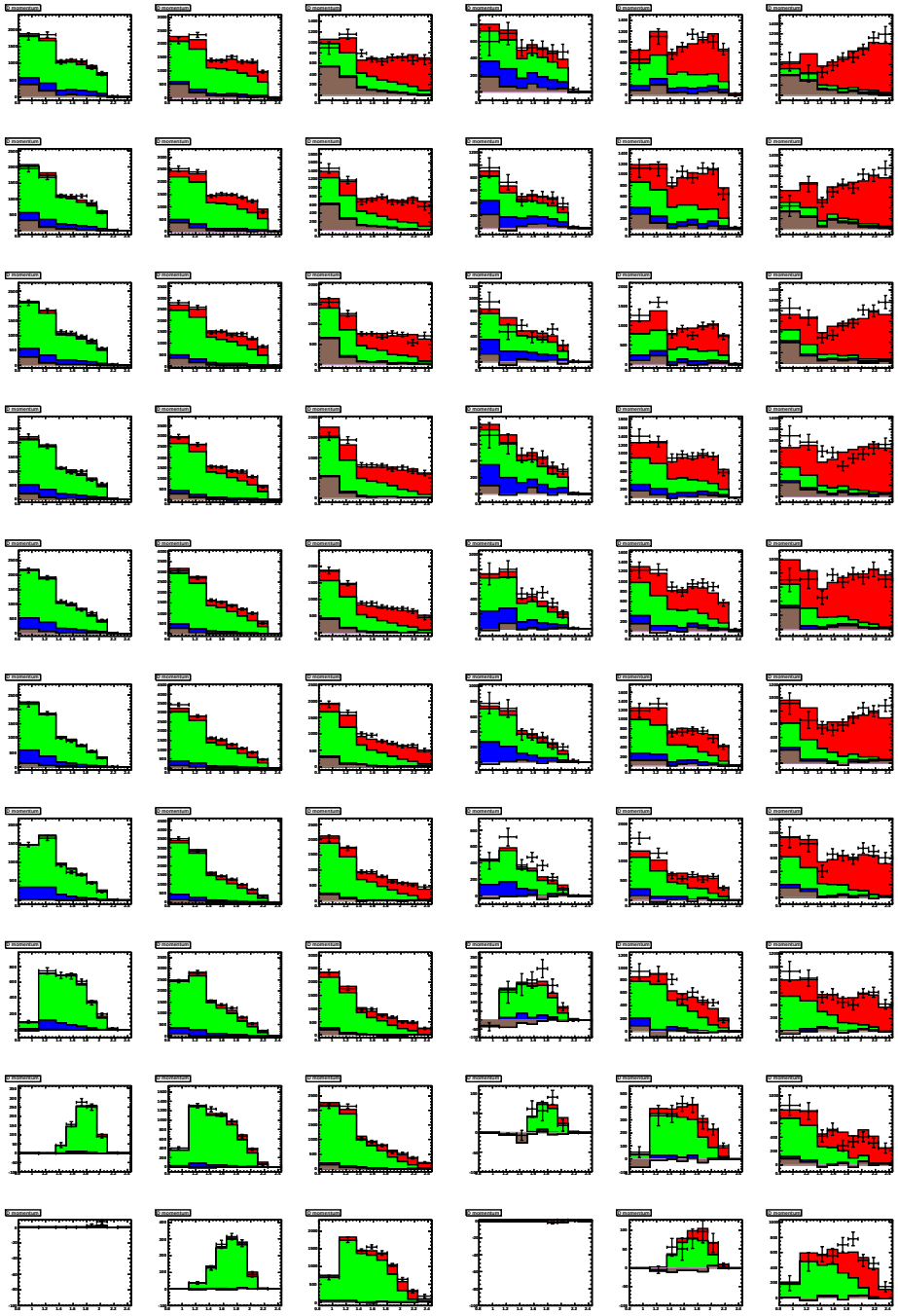

Figure 8.4: [**All bin plots (Nominal fit)**] Data and fit results showing all bins for the electron sample. The left three columns are for the D^0e sample and the right three columns are for the D^+e sample. The tree columns correspond to the three bins of $\cos\theta_{B-Dl}$. The ten rows correspond to the ten bins of p_ℓ. The eight bins in each plot correspond to the eight bins of p_D. The binning is given in section 6.2. Black points are OnPeak - OffPeak data. The red histogram is $B \to D\ell\nu$, green is $B \to D^*\ell\nu$, blue is $B \to D^{(*)}\pi\ell\nu$ and $B \to D^{(*)}\pi\pi\ell\nu$, and brown is background. Note that the y-axis range varies plot by plot.

Chapter 9

Systematic Uncertainties

Systematic uncertainties are evaluated by varying assumptions, such as form factor models and detector modeling, and input values in the fit. We keep track of the sign of the deviations caused by varying inputs; systematic errors are negative when the corresponding fitted values decrease as an assumption is changed or a input parameter increases. When we vary input parameters by $\pm 1\sigma$, we take the larger deviation as a systematic error. There are a few exceptions and details are given in the following sections. The resulting systematic uncertainties are shown in Tables 9.1 and 9.2.

9.1 Form factors

9.1.1 R_1 and R_2

We use R_1 and R_2 as input

$$\begin{aligned} &R_1 = 1.429, \quad \sigma_1 = \sqrt{0.061^2 + 0.044^2} = 0.075 \\ &R_1 = 0.827, \quad \sigma_2 = \sqrt{0.038^2 + 0.022^2} = 0.044 \\ &\text{correlation}: \ \rho_{12} = -0.84 \end{aligned} \tag{9.1}$$

The associated error matrix is given by

$$M = \begin{pmatrix} \sigma_1^2 & \sigma_1\sigma_2\ \rho_{12} \\ \sigma_1\sigma_2\ \rho_{12} & \sigma_2^2 \end{pmatrix} \tag{9.2}$$

We transform variables (R_1, R_2) to (y_1, y_2) to diagonalize the error matrix. Then we vary y_1 and y_2 independently to estimate the systematic uncertainty due to R_1 and R_2. The variation of y_1 gives (R_1,R_2) set A :

$$\delta R_1 = \pm 0.075, \quad \delta R_2 = \mp 0.040 \tag{9.3}$$

and the variation of y_2 gives (R_1,R_2) set B :

$$\delta R_1 = \pm 0.010, \quad \delta R_2 = \mp 0.019 \tag{9.4}$$

9.1.2 $B \to D^{**}\ell\nu$ decay form factors

There are two sources of systematic uncertainty from D^{**} form factors :

- FF slope : $\tilde{\tau}' = -1.5 \pm 0.5$
- Approximation B_1; we take Approximation B_2 as an alternative.

The slope range is what recommended in the LLSW paper [45].

9.2 Effect of $B \to D^{(*)}\pi\ell\nu$ decays

9.2.1 $\mathcal{B}(B^+ \to D^{(*)}\pi\ell\nu)$

As described in section 8, we use

- $\mathcal{B}(B^+ \to D^{(*)}\pi\ell\nu) = 0.0151 \pm 0.0015$

9.2.2 BF ratios

We have five BF ratios as input (see section 8):

- $f_{D_2^*/D_1} = 0.74 \pm 0.20$
- $f_{D_0^* D\pi/D_1 D_2^*} = 0.87 \pm 0.43$
- $f_{D_1' D^*\pi/D_1 D_2^*} = 0.68 \pm 0.25$
- $f_{D\pi/D_0^*} = 0.21 \pm 0.21$
- $f_{D^*\pi/D_1'} = 0.07 \pm 0.07$

We vary these ratios independently in evaluating systematic uncertainties.

9.2.3 Non-resonant $B \to D^{(*)}\pi\ell\nu$ decay BF

Non-resonant $B \to D^{(*)}\pi\ell\nu$ decay BFs are not well measured. Thus we assign 100 % uncertainty on these BF, which is covered by above BF ratios. We also need to change the ratio $f_{D^*\pi/D\pi} \equiv \mathcal{B}^{NR}(B^+ \to D^{*-}\pi^+\ell^+\nu)/\mathcal{B}^{NR}(B^+ \to D^-\pi^+\ell^+\nu)$. In nominal fit this ratio is set to 0.3.

- We change the ratio $f_{D^*\pi/D\pi}$ to 0.1 and 1.0

9.3 Effect of $B \to D^{(*)}\pi\pi\ell\nu$ decays

9.3.1 $B \to D^{(*)}\pi\pi\ell\nu$ decay BF

As described in section 8, we assign 100 % uncertainty on this BF

- $\mathcal{B}(B^+ \to D^{(*)}\pi\pi\ell\nu) = 0.011 \pm 0.011$

9.3.2 Modeling

In nominal fit we combine X, X^*, Y and Y^* with equal rates. To evaluate systematic uncertainty, we vary these ratios

- Vector - scalar ratio

  We change X^*/X and Y^*/Y to 2 and 0.5

- X - Y ratio

  We change X/Y and X^*/Y^* to 2 and 0.5

$B \to D^{(*)}\pi\pi\ell\nu$ decays may include $B \to D_1\ell\nu$ (a mix of $D_1 \to D^{(*)}\pi\pi$ and $D_1 \to D^{(*)}\eta$) decays. Thus,

- We replace the half of nominal X, X^*, Y and Y^* by D_1

9.4 Input parameters

As described in section 5.2.1, we have one parameter to calculate the D_2^* decay branching fractions :

- $f_{D_2^*} = 1.7 \pm 0.4$

Other input parameters are

- $\mathcal{B}(D^{*+} \to D^0\pi^+) = 0.677 \pm 0.005$
- $\mathcal{B}(D^0 \to K^-\pi^+) = 0.0389 \pm 0.0005$
- $\mathcal{B}(D^+ \to K^-\pi^+\pi^+) = 0.0922 \pm 0.0021$
- $t_{+0} \equiv \frac{\tau_{B^+}}{\tau_{B^0}} = 1.071 \pm 0.009$
- $f_{+0} \equiv \frac{f_{+-}}{f_{00}} = 1.065 \pm 0.026$

9.4.1 Luminosity normalization

For $B\bar{B}$ MC

- There is 1.1 % uncertainty (statistical + systematic).

For OffPeak data

- There is 0.25 % uncertainty.

9.5 Various corrections

9.5.1 Beam energy re-weighting

The measured OnPeak beam energy (mean) has an uncertainty of 0.2 MeV.

9.5.2 Electron PID efficiency

The following weight, w_f, approximates the correction to the PID weights due to the presence of other tracks and photons in the event.

- $w_f = 0.966$ (for $p_\ell < 1.0$ GeV)
- $w_f = 0.921 + 0.056 p_\ell - 0.011 p_\ell^2$ (for $1.0 < p_\ell < 2.5$ GeV)
- $w_f = 0.993$ (for $p_\ell > 2.5$ GeV)

where p_ℓ is the electron momentum. We take 50 % of the difference between applying these additional weights and not applying them as systematic error.

9.5.3 Muon PID efficiency

We evaluate muon PID efficiency systematic uncertainty from two sources :

- Effect on the shape of the histograms entering the fit

  We evaluate this by fitting without the PID correction but keeping the same average PID efficiency.

- Overall efficiency scale

  We take 4 % uncertainty on muon PID efficiency.

9.5.4 Lepton PID fake rate

We increase and decrease the fake rate correction factors by 15 %.

9.5.5 Kaon PID correction

We take the difference between the fit results with and without kaon PID correction as a systematic error.

9.5.6 Tracking efficiency correction

We take the difference between the fit results with and without tracking efficiency correction as a systematic error.

9.5.7 Radiative corrections : PHOTOS

We study the effect of radiative corrections at the event generator level by comparing MC generated with and without PHOTOS. PHOTOS [49] is the software used to calculate QED radiative corrections in our MC.

1. We generate $B \to X_c \ell \nu$ events with and without PHOTOS.

2. We produce 3D histograms as we do in our analysis with the above generated MC.

3. We divide the above histograms, bin by bin, to produce the ratio histograms.

4. We multiply the corresponding histograms used in the nominal fit by the off/on ratio histograms to get histograms without radiative corrections, which we use to fit the data.

We take 25 % of the differences in the fit results as systematic uncertainties. Using 25 % is consistent with the procedure used in previous BaBar analysis, and is based roughly on a comparison of PHOTOS with a dedicated matrix element calculation [50].

9.5.8 Bremsstrahlung

Due to emission of bremsstrahlung photons, the electron loses energy when traveling through the detector material. Since the amount of detector material is not known exactly, the effect due to Bremsstrahlung also has uncertainty. This was studied in detail in [51]. We apply this method in our fitting. First, we create 3D histograms corresponding to more and less detector material. Then, we compare fit results.

9.5.9 Vertexing

The vertexing cut is described in the event selection in chapter 3. Nominal cuts are

$$\begin{aligned} P^D(\chi^2, dof) &> 0.001 \\ P^B(\chi^2, dof) &> 0.01 \end{aligned} \tag{9.5}$$

To evaluate the systematic uncertainty of these cuts, we change them to one step looser cuts

$$\begin{aligned} P^D(\chi^2, dof) &> 0.0001 \\ P^B(\chi^2, dof) &> 0.001 \end{aligned} \tag{9.6}$$

The differences between fit results are smaller than the statistical uncertainties. Thus, the differences could be just statistical fluctuation. However, we take a conservative approach and quote the differences as systematic uncertainties.

item	ρ_D^2	ρ^2	$\mathcal{B}(D^0\ell\nu)$	$\mathcal{B}(D^{*0}\ell\nu)$	$\mathcal{F}(1)\|V_{cb}\|$	$\mathcal{G}(1)\|V_{cb}\|$
(R_1,R_2) set A	0.45	2.78	0.69	-0.38	0.60	0.71
(R_1,R_2) set B	-0.38	1.04	-0.18	0.30	-0.31	0.49
D^{**} slope	-1.11	-2.65	-0.09	-0.10	-0.68	-0.91
D^{**} B_2	-0.84	0.58	-0.11	0.20	-0.53	0.29
FF total	**1.51**	**4.02**	**0.73**	**0.53**	**1.10**	**1.29**
$\mathcal{B}(B^+ \to D^{(*)}\pi\ell\nu)$	0.42	-0.37	-0.11	-0.88	0.19	-0.56
$f_{D_2^*/D_1}$	-0.32	0.14	-0.33	0.14	-0.35	0.12
$f_{D_0^* D\pi/D_1 D_2^*}$	-2.16	1.16	-1.52	0.97	-2.02	0.86
$f_{D_1^* D^*\pi/D_1 D_2^*}$	1.10	-0.70	0.82	-0.45	1.03	-0.45
$f_{D\pi/D_0^*}$	-0.75	-1.14	0.31	0.15	-0.27	-0.30
$f_{D^*\pi/D_1^*}$	-0.18	-0.05	-0.12	0.19	-0.16	0.08
NR D^*/D ratio	0.70	-0.14	0.27	-0.16	0.53	-0.10
$D^{(*)}\pi\ell\nu$ **total**	**2.69**	**1.82**	**1.81**	**1.42**	**2.38**	**1.17**
$\mathcal{B}(B^+ \to D^{(*)}\pi\pi\ell\nu)$	1.14	-2.03	0.25	-1.29	0.77	-1.30
X^*/X and Y^*/Y ratio	0.59	-1.18	0.09	-0.28	0.38	-0.52
X/Y and X^*/Y^* ratio	0.73	-0.85	0.20	-0.66	0.51	-0.61
$D_1 \to D\pi\pi$	2.12	-1.59	0.74	-1.08	1.60	-1.06
$D^{(*)}\pi\pi\ell\nu$ **total**	**2.58**	**2.96**	**0.81**	**1.83**	**1.89**	**1.86**
$f_{D_2^*}$	-0.11	-0.01	-0.09	0.06	-0.11	0.03
$\mathcal{B}(D^{*+} \to D^0\pi^+)$	0.70	-0.01	0.43	-0.34	0.61	-0.17
$\mathcal{B}(D^+ \to K^-\pi^+\pi^+)$	-1.37	-0.42	-2.16	0.31	-1.85	0.02
$\mathcal{B}(D^0 \to K^-\pi^+)$	0.67	0.01	-0.20	-1.64	0.29	-0.82
t_{+0}	0.24	0.17	0.62	0.27	0.45	0.19
f_{+0}	0.84	0.44	0.66	-0.54	0.81	-0.13
MC Luminosity	0.00	-0.00	-1.11	-1.11	-0.56	-0.55
OffPeak Luminosity	0.05	0.01	-0.02	-0.00	0.02	0.00
Input parms total	**1.90**	**0.63**	**2.64**	**2.13**	**2.25**	**1.03**
Beam energy	-0.90	0.64	1.28	-0.55	-1.11	0.48
Lepton PID eff	0.48	0.17	1.20	0.83	0.88	0.47
Lepton PID Fake	0.03	0.01	-0.01	-0.01	0.02	-0.00
Kaon PID	0.06	0.83	0.27	0.24	0.17	0.39
Tracking eff	-0.93	-0.46	-3.31	-2.02	-2.19	-1.16
PHOTOS	-2.98	-1.07	-2.87	-0.72	-2.98	-0.71
Bremsstrahlung	0.07	-0.00	-0.13	-0.29	-0.03	-0.14
Vertexing	0.81	-0.67	0.63	0.60	0.78	0.08
Corrections total	**3.38**	**1.71**	**4.77**	**2.46**	**4.04**	**1.57**
Background total	**1.39**	**1.12**	**0.64**	**0.34**	**1.07**	**0.51**
Total	**5.76**	**5.72**	**5.89**	**4.04**	**5.74**	**3.21**

Table 9.1: [**Systematics : Electron fit**] Systematic uncertainties for the electron sample. Numbers are given in %.

item	ρ_D^2	ρ^2	$\mathcal{B}(D^0\ell\nu)$	$\mathcal{B}(D^{*0}\ell\nu)$	$\mathcal{F}(1)\lvert V_{cb}\rvert$	$\mathcal{G}(1)\lvert V_{cb}\rvert$
(R_1,R_2) set A	0.47	2.70	0.73	-0.40	0.61	0.70
(R_1,R_2) set B	-0.43	0.98	-0.19	0.30	-0.32	0.48
D^{**} slope	-1.04	-2.73	-0.12	-0.12	-0.60	-0.97
D^{**} B_2	-1.00	0.61	-0.12	0.22	-0.59	0.31
FF total	**1.57**	**4.01**	**0.77**	**0.56**	**1.09**	**1.32**
$\mathcal{B}(B^+ \to D^{(*)}\pi\ell\nu)$	0.77	-0.43	-0.01	-0.95	0.40	-0.62
$f_{D_2^*/D_1}$	-0.41	0.15	-0.36	0.16	-0.40	0.13
$f_{D_0^* D\pi/D_1 D_2^*}$	-2.91	1.27	-1.53	1.03	-2.34	0.94
$f_{D_1^* D^*\pi/D_1 D_2^*}$	1.46	-0.72	0.85	-0.50	1.19	-0.49
$f_{D\pi/D_0^*}$	-0.70	-1.10	0.27	0.16	-0.24	-0.29
$f_{D^*\pi/D_1^*}$	-0.26	-0.04	-0.14	0.21	-0.21	0.09
NR D^*/D ratio	0.83	-0.13	0.27	-0.17	0.58	-0.12
$D^{(*)}\pi\ell\nu$ **total**	**3.55**	**1.89**	**1.83**	**1.53**	**2.76**	**1.27**
$\mathcal{B}(B^+ \to D^{(*)}\pi\pi\ell\nu)$	1.87	-1.77	0.40	-1.21	1.18	-1.19
X^*/X and Y^*/Y ratio	0.70	-1.04	0.08	-0.24	0.41	-0.47
X/Y and X^*/Y^* ratio	1.03	-0.79	0.24	-0.63	0.66	-0.58
$D_1 \to D\pi\pi$	2.60	-1.53	0.75	-1.07	1.77	-1.04
$D^{(*)}\pi\pi\ell\nu$ **total**	**3.44**	**2.68**	**0.89**	**1.75**	**2.27**	**1.75**
$f_{D_2^*}$	-0.13	-0.01	-0.09	0.06	-0.11	0.03
$\mathcal{B}(D^{*+} \to D^0\pi^+)$	0.76	-0.01	0.41	-0.34	0.60	-0.17
$\mathcal{B}(D^+ \to K^-\pi^+\pi^+)$	-1.33	-0.43	-2.08	0.28	-1.73	-0.00
$\mathcal{B}(D^0 \to K^-\pi^+)$	0.89	0.10	-0.26	-1.69	0.35	-0.81
t_{+0}	0.20	0.17	0.58	0.28	0.39	0.20
f_{+0}	0.86	0.49	0.57	-0.53	0.74	-0.10
MC Luminosity	0.00	-0.00	-1.11	-1.11	-0.56	-0.55
OffPeak Luminosity	0.06	0.00	-0.02	-0.00	0.02	-0.00
Input parms total	**1.98**	**0.68**	**2.55**	**2.16**	**2.12**	**1.02**
Beam energy	1.22	-0.10	1.25	-0.66	1.28	-0.36
Lepton PID shape	-3.19	0.05	3.00	4.12	-0.20	2.06
Lepton PID scale	0.09	-0.07	-4.10	-4.17	-1.98	-2.09
Lepton PID Fake	2.52	0.71	-0.58	-0.50	1.03	-0.01
Kaon PID	0.97	0.73	0.35	0.29	0.69	0.39
Tracking eff	-0.54	-0.30	-3.33	-2.11	-1.96	-1.16
PHOTOS	-0.71	-0.62	-0.82	-0.24	-0.78	-0.33
Bremsstrahlung	0.00	0.00	0.00	0.00	0.00	0.00
Vertexing	1.69	-0.77	0.96	0.54	1.38	0.01
Corrections total	**4.75**	**1.46**	**6.37**	**6.32**	**3.67**	**3.21**
Background total	**1.58**	**1.09**	**0.67**	**0.38**	**1.16**	**0.49**
Total	**7.48**	**5.53**	**7.23**	**7.10**	**5.77**	**4.25**

Table 9.2: [**Systematics : Muon fit**] Systematic uncertainties for the muon sample. Numbers are given in %.

9.6 Background

As described in chapter 5, we re-weight branching fractions of background components. We change those BF by ± one standard deviation and take larger deviations as systematic uncertainties. Results are listed in Tables 9.3 and 9.4. We use different methods for inclusive $B \to D$ decay BFs and correlated cascade $B \to D^{(*)}\tau\nu$ background as explained in the following subsection.

9.6.1 D momentum dependent inclusive $B \to D(D_s)$ BF re-weighting

As described in section 5.1.3, we fit the D (D_s) momentum dependent weights with a 4-th (3-rd) order polynomial, and we use the fitted function to re-weight the MC. To estimate the systematic uncertainty due to the uncertainty on weights, we use the following procedure :

1. We fluctuate each weight using Gaussian random numbers.
2. We fit the distribution of weights using a 4-th (3-rd) order polynomial.
3. We re-weight the MC using the fitted function to create 3D histograms.
4. Using the histograms, we perform fitting.
5. We iterate steps 1 to 4 100 times.
6. We record the standard deviation of the set of fits as a systematic uncertainty.

To estimate the systematic uncertainty due to the choice of fit functions, we re-weight the MC with following two alternatives :

- Use a 7-th (4-th) order polynomial for fitting the D (D_s) momentum dependent weights.
- Use the binned weights without fitting.

item	ρ_D^2	ρ^2	$\mathcal{B}(D^0\ell\nu)$	$\mathcal{B}(D^{*0}\ell\nu)$	$\mathcal{F}(1)\lvert V_{cb}\rvert$	$\mathcal{G}(1)\lvert V_{cb}\rvert$
$B \to D$ weight error	1.32	0.93	0.46	0.27	0.97	0.42
$B \to D$ different fit	-0.15	-0.07	-0.09	-0.05	-0.13	-0.05
$B \to D$ no fit	-0.37	-0.60	-0.42	-0.14	-0.42	-0.26
$B \to D$ **BF total**	**1.38**	**1.11**	**0.63**	**0.31**	**1.06**	**0.50**
$D^0 \to K^{*-}\ell\nu$	-0.02	-0.01	-0.01	-0.00	-0.01	-0.00
$D^0 \to K^-\ell\nu$	-0.05	-0.02	-0.02	-0.00	-0.04	-0.01
$D^0 \to \pi^-\ell\nu$	-0.02	-0.01	-0.01	-0.00	-0.01	-0.00
$D^0 \to \rho^-\ell\nu$	-0.01	-0.00	-0.00	-0.00	-0.00	-0.00
$D^+ \to K^{*0}\ell\nu$	-0.01	-0.01	-0.01	-0.00	-0.01	-0.00
$D^+ \to K^0\ell\nu$	-0.11	-0.03	-0.05	-0.00	-0.09	-0.01
$D^+ \to \pi^0\ell\nu$	-0.03	-0.01	-0.01	-0.00	-0.02	-0.00
$D^+ \to \rho^0\ell\nu$	-0.00	-0.00	-0.00	-0.00	-0.00	-0.00
$D^+ \to \omega\ell\nu$	-0.00	-0.00	-0.00	-0.00	-0.00	-0.00
$D_s^+ \to \phi\ell\nu$	-0.00	0.00	-0.00	-0.00	-0.00	0.00
$D_s^+ \to \eta\ell\nu$	-0.03	0.06	-0.00	-0.01	-0.02	0.01
$D_s^+ \to \eta'\ell\nu$	-0.00	0.00	-0.00	-0.00	-0.00	0.00
$B^+ \to \bar{X}^0\ell^+\nu$	-0.05	-0.10	-0.04	-0.01	-0.05	-0.04
$B^0 \to X^-\ell^+\nu$	-0.09	-0.09	-0.05	-0.02	-0.08	-0.04
CascL Tau	-0.04	-0.02	0.01	-0.15	-0.02	-0.08
Other bkg total	**0.17**	**0.15**	**0.09**	**0.15**	**0.14**	**0.10**
Background total	**1.39**	**1.12**	**0.64**	**0.34**	**1.07**	**0.51**

Table 9.3: [**Systematics : Backgrounds (Electron fit)**] Background systematic uncertainties for the electron sample. Numbers are given in %.

9.6.2 Correlated cascade $B \to D^{(*)}\tau\nu$ background

Measurements of $B \to D^{(*)}\tau\nu$ decay branching fractions have uncertainties up to 30 % [52, 53]. Thus we vary the total amount of correlated cascade $B \to D^{(*)}\tau\nu$ background by 30 %. The contribution of these decays to other backgrounds is small and the effect on fit results is negligible.

9.7 Systematic Covariance Matrix

We construct a covariance matrix to keep track of correlations between systematic uncertainties. When we estimate systematic uncertainty, we vary the value of a quantity (k-th source of systematic uncertainty) and take differences, Δ^{sys}, between

item	ρ_D^2	ρ^2	$\mathcal{B}(D^0\ell\nu)$	$\mathcal{B}(D^{*0}\ell\nu)$	$\mathcal{F}(1)\lvert V_{cb}\rvert$	$\mathcal{G}(1)\lvert V_{cb}\rvert$
$B \to D$ weight error	1.43	0.92	0.44	0.27	0.99	0.42
$B \to D$ different fit	-0.40	-0.07	-0.20	-0.00	-0.31	-0.03
$B \to D$ no fit	-0.36	-0.52	-0.42	-0.11	-0.40	-0.23
$B \to D$ **BF total**	**1.53**	**1.06**	**0.64**	**0.29**	**1.11**	**0.48**
$D^0 \to K^{*-}\ell\nu$	-0.07	-0.04	-0.04	-0.04	-0.06	-0.01
$D^0 \to K^-\ell\nu$	-0.12	-0.05	-0.06	-0.05	-0.09	-0.02
$D^0 \to \pi^-\ell\nu$	-0.06	-0.04	-0.04	-0.04	-0.05	-0.01
$D^0 \to \rho^-\ell\nu$	-0.04	-0.04	-0.03	-0.04	-0.04	-0.01
$D^+ \to K^{*0}\ell\nu$	-0.06	-0.04	-0.04	-0.04	-0.05	-0.01
$D^+ \to K^0\ell\nu$	-0.25	-0.08	-0.11	-0.05	-0.19	-0.02
$D^+ \to \pi^0\ell\nu$	-0.06	-0.04	-0.04	-0.04	-0.05	-0.01
$D^+ \to \rho^0\ell\nu$	-0.04	-0.04	-0.03	0.04	-0.04	-0.01
$D^+ \to \omega\ell\nu$	-0.04	-0.04	-0.03	-0.04	-0.04	-0.01
$D_s^+ \to \phi\ell\nu$	-0.19	0.12	-0.07	-0.09	-0.13	0.01
$D_s^+ \to \eta\ell\nu$	-0.06	0.10	0.03	-0.06	-0.04	0.02
$D_s^+ \to \eta'\ell\nu$	-0.04	0.04	0.03	-0.04	-0.03	0.01
$B^+ \to \bar{X}^0\ell^+\nu$	-0.09	-0.12	-0.05	-0.06	-0.07	-0.04
$B^0 \to X^-\ell^+\nu$	-0.14	-0.12	-0.08	-0.06	-0.11	-0.05
CascL Tau	0.05	-0.00	0.05	-0.16	0.05	-0.08
Other bkg total	**0.41**	**0.27**	**0.21**	**0.25**	**0.32**	**0.11**
Background total	**1.58**	**1.09**	**0.67**	**0.38**	**1.16**	**0.49**

Table 9.4: [**Systematics : Backgrounds (Muon fit)**] Background systematic uncertainties for the muon sample. Numbers are given in %.

	Electron sample				Muon sample			
	ρ_D^2	$\rho_{D^*}^2$	$\mathcal{B}(D)$	$\mathcal{B}(D^*)$	ρ_D^2	$\rho_{D^*}^2$	$\mathcal{B}(D)$	$\mathcal{B}(D^*)$
ρ_D^2	1							
$\rho_{D^*}^2$	-0.02	1						
$\mathcal{B}(D)$	$+0.74$	$+0.12$	1					
$\mathcal{B}(D^*)$	-0.21	$+0.36$	$+0.33$	1				
ρ_D^2	$+0.73$	-0.18	$+0.44$	-0.35	1			
$\rho_{D^*}^2$	-0.06	$+0.98$	-0.05	$+0.31$	-0.15	1		
$\mathcal{B}(D)$	$+0.44$	$+0.02$	$+0.63$	$+0.18$	$+0.13$	-0.00	1	
$\mathcal{B}(D^*)$	-0.17	$+0.19$	$+0.13$	$+0.54$	-0.49	$+0.17$	$+0.69$	1

Table 9.5: [**Systematic correlation coefficients**] Correlations between parameters.

fitted values and nominal values of parameters. For i-th parameter

$$\Delta_{ik}^{sys} = \text{(fitted value - nominal value) of } i\text{-th parameter} \tag{9.7}$$

Then, the ij element of a systematic error matrix is given by

$$\text{cov}_{ij}^{sys} = \sum_k \Delta_{ik}^{sys} \cdot \Delta_{jk}^{sys} \tag{9.8}$$

In cases where we do two fits (one with a + variation and the other with a - variation), we take larger deviation. Systematic correlation coefficients are given in Table 9.5.

Chapter 10

Electron and Muon Combined Results

10.1 Method to combine electron and muon results

We combine electron and muon results by minimizing a χ^2. We put fit results given in Table 8.1 into a vector x_i ($i = 0-3$ for electron and $i = 4-7$ for muon). We sum statistical and systematic covariance matrices to get a full 8×8 covariance (error) matrix, $M(\mathrm{err})_{ij}$. The corresponding correlation matrices are shown in Tables 8.2 and 9.5. Setting $y_0 = y_4 = \rho_D^2$, $y_1 = y_5 = \rho^2$, $y_2 = y_6 = \mathcal{B}(D\ell\nu)$ and $y_3 = y_7 = \mathcal{B}(D^*\ell\nu)$, χ^2 is given by

$$\chi^2 = \sum_{i,j}(y_i - x_i)M(\mathrm{err})^{-1}_{ij}(y_j - x_j) \tag{10.1}$$

where $M(\mathrm{err})^{-1}_{ij}$ is the inverse error matrix. The χ^2 is minimized to solve for the four parameters : ρ_D^2, ρ^2, $\mathcal{B}(D\ell\nu)$ and $\mathcal{B}(D^*\ell\nu)$.

10.1.1 Determination of statistical uncertainty

The combined fit described above produces only total uncertainties of the fit parameters. In order to determine the purely statistical uncertainties, we fit to the combined

lepton sample. The results are

$$\begin{aligned} &\rho_D^2 = 1.224 \pm 0.037, \quad \rho^2 = 1.234 \pm 0.019 \\ &\mathcal{B}(D\ell\nu) = (2.345 \pm 0.025)\%, \quad \mathcal{B}(D^*\ell\nu) = (5.314 \pm 0.025)\% \end{aligned} \tag{10.2}$$

We take these statistical errors as the ones for the combined fit. This is also a good cross-check for the combined results given in Table 10.1.

10.2 Electron and Muon combined fit results

The fit results are given in Table 10.1 along with electron and muon separated results. Correlations are shown in Table 10.2. We calculate $\mathcal{G}(1)|V_{cb}|$ and $\mathcal{F}(1)|V_{cb}|$ from the fit results

$$\begin{aligned} \mathcal{G}(1)|V_{cb}| &= (43.8 \pm 0.8 \pm 2.3) \times 10^{-3} \\ \mathcal{F}(1)|V_{cb}| &= (35.7 \pm 0.2 \pm 1.2) \times 10^{-3} \end{aligned} \tag{10.3}$$

with correlations

$$\begin{aligned} \mathcal{G}(1)|V_{cb}| \text{ and } \mathcal{F}(1)|V_{cb}| &: -0.05 \\ \mathcal{G}(1)|V_{cb}| \text{ and } \rho_D^2 &: +0.63 \\ \mathcal{F}(1)|V_{cb}| \text{ and } \rho^2 &: +0.56 \end{aligned} \tag{10.4}$$

Using these results and values in Equations (4.15) and (4.16), we extract $|V_{cb}|$

$$\begin{aligned} \mathcal{G}(1) \Rightarrow |V_{cb}| &= (40.5 \pm 0.8 \pm 2.1 \pm 0.9) \times 10^{-3} \\ \mathcal{F}(1) \Rightarrow |V_{cb}| &= (38.5 \pm 0.2 \pm 1.3 \pm 1.0) \times 10^{-3} \end{aligned} \tag{10.5}$$

Parameters	Electron fit	Muon fit	combined result
ρ_D^2	$1.26 \pm 0.05 \pm 0.07$	$1.15 \pm 0.06 \pm 0.09$	$1.22 \pm 0.04 \pm 0.07$
ρ^2	$1.22 \pm 0.02 \pm 0.07$	$1.23 \pm 0.03 \pm 0.07$	$1.21 \pm 0.02 \pm 0.07$
$\mathcal{B}(\bar{D}^0\ell^+\nu)(\%)$	$2.41 \pm 0.03 \pm 0.14$	$2.29 \pm 0.04 \pm 0.16$	$2.36 \pm 0.03 \pm 0.12$
$\mathcal{B}(\bar{D}^{*0}\ell^+\nu)(\%)$	$5.41 \pm 0.03 \pm 0.22$	$5.23 \pm 0.04 \pm 0.37$	$5.37 \pm 0.02 \pm 0.21$
χ^2/ndof (P-value)	424/470 (0.94)	496/466 (0.16)	2.1/4 (0.72)

Table 10.1: [**Combined fit results**] Fit results on the electron and muon samples and the combined results.

	ρ_D^2	ρ^2	$\mathcal{B}(D^0\ell\nu)$	$\mathcal{B}(D^{*0}\ell\nu)$
ρ_D^2	1			
ρ^2	-0.131	1		
$\mathcal{B}(D^0\ell\nu)$	+0.598	+0.055	1	
$\mathcal{B}(D^{*0}\ell\nu)$	-0.283	+0.310	+0.302	1

Table 10.2: [**Combined fit correlation coefficients**] Correlations between parameters of combined fit.

where the third errors correspond to the theory errors on $\mathcal{G}(1)$ and $\mathcal{F}(1)$. We also calculate the ratio $\mathcal{G}(1)/\mathcal{F}(1)$ to compare directly with theory (lattice QCD)

$$\text{Measured}: \quad \mathcal{G}(1)/\mathcal{F}(1) = 1.23 \pm 0.09 \tag{10.6}$$

$$\text{Theory}: \quad \mathcal{G}(1)/\mathcal{F}(1) = 1.17 \pm 0.04 \tag{10.7}$$

where we assumed the theory errors on $\mathcal{G}(1)$ and $\mathcal{F}(1)$ are independent. The measured ratio is consistent with the predicted ratio.

Chapter 11

Discussion

The form factor slopes and branching fractions agree with the world average [36], which is

$$\begin{aligned} \rho_D^2 &= 1.17 \pm 0.18 \\ \rho^2 &= 1.17 \pm 0.05 \\ \mathcal{B}(B^+ \to \bar{D}^0 \ell\nu) &= (2.32 \pm 0.13)\% \\ \mathcal{B}(B^+ \to \bar{D}^{*0} \ell\nu) &= (5.53 \pm 0.31)\% \end{aligned} \tag{11.1}$$

We added one more contribution to $\mathcal{B}(B^+ \to \bar{D}^{*0}\ell\nu)$. The value of this branching fraction seems to be converging. We give an average of recent BaBar measurements below. The precision of our D slope, ρ_D^2, is twice as good as the world average. As our fit gives good χ^2 by adding $B \to D^{(*)}\pi\pi\ell\nu$ component, this suggests that there is a missing component other than $B \to D\ell\nu$, $B \to D^*\ell\nu$ and $B \to D^{(*)}\pi\ell\nu$. This also suggests that the missing component has similar kinematic properties to $B \to D^{(*)}\pi\pi\ell\nu$ decays.

11.1 Combined BaBar results

There are three recent BaBar measurements of $B \to D^{(*)}\ell\nu$ decays. Ref. [44] reconstructs $B^0 \to D^{*-}\ell^+\nu_\ell$ decays and measures

$$\begin{aligned} \mathcal{F}(1)|V_{cb}| &= (34.4 \pm 0.3 \pm 1.1) \times 10^{-3} \\ \rho^2 &= 1.191 \pm 0.048 \pm 0.028 \\ \mathcal{B}(B^0 \to D^{*-}\ell^+\nu_\ell) &= (4.69 \pm 0.04 \pm 0.34)\% \end{aligned} \tag{11.2}$$

Ref. [54] reconstructs $B^- \to D^{*0}e^-\bar{\nu}_e$ decays and obtains

$$\begin{aligned} \mathcal{F}(1)|V_{cb}| &= (35.9 \pm 0.6 \pm 1.4) \times 10^{-3} \\ \rho^2 &= 1.16 \pm 0.06 \pm 0.08 \\ \mathcal{B}(B^- \to D^{*0}e^-\bar{\nu}_e) &= (5.56 \pm 0.08 \pm 0.41)\% \end{aligned} \tag{11.3}$$

Ref. [11] fully reconstructs one B and looks at the other B decaying semileptonically. It quotes

$$\begin{aligned} \mathcal{B}(B^- \to D^0\ell\bar{\nu}) &= (2.33 \pm 0.09 \pm 0.09)\% \\ \mathcal{B}(B^- \to D^{*0}\ell\bar{\nu}) &= (5.83 \pm 0.15 \pm 0.30)\% \\ \mathcal{B}(\bar{B}^0 \to D^+\ell\bar{\nu}) &= (2.21 \pm 0.11 \pm 0.12)\% \\ \mathcal{B}(\bar{B}^0 \to D^{*+}\ell\bar{\nu}) &= (5.49 \pm 0.16 \pm 0.25)\% \end{aligned} \tag{11.4}$$

The global fit results are consistent with these results. The $\mathcal{F}(1)|V_{cb}|$ versus ρ^2 are plotted in Figure 11.1 to show the good agreement between BaBar results.

We combine results from the three previous BaBar analysis with the global fit results. We impose isospin symmetry to previous results, and rescale previous results using new values for f_{+0} and charm decay branching fractions if applicable. Ref. [44] and Ref. [54] are statistically independent. Ref. [11] use one B fully reconstruct sample and statistical overlap with others are expected to be small. The global fit is a large superset of others and have very small statistical errors. Thus, statistical

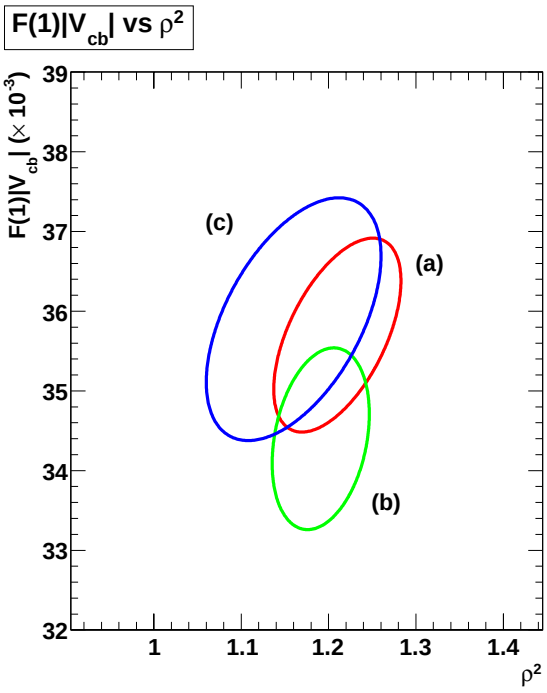

Figure 11.1: [$\mathcal{F}(1)|V_{cb}|$ **vs** ρ^2] Comparison of BaBar measurements of $\mathcal{F}(1)|V_{cb}|$ and ρ^2. (a) red is global fit, (b) green is Ref. [44] and (c) blue is Ref. [54].

correlations between 4 analysis is negligible. We categorize systematic uncertainties into detector effects, background, R_2 and R_2, D^0 decay BF and so on, and assume maximum correlation in each category between 4 analysis. The combined results are

$$\begin{aligned}
&\mathcal{B}(B^- \to D^0 \ell\bar{\nu}) = (2.33 \pm 0.09)\% \\
&\mathcal{B}(B^- \to D^{*0} \ell\bar{\nu}) = (5.47 \pm 0.19)\% \\
&\rho^2 = 1.19 \pm 0.04 \\
&\mathcal{F}(1)|V_{cb}| = (34.8 \pm 0.8) \times 10^{-3}
\end{aligned} \tag{11.5}$$

with χ^2 probabilities 0.85, 0.38, 0.90 and 0.33, respectively. The χ^2 probabilities show that four BaBar measurements agree well.

Parameters	Electron fit	Muon fit	combined result
ρ_D^2	$1.24 \pm 0.05 \pm 0.09$	$1.12 \pm 0.07 \pm 0.09$	$1.18 \pm 0.04 \pm 0.07$
ρ^2	$1.32 \pm 0.05 \pm 0.09$	$1.31 \pm 0.06 \pm 0.09$	$1.31 \pm 0.04 \pm 0.09$
R_1	$1.56 \pm 0.09 \pm 0.14$	$1.50 \pm 0.10 \pm 0.16$	$1.53 \pm 0.07 \pm 0.14$
R_2	$0.68 \pm 0.07 \pm 0.09$	$0.70 \pm 0.08 \pm 0.10$	$0.67 \pm 0.05 \pm 0.09$
$\mathcal{B}(B^+ \to \bar{D}^0 \ell^+ \nu)$ (%)	$2.40 \pm 0.04 \pm 0.15$	$2.26 \pm 0.04 \pm 0.17$	$2.33 \pm 0.03 \pm 0.13$
$\mathcal{B}(B^+ \to \bar{D}^{*0} \ell^+ \nu)$ (%)	$5.48 \pm 0.05 \pm 0.23$	$5.32 \pm 0.06 \pm 0.37$	$5.46 \pm 0.04 \pm 0.22$
χ^2/ndof (P-value)	418/468 (0.95)	490/464 (0.20)	2.0/6 (0.92)

Table 11.1: [R_1 **and** R_2 **floated fit results**] Fit results on the electron and muon samples and the combined results.

	ρ_D^2	ρ^2	R_1	R_2	$\mathcal{B}(D\ell\nu)$	$\mathcal{B}(D^*\ell\nu)$
ρ_D^2	1					
ρ^2	-0.426	1				
R_1	-0.212	+0.736	1			
R_2	+0.506	-0.782	-0.719	1		
$\mathcal{B}(D\ell\nu)$	+0.598	-0.031	+0.140	+0.097	1	
$\mathcal{B}(D^*\ell\nu)$	-0.319	+0.418	+0.144	-0.315	+0.217	1

Table 11.2: [R_1 **and** R_2 **floated fit correlation coefficients**] Correlations between parameters.

11.2 Results when floating R_1 and R_2

In addition to the nominal fit, we also performed a fit with R_1 and R_2 as free parameters. The results are summarized in Table 11.1. The correlations corresponding to combined result are given in Table 11.2. We compare our results with previous BaBar measurement [44] :

$$\begin{aligned} \rho^2 &= 1.191 \pm 0.048 \pm 0.028 \\ R_1 &= 1.429 \pm 0.061 \pm 0.044 \\ R_2 &= 0.827 \pm 0.038 \pm 0.022 \end{aligned} \tag{11.6}$$

The two results, compared in the space of the three form factor parameters, are consistent at 36 % CL (Confidence Level).

Chapter 12

Conclusion

We reconstruct $D^0\ell$ and $D^+\ell$ pairs to access exclusive decays of the type $B \to D^{(*)}(\pi)\ell\nu$. Instead of explicitly reconstruct D^* and D^{**}, kinematic variables, p^*_ℓ, p^*_D and $\cos\Theta_{B-D\ell}$ are used to distinguish each exclusive mode and background. We use a global fit to measure two form factor slopes

$$\begin{aligned} \rho^2_D &= 1.22 \pm 0.04(stat.) \pm 0.07(syst.) \\ \rho^2 &= 1.21 \pm 0.02(stat.) \pm 0.07(syst.) \end{aligned} \tag{12.1}$$

and two branching fractions

$$\begin{aligned} \mathcal{B}(B^+ \to \bar{D}^0\ell^+\nu) &= (2.36 \pm 0.03(stat.) \pm 0.12(syst.))\% \\ \mathcal{B}(B^+ \to \bar{D}^{*0}\ell^+\nu) &= (5.37 \pm 0.02(stat.) \pm 0.21(syst.))\% \end{aligned} \tag{12.2}$$

These results have good agreement with world average. We also determine

$$\begin{aligned} \mathcal{G}(1)|V_{cb}| &= (43.8 \pm 0.8(stat.) \pm 2.3(syst.)) \times 10^{-3} \\ \mathcal{F}(1)|V_{cb}| &= (35.7 \pm 0.2(stat.) \pm 1.2(syst.)) \times 10^{-3} \end{aligned} \tag{12.3}$$

The $\mathcal{G}(1)|V_{cb}|$ is twice as precise as world average and the precision of $\mathcal{F}(1)|V_{cb}|$ is similar to the best single measurement. This analysis method is different from and complementary to previous BaBar measurements [11, 44, 54]; the results are

consistent.

From these results, we extract $|V_{cb}|$. From $\mathcal{G}(1)|V_{cb}|$

$$|V_{cb}| = (40.5 \pm 0.8(stat.) \pm 2.1(syst.) \pm 0.9(theo.)) \times 10^{-3} \tag{12.4}$$

and from $\mathcal{F}(1)|V_{cb}|$

$$|V_{cb}| = (38.5 \pm 0.2(stat.) \pm 1.3(syst.) \pm 1.0(theo.)) \times 10^{-3} \tag{12.5}$$

These are consistent with each other. We also take a ratio

$$\frac{\mathcal{G}(1)}{\mathcal{F}(1)} = 1.23 \pm 0.09 \tag{12.6}$$

which agrees with theoretical prediction.

Bibliography

[1] BELLE Collaboration, K. Abe *et al.*, *"Determination of $|V_{cb}|$ using the semileptonic decay $\bar{B}^0 \to D^{*+} e^- \bar{\nu}$"*, Phys. Lett. B**526**, 247 (2002), hep-ex/0111060.

[2] DELPHI Collaboration, P. Abreu *et al.*, *"Measurement of V_{cb} from the decay process $\bar{B}^0 \to D^{*+} \ell^- \bar{\nu}$"*, Phys. Lett. B**510**, 55 (2001), hep-ex/0104026.

[3] BABAR Collaboration, B. Aubert *et al.*, *"Measurement of the $\bar{B}^0 \to D^{*+} l^- \bar{\nu}_l$ Decay Rate and $|V_{cb}|$"*, Phys. Rev. D**71**, 051502 (2005), hep-ex/0408027.

[4] OPAL Collaboration, G. Abbiendi *et al.*, *"Measurement of $|V_{cb}|$ using $B^0 \to D^* l\nu$ decays"*, Phys. Lett. B**482**, 15 (2000), hep-ex/0003013.

[5] ALEPH Collaboration, D. Buskulic *et al.*, *"Measurements of $|V_{cb}|$, form-factors and branching fractions in the decays $\bar{B}^0 \to D^{*+} l^- \bar{\nu}_l$ and $\bar{B}^0 \to D^+ l^- \bar{\nu}_l$"*, Phys. Lett. B**395**, 373 (1997).

[6] DELPHI Collaboration, J. Abdallah *et al.*, *"Measurement of $|V_c b|$ using the semileptonic decay $\bar{B}^0_d \to D^{*+} l^- \bar{\nu}_l$"*, European. Phys. J. C**33**, 213 (2004), hep-ex/0401023.

[7] CLEO Collaboration, N. E. Adam *et al.*, *"Determination of the $\bar{B} \to D^* l\bar{\nu}$ Decay Width and $|V_{cb}|$"*, Phys. Rev. D**67**, 032001 (2003), hep-ex/0210040.

[8] BELLE Collaboration, K. Abe *et al.*, *"Measurement of $\mathcal{B}(\bar{B} \to D^+ l^- \bar{\nu})$ and Determination of $|V_{cb}|$"*, Phys. Lett. B**526**, 258 (2002), hep-ex/0111082.

[9] CLEO Collaboration, J. Bartelt *et al.*, *"Measurement of the $B \to D\ell\nu$ Branching Fractions and Form Factor"*, Phys. Rev. Lett.**82**, 3746 (2003), hep-ex/9811042.

[10] Particle Data Group, C. Amsler *et al.*, *"Review of Particle Physics"*, Phys. Lett. B**667**, 1 (2008).

[11] BABAR Collaboration, *"A Measurement of the Branching Fractions of Exclusive $\bar{B} \to D^{(*)}(\pi)\ell^-\bar{\nu}_\ell$ Decays in Events with a Fully Reconstructed B Meson"*, Phys. Rev. Lett. **100**, 151802 (2008), arXiv:0712.3503v1 [hep-ex].

[12] D. Griffiths, *"Introduction to Elementary Particles"*, John Wiley & Sons, Inc. (1987).

[13] W. N. Cottingham and D. A. Greenwood, *"An Introduction to the Standard Model of Particle Physics"*, Cambridge Univ. Press (1998).

[14] T. Morii, C. S. Lim and S. N. Mukherjee, *"The Physics of the Standard Model and Beyond"*, World Scientific (2004).

[15] B. Kayser, *"Nautrino Physics"*, Lectures Presented at the 2004 SLAC Summer Institute, hep-ph/0506165.

[16] N. Cabbibo, *"Unitary Symmetry and Leptonic Decays"*, Phys. Rev. Lett. **10**, 531 (1963).

[17] M. Kobayashi and T. Maskawa, *"CP-Violation in the Renormalizable Theory of Weak Interaction"*, Prog. Theor. Phys. **49**, 652 (1973).

[18] C. Jarlskog, *"Introduction to CP Violation"*, in "CP Violation" (ed. C. Jarlskog), World Scientific (1989).

[19] H. J. Lipkin, *"Physics at B-Fcatories (A Theretical Talk)"*, Presented at Tel Aviv University (1993), arXiv:hep-ph/9302204.

[20] A. V. Manohar and M. B. Wise, *"Heavy Quark Physics"*, Cambridge University Press (2000).

[21] M. Neubert, *"Heavy Quark Symmetry"*, Phys. Rept. **245**, 259 (1994), hep-ph/9306320.

[22] J. D. Richman and P. R. Burchat., *"Leptonic and Semileptonic Decays of Charm and Bottom Hadrons"*, Rev. Mod. Phys. **67**, 893 (1995), hep-ph/9508250.

[23] M. Okamoto *et al.*, *"Semileptonic $D \to \pi/K$ and $B \to \pi/D$ decays in 2+1 flavor lattice QCD"*, Nucl. Phys. Proc. Suppl. **140**, 461 (2005), hep-lat/0409116.

[24] I. Caprini, L. Lellouch and M.Neubert., *"Dispersive Bounds on the Shape of $B \to D^{(*)} l\nu$ Form Factors"*, Nucl. Phys. B**530**, 153 (1998), hep-ph/9712417.

[25] *"PEP-II Conceptual Design Report"*, SLAC-0418 (2002).

[26] D. J. Lange, *"The EvtGen particle decay simulation package"*, Nucl. Instrum. Meth. **A462**, 152 (2001).

[27] D. Scora and N. Isgur., *"Semileptonic Meson Decays in the Quark Model: An Update"*, Phys. Rev. D**52**, 2783 (1995), hep-ph/9503486.

[28] N. Isgur, D. Scora, B. Grinstein and M. B. Wise., *"Semileptonic Meson Decays in the Quark Model"*, Phys. Rev. D**39**, 2783 (1989).

[29] J. L. Goity, *"Chiral perturbation theory for SU(3) breaking in heavy meson systems"*, Phys. Rev. D**46**, 3929 (1992), hep-ph/9206230.

[30] J. L. Goity and W. Roberts., *"Soft Pion Emission in Semileptonic B-Meson Decays"*, Phys. Rev. D**51**, 3459 (1995), hep-ph/9406236.

[31] Geant 4 Collaboration, S. Agostinelli *et al.*, *"GEANT4: A Simulation toolkit"*, Nucl. Instrum. Meth. **A506**, 250 (2003).

[32] BABAR Collaboration, B. Aubert *et al.*, *"The BABAR Detector"*, Nucl. Instrum. Meth. **A479**, 1 (2002), hep-ex/0105044.

[33] W. D. Hulsbergen, *"Decay Chain Fitting with a Kalman Filter"*, Nucl. Instrum. Meth. **A552**, 566 (2005).

[34] C. Bernard *et al.*, *"$\bar{B} \to D^* \ell \nu$ form factor at zero recoil from three-flavor lattice QCD: A model independent determination of $|V_{cb}|$"*, arXiv:0808.2519v1[hep-lat].

[35] A. Sirlin, *"Large $m(W)$, $m(Z)$ Behavior of the mathcal$O(\alpha)$ Corrections to Semileptonic Processes Mediated by W."*, Nucl. Phys. B**196**, 83 (1982).

[36] Heavy Flavor Averaging Group (HFAG), http://www.slac.stanford.edu/xorg/hfag/index.html.

[37] Babar Collaboration, B. Barate*et al.*, *"Study of inclusive charm production in B meson decays with the BaBar experiment"*, Babar Analysis Document 1234, (2006).

[38] Babar Collaboration, B. Barate*et al.*, *"Study of Inclusive B^- and $\bar{B}^0$ Decays to Flavor-Tagged D, D_s and Λ_c^+"*, Phys. Rev. D **75**, 072002 (2007), hep-ex/0606026.

[39] BELLE Collaboration, K. Abe *et al.*, *"Observation of the $D_1(2420) \to D\pi^+\pi^-$ decays"*, Phys. Rev. Lett. **94**, 221805 (2005), hep-ex/0410091.

[40] A. E. Snyder., *"Effect of Lepton mass on Semileptonic Branching Fraction, $|V_{cb}|$ and Form Factor Measurements."*, Babar Analysis Document 1883.

[41] M. Mazur and J. Richman, *"Study of the Exclusive Semileptonic Decays $B \to D\tau^-\bar{\nu}_\tau$ and $B \to D^*\tau^-\bar{\nu}_\tau$"*, Babar Analysis Document 1111.

[42] J. G. Korner and G. A. Schuler, *"Exclusive Semileptonic Heavy Meson Decays Including Lepton Mass Effects."*, Z. Phys. C**46**, 93 (1990); J. G. Korner, G. A. Schuler and Y. L. Wu, *"T-odd and CP-odd Triple Momentum Correlations in the Exclusive Semileptonic Bottom Meson Decay $B \to D^* \ell \nu$"*, Phys. Lett. B**242**, 119 (1990).

[43] BABAR Collaboration, B. Aubert *et al.*, *"Measurements of the B to D^* Form Factors Using the Decay $B^0 \to D^* e \nu_e$"*, Phys. Rev. D**74**, 092004 (2006), hep-ex/0602023.

[44] BABAR Collaboration, B. Aubert *et al.*, *"Determination of the Form Factors for the Decay $B^0 \to D^{*-} \ell^+ \nu_\ell$ and of the CKM Matrix Element $|V_{cb}|$"*, Phys. Rev. D**77**, 032002 (2008), arXiv:0705.4008 [hep-ex].

[45] A. K. Leibovich, Z. Ligeti, I. W. Stewart, M. B. Wise., *"Model independent results for $B \to D_1(2420) \ell \bar{\nu}$ and $B \to D_2^*(2460) \ell \bar{\nu}$ at order $\Lambda_{QCD}/m_{c,b}$"*, Phys. Rev. Lett.**78**, 3995 (1997), hep-ph/9703213.

[46] A. K. Leibovich, Z. Ligeti, I. W. Stewart, M. B. Wise., *"Semileptonic B decays to excited charmed mesons"*, Phys. Rev. D**57**, 308 (1998), hep-ph/9705467.

[47] BABAR Collaboration, B. Aubert *et al.*, *"Measurement of Semileptonic B Decays into Orbitally-Excited Charm States."*, submitted to Phys. Rev. Lett., arXiv:0808.0333 [hep-ex].

[48] BABAR Collaboration, B. Aubert *et al.*, *"Measurement of the Branching Fractions of $\bar{B} \to D^{**} \ell^- \bar{\nu}_\ell$ Decays in Events Tagged by a Fully Reconstructed B Meson."*, submitted to Phys. Rev. Lett., arXiv:0808.0528 [hep-ex].

[49] E. Barbeiro and Z. Was, *"Photos: A universal monte carlo for QED radiative corrections. Version 2.0"*, Comput. Phys. Commun. **79**, 291 (1994); E. Bar-

beiro, B. van Eijk and Z. Was, *"Photos: A universal monte carlo for QED radiative corrections in decays"*, Comput. Phys. Commun. **66**, 115 (1991).

[50] E. S. Ginsberg, *"Radiative Correction to K_{13} Decays"*, Phys. Rev. **142**, 1035 (1966).

[51] F. Bernlochner *et al.*, *"On the Effects of Additional Bremsstrhlung due Detector Geometry Uncertainties on Monte Carlo Simulatated Electron Energy Spectra"*, Babar Analysis Document 1911.

[52] BABAR Collaboration, B. Aubert *et al.*, *"Observation of the Semileptonic Decays $B \to D^*\tau\bar{\nu}_\tau$ and Evidence for $B \to D\tau\bar{\nu}_\tau$"*, Phys. Rev. D **76**, 051104 (2007), arXiv:0709.1698 [hep-ex].

[53] BELLE Collaboration, A. Matyia *et al.*, *"Observation of $B^0 \to D^{*-}\tau^+\nu_\tau$ decay at Belle"*, arXiv:0706.4429 [hep-ex].

[54] BABAR Collaboration, B. Aubert *et al.*, *"Measurements of the Decay $B^- \to D^{*0}e^-\bar{\nu}_e$"*, Phys. Rev. Lett.**100**, 231803 (2008), arXiv:0712.3493 [hep-ex].

Appendix A

Decay modes to consider

A.1 Semileptonic $B \to D^{(*,**)}\ell\nu$ decays

A.1.1 Semileptonic B^+ decays

There are three types of decay modes (Figure A.1).

- $B^+ \to \bar{D}^{(*,**)0}\ell^+\nu_\ell$
- $B^+ \to \bar{D}^{(*)0}\pi^0\ell^+\nu_\ell$
- $B^+ \to D^{(*)-}\pi^+\ell^+\nu_\ell$

A.1.2 Semileptonic B^0 decays

There are three types of decay modes (Figure A.1).

- $B^0 \to D^{(*,**)-}\ell^+\nu_\ell$
- $B^0 \to D^{(*)-}\pi^0\ell^+\nu_\ell$
- $B^0 \to \bar{D}^{(*)0}\pi^-\ell^+\nu_\ell$

A.2 D^* and D^{**} decays

A.2.1 $D^{*,**+}$ decays

There are three types of decay modes (Figure A.2).

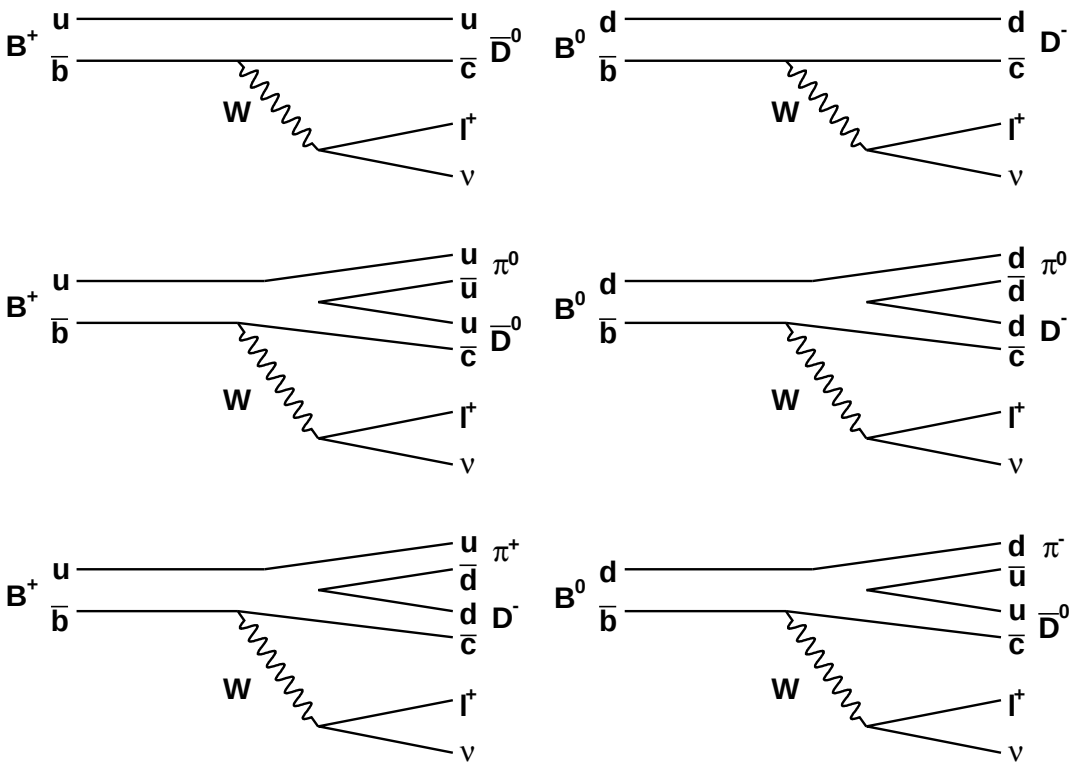

Figure A.1: Feynman diagrams of semileptonic $B \to D^{(*,**)}\ell\nu$ decays

- $D^{*,**+} \to D^{(*)0}\pi^+$
- $D^{*,**+} \to D^{(*)+}\pi^0$
- $D^{*,**+} \to D^{(*)+}\gamma$

Note that

- $D^{**+} \to D^{*+}\gamma$ is negligible because it is an electromagnetic process and small compared to strong processes.
- $D^{*+} \to D^{*+}\gamma$ is allowed because strong processes are suppressed by phase space, the EM process amplitude has comparable size to strong processes.

A.2.2 $D^{*,**0}$ decays

There are three types of decay modes (Figure A.2).

- $D^{*,**0} \to D^{(*)+}\pi^-$
- $D^{*,**0} \to D^{(*)0}\pi^0$
- $D^{*,**0} \to D^{(*)0}\gamma$

Note that

- $D^{**0} \to D^{*0}\gamma$ is negligible
- $D^{*0} \to D^+\pi^-$ is not allowed because $m_{D^{*0}} < m_{D^+} + m_{\pi^-}$

A.3 D^0 and D^+ decays

A.3.1 D^0 decays

There are four decay modes used in the reconstruction of D^0 (Figure A.3).

- $D^0 \to K^-\pi^+$

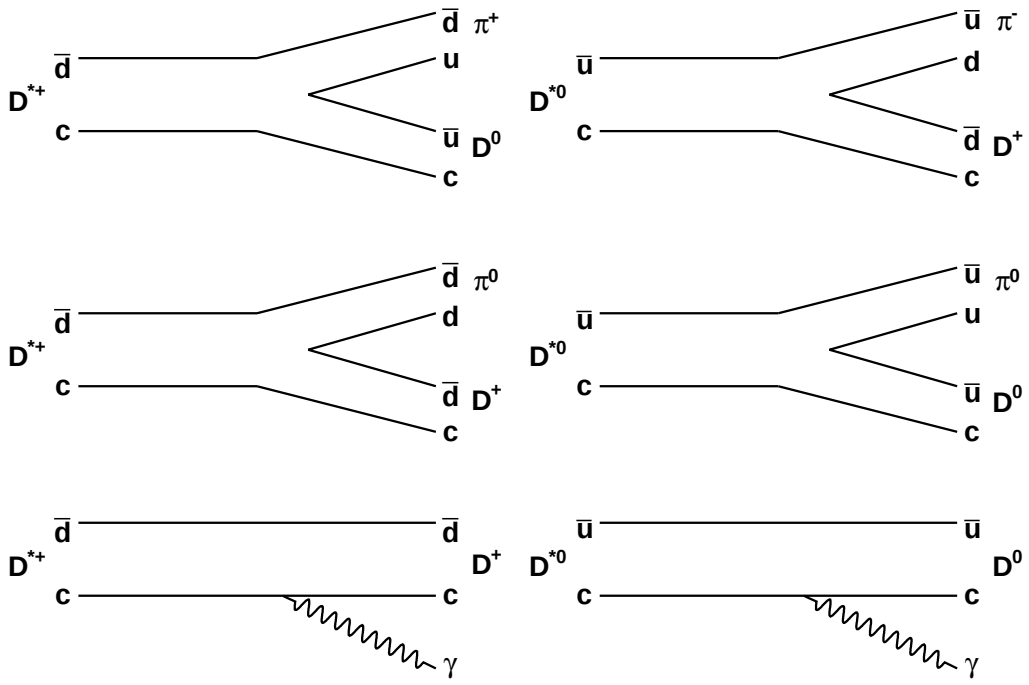

Figure A.2: Feynman diagrams of $D^{*,**}$ decays

- $D^0 \to K^-\pi^+\pi^+\pi^-$
- $D^0 \to K^-\pi^+\pi^0$
- $D^0 \to K^0_s\pi^+\pi^-$

A.3.2 D^+ decays

There are two decay modes used in the reconstruction of D^+ (Figure A.3).

- $D^+ \to K^-\pi^+\pi^+$
- $D^+ \to \bar{K}^0_s\pi^+$

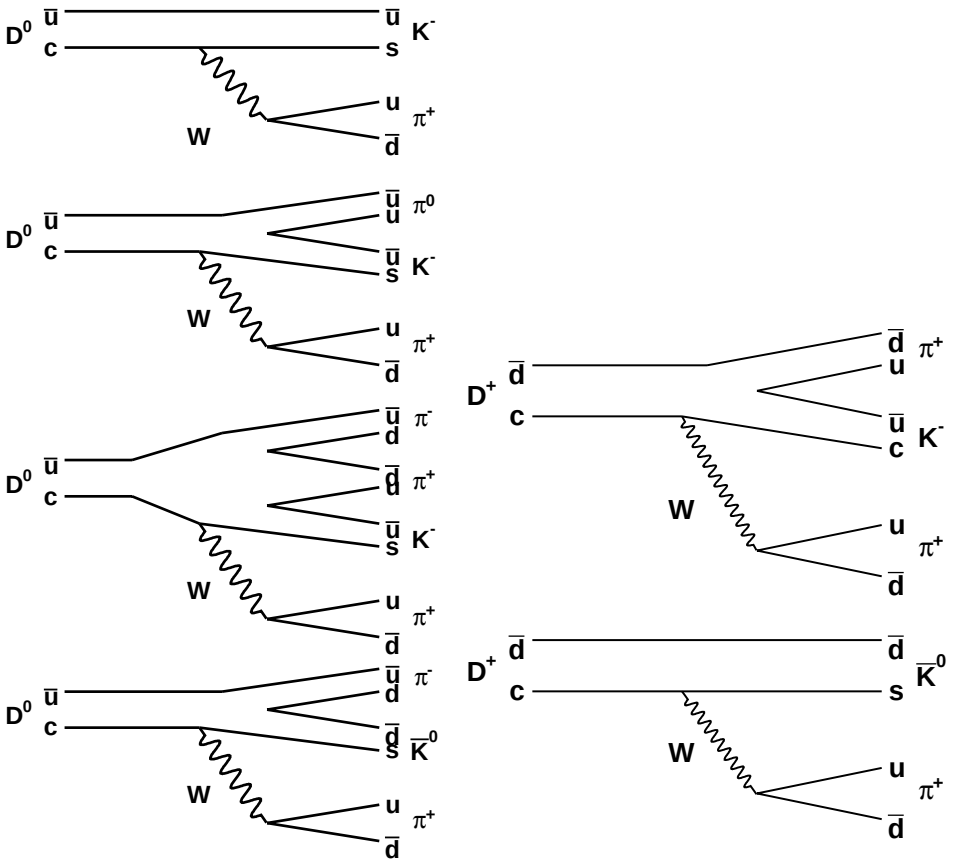

Figure A.3: Feynman diagrams of D decays

A.4 Decay chain

A.4.1 B^+ decay chain

1. $B^+ \to \bar{D}^0 \ell^+ \nu_\ell$ (D^0)
2. $B^+ \to \bar{D}^{*0} \ell^+ \nu_\ell$
   - $D^- \pi^+$ (not possible)
   - $\bar{D}^0 \pi^0$ (D^0)
   - $\bar{D}^0 \gamma$ (D^0)
3. $B^+ \to \bar{D}^{**0} \ell^+ \nu_\ell$
   - $D^- \pi^+$ (D^+)
   - $\bar{D}^0 \pi^0$ (D^0)
   - $\bar{D}^0 \gamma$ (negligible)
   - $D^{*-} \pi^+$
     - $\bar{D}^0 \pi^-$ (D^0)
     - $D^- \pi^0$ (D^+)
     - $D^- \gamma$ (D^+)
   - $\bar{D}^{*0} \pi^0$
     - $D^- \pi^+$ (not possible)
     - $\bar{D}^0 \pi^0$ (D^0)
     - $\bar{D}^0 \gamma$ (D^0)
   - $\bar{D}^{*0} \gamma$ (negligible)
4. $B^+ \to \bar{D}^0 \pi^0 \ell^+ \nu_\ell$ (D^0)
5. $B^+ \to D^- \pi^+ \ell^+ \nu_\ell$ (D^+)

6. $B^+ \to \bar{D}^{*0}\pi^0\ell^+\nu_\ell$
   - $\to D^-\pi^+$ (not possible)
   - $\to \bar{D}^0\pi^0$ (D^0)
   - $\to \bar{D}^0\gamma$ (D^0)
7. $B^+ \to D^{*-}\pi^+\ell^+\nu_\ell$
   - $\to \bar{D}^0\pi^-$ (D^0)
   - $\to D^-\pi^0$ (D^+)
   - $\to D^-\gamma$ (D^+)

A.4.2 B^0 decay chain

1. $B^0 \to D^-\ell^+\nu_\ell$ (D^0)
2. $B^0 \to D^{*-}\ell^+\nu_\ell$
   - $\to \bar{D}^0\pi^-$ (D^0)
   - $\to D^-\pi^0$ (D^+)
   - $\to D^-\gamma$ (D^+)

3. $B^0 \to D^{**-}\ell^+\nu_\ell$
   - $\bar{D}^0\pi^-$ (D^0)
   - $D^-\pi^0$ (D^+)
   - $D^-\gamma$ (negligible)
   - $D^{*-}\pi^0$
     - $\bar{D}^0\pi^-$ (D^0)
     - $D^-\pi^0$ (D^+)
     - $D^-\gamma$ (D^+)
   - $\bar{D}^{*0}\pi^-$
     - $D^-\pi^+$ (not possible)
     - $\bar{D}^0\pi^0$ (D^0)
     - $\bar{D}^0\gamma$ (D^0)
   - $\bar{D}^{*-}\gamma$ (negligible)
4. $B^0 \to D^-\pi^0\ell^+\nu_\ell$ (D^+)
5. $B^0 \to \bar{D}^0\pi^-\ell^+\nu_\ell$ (D^0)
6. $B^0 \to D^{*-}\pi^0\ell^+\nu_\ell$
   - $\bar{D}^0\pi^-$ (D^0)
   - $D^-\pi^0$ (D^+)
   - $D^-\gamma$ (D^+)
7. $B^0 \to \bar{D}^{*0}\pi^-\ell^+\nu_\ell$
   - $D^-\pi^+$ (not possible)
   - $\bar{D}^0\pi^0$ (D^0)
   - $\bar{D}^0\gamma$ (D^0)

Appendix B

Classification of D^{**}

B.1 Angular momentum of a meson

In atomic spectroscopy, there are two useful schemes to add angular momentum: LS-coupling and jj-coupling.

- LS-coupling

$$\begin{aligned} \boldsymbol{S} &= \boldsymbol{s}_1 + \boldsymbol{s}_2 \\ \boldsymbol{J} &= \boldsymbol{L} + \boldsymbol{S} \end{aligned} \tag{B.1}$$

- jj-coupling

$$\begin{aligned} \boldsymbol{j}_1 &= \boldsymbol{L} + \boldsymbol{s}_1 \\ \boldsymbol{J} &= \boldsymbol{j}_1 + \boldsymbol{s}_2 \end{aligned} \tag{B.2}$$

where s, l and j are the spin, orbital angular momentum and total angular momentum of individual particles, and S, L and J are the spin, orbital angular momentum and total angular momentum of the system.

B.2 Parity of a meson ($Q\bar{q}$-system) : $P = (-1)^{L+1}$

The parity of

- Quark [1] : $P_Q = +1$
- Anti-quark : $P_{\bar{q}} = -1$
- Orbital angular momentum L : $(-1)^L$

Thus, the parity of a $Q\bar{q}$-system is given by

$$P = (P_Q)(P_{\bar{q}})(-1)^L = (+1)(-1)(-1)^L = (-1)^{L+1} \tag{B.3}$$

Hence, $P = (-)$ for $L = 0$ and $P = (+)$ for $L = 1$.

B.3 Standard classification of mesons

For equal-mass meson system, it is traditional to couple the orbital angular momentum, $\boldsymbol{L}$, with the total spin of the quark and anti-quark, $\boldsymbol{S}$ (LS-coupling scheme).

$$\begin{aligned} \boldsymbol{S} &= \boldsymbol{s}_1 + \boldsymbol{s}_2 \\ \boldsymbol{J} &= \boldsymbol{L} + \boldsymbol{S} \end{aligned} \tag{B.4}$$

This is the standard practice for light mesons and heavy quarkonium ($c\bar{c}$ and $b\bar{b}$). The good quantum numbers are then S, L and J.

There are spin-singlet and spin-triplet levels because S is always $S = 0$ or $S = 1$.

- For $L = 0$ and $S = 0$, $J = 0$: $^1S_0$
- For $L = 0$ and $S = 1$, $J = 1$: $^3S_1$
- For $L = 1$ and $S = 0$, $J = 1$: $^1P_1$
- For $L = 1$ and $S = 1$, $J = 0, 1, 2$: $^3P_0$, $^3P_1$ or $^3P_2$

[1] One could define the parity of quark to be (-1). Then its of anti-quark is (+1). But, as far as P(quark) = - P(anti-quark), the final result won't change.

	Particle	J^P
$^1S_0$	D	0^-
$^3S_1$	D^*	1^-
$^1P_1$	D_1	1^+
$^3P_0$	D_0^*	0^+
$^3P_1$	D_1^*	1^+
$^3P_2$	D_2^*	2^+

Table B.1: Traditional spectroscopic notation of D, D^* and D^{**} mesons.

In general, for $S = 0$ and $S = 1$

$$^1L_L \quad \text{and} \quad ^3L_{L-1,L,L+1} \tag{B.5}$$

We may apply this classification to D, D^* and D^{**} mesons. It is summarized in Table B.1. In this classification D^{**} consists of one singlet (D_1) and a triplet (D_0^*, D_1^* and D_2^*).

B.4 Heavy Quark Effective Theory (HQET) and D, D^* and D^{**} mesons

In HQET, the spin symmetry suggests that the spin of heavy quark is conserved. Thus, for the mesons consist of heavy and light quarks, we can apply jj coupling scheme. First, we can add the angular momentum (L) and the spin of the light quark (s_l) to get the angular momentum of light constituent (j_l). Then we can add the spin of the heavy quark (s_h) to j_l.

$$\begin{aligned} \boldsymbol{j}_l &= \boldsymbol{L} + \boldsymbol{s}_l \\ \boldsymbol{J} &= \boldsymbol{j}_l + \boldsymbol{s}_h \end{aligned} \tag{B.6}$$

For $L = 0$ and $s_l = 1/2$, $j_l = 1/2$ only, and for $L = 1$ and $s_l = 1/2$, $j_l = 1/2$ or $j_l = 3/2$. Hence,

- $L = 0$, $j_l = 1/2 \rightarrow J = 0$ (D) or 1 (D^*)

j_l^P	Particles	J^P	mass (GeV)
$\frac{1}{2}^+$	D, D^*	0^-, 1^-	1.971
$\frac{1}{2}^-$	D_0^*, D_1'	0^+, 1^+	2.40
$\frac{3}{2}^-$	D_1, D_2^*	1^+, 2^+	2.445

Table B.2: Spin parity of charmed meson doublets

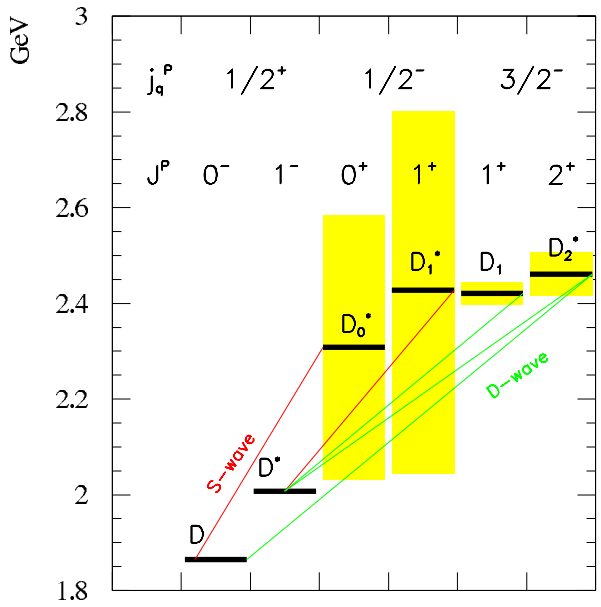

Figure B.1: Charmed meson levels and transitions. $j_q = j_l$ in the text. The yellow bands show the width of each D^{**} state

.

- $L = 1$, $j_l = 1/2 \rightarrow J = 0$ (D_0^*) or 1 (D_1')
- $L = 1$, $j_l = 3/2 \rightarrow J = 1$ (D_1) or 2 (D_2^*)

These are summarized in Table B.2. In this classification, D^{**} consists of two doublets : $(D_0^*,\ D_1')$ and $(D_1,\ D_2^*)$.

B.5 Decay modes of D^{**}

The HQET based classification implies that the $j = 3/2$ states will decay only through the d-wave ($D_1 \rightarrow D^*$ and $D_2^* \rightarrow D$) and so will be narrow. The $j = 1/2$ states can decay through the s-wave ($D_0^* \rightarrow D$ and $D_1' \rightarrow D^*$) and, in general, will be broad.

Initial state	Final state	ΔL	description
D_0^*	$D\pi$	0	broad S-wave transition
	$D^*\pi$	1	parity violation
D_1'	$D\pi$	1	parity violation
	$D^*\pi$	0	broad S-wave transition
		2	heavy quark spin symmetry violation
D_1	$D\pi$	1	parity violation
	$D^*\pi$	0	heavy quark spin symmetry violation
		2	narrow D-wave transition
D_2^*	$D\pi$	2	narrow D-wave transition
	$D^*\pi$	2	narrow D-wave transition

Table B.3: D^{**} decay modes.

This is shown in Figure B.1 and summarized in Table B.3. We consider this in detail.

Spin-parity of $D\pi$ system is

- Since $D : S = 0, P = (-)$ and $\pi : S = 0, P = (-)$
- if $L = 0$, $J = 0$ and $P = (-)(-)(-)^0 = (+)$, then $J^P = 0^+$
- if $L = 1$, $J = 1$ and $P = (-)(-)(-)^1 = (-)$, then $J^P = 1^-$
- if $L = 2$, $J = 2$ and $P = (-)(-)(-)^2 = (+)$, then $J^P = 2^+$

Note that $P = (-)^L$ for a orbital angular momentum L system. Spin-parity of $D^*\pi$ system is

- Since $D^* : S = 1, P = (-)$ and $\pi : S = 0, P = (-)$
- if $L = 0$, $J = 1$ and $P = (-)(-)(-)^0 = (+)$, then $J^P = 1^+$
- if $L = 1$, $J = 2, 1, 0$ and $P = (-)(-)(-)^1 = (-)$, then $J^P = 0^-, 1^-, 2^-$
- if $L = 2$, $J = 3, 2, 1$ and $P = (-)(-)(-)^2 = (+)$, then $J^P = 1^+, 2^+, 3^+$

Thus,

- $J^P = 0^+$ state (D_0^*) can decay only to $D\pi$ and $\Delta L = 0$
- $J^P = 1^+$ state (D_1 and D_1') can decay only to $D^*\pi$ and $\Delta L = 0, 2$
- $J^P = 2^+$ state (D_2^*) can decay both to $D\pi$ and to $D^*\pi$ and $\Delta L = 2$

Next, we consider angular momentum of D_1 and D_1' decays.

- $D_1(L = +1, s_l = +1/2, j_l = +3/2; s_h = -1/2, J = +1)$
  $\rightarrow D^*(s_l = +1/2, s_h = +1/2, j_D = +1) + \pi(j_\pi = 0) + (L = 0); J = +1$
  This violates heavy quark spin symmetry ($s_h = -1/2 \rightarrow s_h = +1/2$)
- $D_1(L = +1, s_l = +1/2, j_l = +3/2; s_h = -1/2, J = +1)$
  $\rightarrow D^*(s_l = -1/2, s_h = -1/2, j_D = -1) + \pi(j_\pi = 0) + (L = +2); J = +1$
  This conserves heavy quark spin symmetry ($s_h = -1/2 \rightarrow s_h = -1/2$)
- $D_1'(L = +1, s_l = -1/2, j_l = +1/2; s_h = +1/2, J = +1)$
  $\rightarrow D^*(s_l = +1/2, s_h = +1/2, j_D = +1) + \pi(j_\pi = 0) + (L = 0); J = +1$
  This conserves heavy quark spin symmetry ($s_h = +1/2 \rightarrow s_h = +1/2$)
- $D_1'(L = +1, s_l = -1/2, j_l = +1/2; s_h = +1/2, J = +1)$
  $\rightarrow D^*(s_l = -1/2, s_h = -1/2, j_D = -1) + \pi(j_\pi = 0) + (L = +2); J = +1$
  This violates heavy quark spin symmetry ($s_h = +1/2 \rightarrow s_h = -1/2$)

Appendix C

Isospin Symmetry

Isospin symmetry is an approximate symmetry due to the similar mass of u and d quarks. These two quarks are treated as a doublet and isospin is assigned such that

$$u : |1/2, +1/2 >, \quad d : |1/2, -1/2 > \tag{C.1}$$

Isospin of other quarks are all zero. Isospin can be treated in the same way as ordinaly spin. Thus, we can use Clebsh-Gordon coefficients to add or subtract two isospins.

C.1 Semileptonic B decays

From isospin symmetry, these B decay rates are identical

$$\begin{aligned} \Gamma(B^+ \to \bar{D}^0 \ell^+ \nu) &= \Gamma(B^0 \to D^- \ell^+ \nu) \\ \Gamma(B^+ \to \bar{D}^{*0} \ell^+ \nu) &= \Gamma(B^0 \to D^{*-} \ell^+ \nu) \\ \Gamma(B^+ \to \bar{D}^{**0} \ell^+ \nu) &= \Gamma(B^0 \to D^{**-} \ell^+ \nu) \end{aligned} \tag{C.2}$$

Isospin symmetry may be applied to non-resonant $B \to D^{(*)} \pi \ell \nu$ decays.

$$\begin{aligned} \Gamma^{NR}(B^+ \to D^- \pi^+ \ell^+ \nu) &= \Gamma^{NR}(B^0 \to \bar{D}^0 \pi^- \ell^+ \nu) \\ \Gamma^{NR}(B^+ \to D^{*-} \pi^+ \ell^+ \nu) &= \Gamma^{NR}(B^0 \to \bar{D}^{*0} \pi^- \ell^+ \nu) \end{aligned} \tag{C.3}$$

$$\begin{aligned}
\Gamma^{NR}(B^+ \to D^- \pi^+ \ell^+ \nu) &= 2\Gamma^{NR}(B^+ \to \bar{D}^0 \pi^0 \ell^+ \nu) \\
\Gamma^{NR}(B^0 \to \bar{D}^0 \pi^- \ell^+ \nu) &= 2\Gamma^{NR}(B^0 \to D^- \pi^0 \ell^+ \nu) \\
\Gamma^{NR}(B^+ \to D^{*-} \pi^+ \ell^+ \nu) &= 2\Gamma^{NR}(B^+ \to \bar{D}^{*0} \pi^0 \ell^+ \nu) \\
\Gamma^{NR}(B^0 \to \bar{D}^{*0} \pi^- \ell^+ \nu) &= 2\Gamma^{NR}(B^0 \to D^{*-} \pi^0 \ell^+ \nu)
\end{aligned} \tag{C.4}$$

The origin of the factor 2 is, for example,

$$\begin{aligned}
&B^+(u\bar{b}) : |1/2, 1/2> \\
&D^-(d\bar{c}) : |1/2, -1/2> \\
&\pi^+(u\bar{d}) : |1, 1> \\
&D^-\pi^+ : |1, 1> \times |1/2, -1/2> = \sqrt{\tfrac{1}{3}}|3/2, 1/2> + \sqrt{\tfrac{2}{3}}|1/2, 1/2> \\
&\bar{D}^0(u\bar{c}) : |1/2, 1/2> \\
&\pi^0(u\bar{u} \text{ or } d\bar{d}) : |1, 0> \\
&\bar{D}^0\pi^0 : |1, 0> \times |1/2, 1/2> = \sqrt{\tfrac{2}{3}}|3/2, 1/2> - \sqrt{\tfrac{1}{3}}|1/2, 1/2>
\end{aligned} \tag{C.5}$$

hence

$$\Gamma(B^+ \to D^- \pi^+ \ell^+ \nu) : \Gamma(B^+ \to \bar{D}^0 \pi^0 \ell^+ \nu) = \frac{2}{3} : \frac{1}{3} = 2 : 1 \tag{C.6}$$

Branching fractions are not same because of the difference in total rate (Γ) or life time (τ) of B^+ and B^0. We define

$$t_{+0} \equiv \frac{\tau_{B^+}}{\tau_{B^0}} = \frac{\Gamma_{B^0}}{\Gamma_{B^+}} \tag{C.7}$$

So, branching fractions are, for example,

$$\frac{\mathcal{B}(B^+ \to \bar{D}^{*0} \ell^+ \nu)}{\mathcal{B}(B^0 \to D^{*-} \ell^+ \nu)} = \frac{\Gamma(B^+ \to D^* \ell \nu)}{\Gamma(B^0 \to D^* \ell \nu)} \frac{\Gamma_{B^0}}{\Gamma_{B^+}} = t_{+0} \tag{C.8}$$

Thus, due to isospin symmetry, we have the following relations between branching fractions of semileptonic B decays.

$$\begin{aligned}
&\mathcal{B}(B^+ \to \bar{D}^0 \ell^+ \nu) = t_{+0}\mathcal{B}(B^0 \to D^- \ell^+ \nu) \\
&\mathcal{B}(B^+ \to \bar{D}^{*0} \ell^+ \nu) = t_{+0}\mathcal{B}(B^0 \to D^{*-} \ell^+ \nu) \\
&\mathcal{B}(B^+ \to \bar{D}^{**0} \ell^+ \nu) = t_{+0}\mathcal{B}(B^0 \to D^{**-} \ell^+ \nu) \\
&\mathcal{B}^{NR}(B^+ \to D^- \pi^+ \ell^+ \nu) = 2\mathcal{B}^{NR}(B^+ \to \bar{D}^0 \pi^0 \ell^+ \nu) \\
&= t_{+0}\mathcal{B}^{NR}(B^0 \to \bar{D}^0 \pi^- \ell^+ \nu) = 2t_{+0}\mathcal{B}^{NR}(B^0 \to D^- \pi^0 \ell^+ \nu) \\
&\mathcal{B}^{NR}(B^+ \to D^{*-} \pi^+ \ell^+ \nu) = 2\mathcal{B}^{NR}(B^+ \to \bar{D}^{*0} \pi^0 \ell^+ \nu) \\
&= t_{+0}\mathcal{B}^{NR}(B^0 \to \bar{D}^{*0} \pi^- \ell^+ \nu) = 2t_{+0}\mathcal{B}^{NR}(B^0 \to D^{*-} \pi^0 \ell^+ \nu)
\end{aligned} \tag{C.9}$$

C.2 D^{**} decays

Isospin symmetry may be applied to D^{**} decays as well.

$$\begin{aligned}
&\Gamma(D^{**0} \to D^+ \pi^-) = \Gamma(D^{**+} \to D^0 \pi^+) \\
&\Gamma(D^{**0} \to D^0 \pi^0) = \Gamma(D^{**+} \to D^+ \pi^0) \\
&\Gamma(D^{**0} \to D^{*+} \pi^-) = \Gamma(D^{**+} \to D^{*0} \pi^+) \\
&\Gamma(D^{**0} \to D^{*0} \pi^0) = \Gamma(D^{**+} \to D^{*+} \pi^0)
\end{aligned} \tag{C.10}$$

And also

$$\begin{aligned}
&\Gamma(D^{**0} \to D^+ \pi^-) = 2\Gamma(D^{**0} \to D^0 \pi^0) \\
&\Gamma(D^{**+} \to D^0 \pi^+) = 2\Gamma(D^{**+} \to D^+ \pi^0) \\
&\Gamma(D^{**0} \to D^{*+} \pi^-) = 2\Gamma(D^{**0} \to D^{*0} \pi^0) \\
&\Gamma(D^{**+} \to D^{*0} \pi^+) = 2\Gamma(D^{**+} \to D^{*+} \pi^0)
\end{aligned} \tag{C.11}$$

This factor 2 has the same origin as B decay case. For example,

$$
\begin{aligned}
&D^{**+} : |1/2, 1/2> \\
&D^{0} : |1/2, -1/2> \\
&\pi^{+} : |1, 1> \\
&D^{0}\pi^{+} : |1, 1> \times |1/2, -1/2> = \sqrt{\tfrac{1}{3}}|3/2, 1/2> + \sqrt{\tfrac{2}{3}}|1/2, 1/2> \\
&D^{+} : |1/2, 1/2> \\
&\pi^{0} : |1, 0> \\
&D^{+}\pi^{0} : |1, 0> \times |1/2, 1/2> = \sqrt{\tfrac{2}{3}}|3/2, 1/2> - \sqrt{\tfrac{1}{3}}|1/2, 1/2>
\end{aligned}
\tag{C.12}
$$

hence

$$
\Gamma(D^{**+} \to D^{0}\pi^{+}) : \Gamma(D^{**+} \to D^{+}\pi^{0}) = \frac{2}{3} : \frac{1}{3} = 2 : 1 \tag{C.13}
$$

Supposing total rates or lifetimes of D^{**0} and D^{**+} are same, branching fractions for D^{**} decays are

$$
\begin{aligned}
&\mathcal{B}(D^{**0} \to D^{+}\pi^{-}) = 2\mathcal{B}(D^{**0} \to D^{0}\pi^{0}) = \mathcal{B}(D^{**+} \to D^{0}\pi^{+}) = 2\mathcal{B}(D^{**+} \to D^{+}\pi^{0}) \\
&\mathcal{B}(D^{**0} \to D^{*+}\pi^{-}) = 2\mathcal{B}(D^{**0} \to D^{*0}\pi^{0}) = \mathcal{B}(D^{**+} \to D^{*0}\pi^{+}) = 2\mathcal{B}(D^{**+} \to D^{*+}\pi^{0})
\end{aligned}
\tag{C.14}
$$

Appendix D

$\cos\theta_{BY}$

Since we are interested in semileptonic B decays and we reconstruct $D\ell$ pairs, we consider the case $Y = D\ell$.

D.1 $B \to D\ell\nu$ decays

In the decay of $B \to Dl + \nu$, 4-momentum conservation gives

$$p_B = p_{Dl} + p_\nu \tag{D.1}$$

As the mass of neutrino is equal to zero

$$0 = p_\nu^2 = (p_B - p_{Dl})^2 = p_B^2 + p_{Dl}^2 - 2p_B \cdot p_{Dl} = m_B^2 + m_{Dl}^2 - 2p_B \cdot p_{Dl} \tag{D.2}$$

Here,

$$p_B \cdot p_{Dl} = E_B E_{Dl} - \boldsymbol{p}_B \cdot \boldsymbol{p}_{Dl} = E_B E_{Dl} - |\boldsymbol{p}_B||\boldsymbol{p}_{Dl}| \cos\Theta_{B-Dl} \tag{D.3}$$

Hence

$$\begin{aligned} 0 &= m_B^2 + m_{Dl}^2 - 2(E_B E_{Dl} - |\boldsymbol{p}_B||\boldsymbol{p}_{Dl}| \cos\Theta_{B-Dl}) \\ \Rightarrow m_B^2 + m_{Dl}^2 &= 2E_B E_{Dl} - 2|\boldsymbol{p}_B||\boldsymbol{p}_{Dl}| \cos\Theta_{B-Dl} \end{aligned} \tag{D.4}$$

Therefore

$$\cos\Theta_{B-Dl} = \frac{2E_B E_{Dl} - m_B^2 - m_{Dl}^2}{2|\boldsymbol{p}_B||\boldsymbol{p}_{Dl}|} \tag{D.5}$$

Note that $\cos\Theta_{B-Dl}$ is given by the energy, mass and momentum of B and $D\ell$.

In practice, E_B is given by the half of the beam energy in the CM frame and $|\boldsymbol{p}_B|$ is given by

$$|\boldsymbol{p}_B| = \sqrt{E_B^2 - m_B^2} \tag{D.6}$$

D.2 $B \to D^*\ell\nu$ decays

If the B decay involves additional particles, $\cos\Theta_{B-Dl} < -1$ is possible. As an example, let us consider $B \to D^*\ell\nu$ decays. In this case, the pion from $D^* \to D\pi$ decay is not included in the $D\ell$. Conservation of 4-momentum gives

$$p_B = p_{Dl} + p_\pi + p_\nu \tag{D.7}$$

Then,

$$\begin{aligned} &(p_\nu + p_\pi)^2 = (p_B - p_{Dl})^2 \\ &\Rightarrow p_\nu^2 + p_\pi^2 + 2p_\nu \cdot p_\pi = p_B^2 + p_{Dl}^2 - 2p_B \cdot p_{Dl} \\ &\Rightarrow 0 + m_\pi^2 + 2p_\nu \cdot p_\pi = m_B^2 + m_{Dl}^2 - 2p_B \cdot p_{Dl} \end{aligned} \tag{D.8}$$

Since $m_\pi \ll m_B$,

$$2p_\nu \cdot p_\pi = m_B^2 + m_{Dl}^2 - 2p_B \cdot p_{Dl} \tag{D.9}$$

and also

$$\begin{aligned} p_\nu \cdot p_\pi &= E_\nu E_\pi - \boldsymbol{p}_\nu \cdot \boldsymbol{p}_\pi = E_\nu E_\pi - |\boldsymbol{p}_\nu||\boldsymbol{p}_\pi| \cos\Theta_{\nu-\pi} \\ &= E_\nu E_\pi - E_\nu E_\pi \cos\Theta_{\nu-\pi} = E_\nu E_\pi \left(1 - \cos\Theta_{\nu-\pi}\right) \geq 0 \end{aligned} \tag{D.10}$$

Let the angle between B and Dl be Θ'_{B-Dl}. Then,

$$p_B \cdot p_{Dl} = E_B E_{Dl} - \boldsymbol{p}_B \cdot \boldsymbol{p}_{Dl} = E_B E_{Dl} - |\boldsymbol{p}_B||\boldsymbol{p}_{Dl}| \cos\Theta'_{B-Dl} \tag{D.11}$$

Hence,

$$\cos\Theta'_{B-Dl} = \frac{2E_B E_{Dl} - m_B^2 - m_{Dl}^2}{2|\boldsymbol{p}_B||\boldsymbol{p}_{Dl}|} + \frac{2p_\nu \cdot p_\pi}{2|\boldsymbol{p}_B||\boldsymbol{p}_{Dl}|} = \cos\Theta_{B-Dl} + \alpha \tag{D.12}$$

where

$$\alpha \equiv \frac{2p_\nu \cdot p_\pi}{2|\boldsymbol{p}_B||\boldsymbol{p}_{Dl}|} \geq 0 \tag{D.13}$$

Considering

$$-1 \leq \cos\Theta'_{B-Dl} \leq 1 \tag{D.14}$$

$\cos\Theta_{B-Dl} = \cos\Theta'_{B-Dl} - \alpha$ is

$$-1 - \alpha \leq \cos\Theta_{B-Dl} \leq 1 - \alpha \tag{D.15}$$

Since $\alpha \geq 0$, the lower end of $\cos\Theta_{B-Dl}$ can be smaller than -1.

D.3 If D and l come from different B

In the case that D and l came from different B, $\cos\Theta_{B-Dl} > 1$ is possible.

$$\begin{aligned} E_{Dl} &= E_D + E_l = \sqrt{m_D^2 + |\boldsymbol{p}_D|^2} + \sqrt{m_l^2 + |\boldsymbol{p}_l|^2} = \sqrt{m_D^2 + |\boldsymbol{p}_D|^2} + |\boldsymbol{p}_l| \\ |\boldsymbol{p}_{Dl}|^2 &= |\boldsymbol{p}_D + \boldsymbol{p}_l|^2 = |\boldsymbol{p}_D|^2 + |\boldsymbol{p}_l|^2 + 2|\boldsymbol{p}_D||\boldsymbol{p}_l|\cos\theta \end{aligned} \tag{D.16}$$

and

$$\begin{aligned} m_{Dl}^2 &= E_{Dl}^2 - |\boldsymbol{p}_{Dl}|^2 \\ &= m_D^2 + |\boldsymbol{p}_D|^2 + |\boldsymbol{p}_l|^2 + 2|\boldsymbol{p}_l|\sqrt{m_D^2 + |\boldsymbol{p}_D|^2} - |\boldsymbol{p}_D|^2 - |\boldsymbol{p}_l|^2 - 2|\boldsymbol{p}_D||\boldsymbol{p}_l|\cos\theta \\ &= m_D^2 + 2|\boldsymbol{p}_l|\sqrt{m_D^2 + |\boldsymbol{p}_D|^2} - 2|\boldsymbol{p}_D||\boldsymbol{p}_l|\cos\theta \\ &= m_D^2 + 2|\boldsymbol{p}_l|(\sqrt{m_D^2 + |\boldsymbol{p}_D|^2} - |\boldsymbol{p}_D|\cos\theta) \end{aligned} \tag{D.17}$$

If D and l come from different B, p_D and p_l are not restricted by energy momentum conservation. The $|\boldsymbol{p}_D|$ and $|\boldsymbol{p}_l|$ can be any value. For example, if $|\boldsymbol{p}_l| \simeq |\boldsymbol{p}_D|$ and

$\cos\theta \simeq -1$, $|\boldsymbol{p}_{Dl}|$ can be very small. However,

$$\begin{aligned} & 2E_B E_{Dl} - m_B^2 - m_{Dl}^2 \\ & \simeq 2E_B(\sqrt{m_D^2 + |\boldsymbol{p}_D|^2} + |\boldsymbol{p}_D|) - m_B^2 - m_D^2 - 2|\boldsymbol{p}_D|(\sqrt{m_D^2 + |\boldsymbol{p}_D|^2} + |\boldsymbol{p}_D|) \\ & = 2(\sqrt{m_D^2 + |\boldsymbol{p}_D|^2} + |\boldsymbol{p}_D|)(E_B - |\boldsymbol{p}_D|) - m_B^2 - m_D^2 \end{aligned} \tag{D.18}$$

is not necessarily small. For example, if $|\boldsymbol{p}_D| \ll m_D$

$$2E_B E_{Dl} - m_B^2 - m_{Dl}^2 \simeq 2m_D E_B - m_B^2 - m_D^2 \simeq -(m_B - m_D)^2 \tag{D.19}$$

Hence

$$\cos\Theta_{B-Dl} = \frac{2E_B E_{Dl} - m_B^2 - m_{Dl}^2}{2|\boldsymbol{p}_B||\boldsymbol{p}_{Dl}|} \tag{D.20}$$

can be large negative number. And, if $|\boldsymbol{p}_D| \simeq 1.2\, m_D$

$$2E_B E_{Dl} - m_B^2 - m_{Dl}^2 \simeq 5.4\, m_D(m_B - m_D) - m_B^2 - m_D^2 > 0 \tag{D.21}$$

Hence

$$\cos\Theta_{B-Dl} = \frac{2E_B E_{Dl} - m_B^2 - m_{Dl}^2}{2|\boldsymbol{p}_B||\boldsymbol{p}_{Dl}|} \tag{D.22}$$

can be larger than 1.

Appendix E

Velocity transfer w

E.1 w and q^2

In the framework of Heavy Quark Effective Theory (HQET) it is convenient to use the velocity transfer w instead of momentum transfer q^2. In semileptonic $B \to D^{(*)}\ell\nu$ decays, w is defined as the product of 4-velocities of B and $D^{(*)}$

$$w \equiv v_B \cdot v_{D^{(*)}} = \frac{p_B \cdot p_{D^{(*)}}}{m_B m_{D^{(*)}}} \tag{E.1}$$

The momentum transfer q^2 from B to $D^{(*)}$ (or the invariant mass of the virtual W) is given by

$$q = p_\ell + p_\nu = p_B - p_{D^{(*)}} \tag{E.2}$$

Thus

$$\begin{aligned} &q^2 = (p_B - p_{D^{(*)}})^2 = p_B^2 + p_{D^{(*)}}^2 - 2p_B \cdot p_{D^{(*)}} = m_B^2 + m_{D^{(*)}}^2 - 2p_B \cdot p_{D^{(*)}} \\ &\Rightarrow p_B \cdot p_{D^{(*)}} = \frac{m_B^2 + m_{D^{(*)}}^2 - q^2}{2} \end{aligned} \tag{E.3}$$

Hence

$$w = \frac{m_B^2 + m_{D^{(*)}}^2 - q^2}{2m_B m_{D^{(*)}}} \tag{E.4}$$

w is a Lorentz invariant and linearly related to q^2.

w corresponds to the relativistic boost γ of the $D^{(*)}$ in the B rest frame.

$$\gamma_{D^{(*)}} = \frac{E_{D^{(*)}}}{m_{D^{(*)}}} \tag{E.5}$$

E.2 $1 \leq w \lesssim 1.6$

The range of w and q^2 are restricted by kinematics of the decay. When $q^2 = 0$, w is maximum

$$w_{\max} = \frac{m_B^2 + m_{D^{(*)}}^2}{2 m_B m_{D^{(*)}}} \tag{E.6}$$

Using $m_B = 5279$, $m_D = 1867$ and $m_{D^*} = 2008$ MeV,

$$\frac{m_B^2 + m_D^2}{2 m_B m_D} = 1.590, \quad \frac{m_B^2 + m_{D^*}^2}{2 m_B m_{D^*}} = 1.504 \tag{E.7}$$

Using $m_{D_0^*} = 2400$, $m_{D_1'} = 2430$, $m_{D_1} = 2420$ and $m_{D_2^*} = 2460$ MeV,

$$\begin{aligned} \frac{m_B^2 + m_{D_0^*}^2}{2 m_B m_{D_0^*}} = 1.327, \quad \frac{m_B^2 + m_{D_1'}^2}{2 m_B m_{D_1'}} = 1.316, \\ \frac{m_B^2 + m_{D_1}^2}{2 m_B m_{D_1}} = 1.320, \quad \frac{m_B^2 + m_{D_2^*}^2}{2 m_B m_{D_2^*}} = 1.306 \end{aligned} \tag{E.8}$$

The minimum of the w is

$$w_{\min} = 1 \tag{E.9}$$

which corresponds to

$$q^2_{\max} = (m_B - m_{D^{(*)}})^2 \tag{E.10}$$

where

$$(m_B - m_D)^2 = 11.64, \quad (m_B - m_{D^*})^2 = 10.69 \ (\mathrm{GeV}/c^2)^2 \tag{E.11}$$

and

$$(m_B - m_{D_0^*})^2 = 8.29, \quad (m_B - m_{D_1'})^2 = 8.12 \ (\mathrm{GeV}/c^2)^2, \tag{E.12}$$

$$(m_B - m_{D_1})^2 = 8.17, \quad (m_B - m_{D_2^*})^2 = 7.95 \ (\mathrm{GeV}/c^2)^2 \tag{E.13}$$

E.3 Practical calculation of w

We can calculate w by the following formula

$$w = \frac{p_B \cdot p_{D^{(*)}}}{m_B m_{D^{(*)}}} = \frac{E_B E_{D^{(*)}} - |\boldsymbol{P}_B||\boldsymbol{P}_{D^{(*)}}| \cos\theta_{B-D}}{m_B m_{D^{(*)}}} \tag{E.14}$$

In practice, E_B is the beam energy in the CM frame, and $|\boldsymbol{P}_B|$ is given by

$$|\boldsymbol{P}_B| = \sqrt{E_B^2 - m_B^2} \tag{E.15}$$

Appendix F

Calculation of $\mathcal{G}(1)|V_{cb}|$ and $\mathcal{F}(1)|V_{cb}|$

F.1 $\mathcal{G}(1)|V_{cb}|$

The differential decay rate for $B \to D\ell\nu$ decays is given in Equation (2.10). Combined with CLN parametrization given in Equation (2.17), the differential decay rate is given by

$$\begin{aligned}
&\frac{d\Gamma(B \to D\ell\nu)}{dw} \\
&= \frac{G_F^2 m_B^5}{48\pi^3} r^3 (w^2-1)^{3/2} (1+r)^2 [1 - 8\rho_D^2 z + (51\rho_D^2 - 10)z^2 - (252\rho_D^2 - 84)z^3]^2 \\
&\quad \times \left(\mathcal{G}(1)|V_{cb}|\right)^2
\end{aligned} \tag{F.1}$$

Note that $\mathcal{G}(1) = h_+(1)$. By integrating over w, we get

$$\begin{aligned}
&\frac{\mathcal{B}(B \to D\ell\nu)}{\tau_B} \\
&= \frac{G_F^2 m_B^5}{48\pi^3} r^3 (1+r)^2 \int (w^2-1)^{3/2} [1 - 8\rho_D^2 z + (51\rho_D^2 - 10)z^2 - (252\rho_D^2 - 84)z^3]^2 dw \\
&\quad \times \left(\mathcal{G}(1)|V_{cb}|\right)^2
\end{aligned} \tag{F.2}$$

where τ_B is the lifetime of the B meson. If we define

$$C^D \equiv \sqrt{\frac{48\pi^3}{G_F^2 m_B^5 \tau_B r^3 (1+r)^2}} \tag{F.3}$$

$$I_1^D \equiv \int (w^2-1)^{3/2}(1-10z^2+84z^3)^2 dw \tag{F.4}$$

$$I_2^D \equiv 2\int (w^2-1)^{3/2}(1-10z^2+84z^3)(8z-51z^2+252z^3) dw \tag{F.5}$$

$$I_3^D \equiv \int (w^2-1)^{3/2}(8z-51z^2+252z^3)^2 dw \tag{F.6}$$

then

$$\mathcal{G}(1)|V_{cb}| = C^D \mathcal{B}(B \to D\ell\nu)^{1/2}[I_1^D - \rho_D^2 I_2^D + (\rho_D^2)^2 I_3^D]^{-1/2} \tag{F.7}$$

Thus, using fit results $\mathcal{B}(B \to D\ell\nu)$ and ρ_D^2, we can calculate $\mathcal{G}(1)|V_{cb}|$. We use the following numerical values

$$\begin{aligned}
&\tau_{B^+} = 1.638 \times 10^{-12}/6.58211915 \times 10^{-25} \ \ \text{GeV}^{-1} \\
&m_{B^+} = 5.2790 \ \ \text{GeV} \\
&m_{D^0} = 1.8645 \ \ \text{GeV} \\
&G_F = 1.166371 \times 10^{-5} \ \ \text{GeV}^{-2}
\end{aligned} \tag{F.8}$$

F.2 $\mathcal{F}(1)|V_{cb}|^2$

The differential decay rate for $B \to D^*\ell\nu$ decays is given in Equation (2.26). Combined with CLN parametrization given in Equation (2.25), the differential decay rate is given by

$$\begin{aligned}
&\frac{d\Gamma(B \to D^*\ell\nu)}{dw} \\
&= \frac{G_F^2 |V_{cb}|^2 m_B^5}{48\pi^3} r^3 (w^2-1)^{1/2}(w+1)^2 \\
&\quad \times [\mathcal{F}(1)]^2 [1 - 8\rho^2 z + (53\rho^2 - 15)z^2 - (231\rho^2 - 91)z^3]^2 (\tilde{h}_+^2 + \tilde{h}_-^2 + \tilde{h}_0^2)
\end{aligned} \tag{F.9}$$

Note that $\mathcal{F}(1) = h_{A_1}(1)$. By integrating over w, we get

$$\begin{aligned}\frac{\mathcal{B}(B \to D^* \ell \nu)}{\tau_B} = \frac{G_F^2 m_B^5}{48\pi^3} r^3 \left(\mathcal{F}(1)|V_{cb}|\right)^2 \\ \int (w^2-1)^{1/2}(w+1)^2(\tilde{h}_+^2 + \tilde{h}_-^2 + \tilde{h}_0^2) \\ \times[1 - 8\rho^2 z + (53\rho^2 - 15)z^2 - (231\rho^2 - 91)z^3]^2 dw \end{aligned} \tag{F.10}$$

Let us simplify this equation. By defining

$$\begin{aligned} k_1 &\equiv -0.12(w-1) + 0.05(w-1)^2 \\ k_2 &\equiv 0.11(w-1) - 0.06(w-1)^2 \end{aligned} \tag{F.11}$$

we get

$$\begin{aligned} &\tilde{h}_+^2 + \tilde{h}_-^2 + \tilde{h}_0^2 \\ &= (1 - 2wr + r^2)\left[1 - 2\sqrt{\frac{w-1}{w+1}}(R_1 + k_1) + \frac{w-1}{w+1}(R_1 + k_1)^2\right] \\ &\quad + (1 - 2wr + r^2)\left[1 + 2\sqrt{\frac{w-1}{w+1}}(R_1 + k_1) + \frac{w-1}{w+1}(R_1 + k_1)^2\right] \\ &\quad + (w-r)^2 - 2(w-r)(w-1)(R_2 + k_2) + (w-1)^2(R_2 + k_2)^2 \\ &= (2 + w^2 - 6wr + 3r^2) + 2(1 - 2wr + r^2)\frac{w-1}{w+1}(R_1^2 + 2k_1 R_1 + k_1^2) \\ &\quad - 2(w-r)(w-1)(R_2 + k_2) + (w-1)^2(R_2^2 + 2k_2 R_2 + k_2^2) \end{aligned} \tag{F.12}$$

Thus, if we define

$$A \equiv (2 + w^2 - 6wr + 3r^2) + 2(1 - 2wr + r^2)\frac{w-1}{w+1}k_1^2 \\ -2(w-r)(w-1)k_2 + (w-1)^2 k_2^2 \tag{F.13}$$

$$B_1 \equiv 4(1 - 2wr + r^2)\frac{w-1}{w+1}k_1 \tag{F.14}$$

$$D_1 \equiv 2(1 - 2wr + r^2)\frac{w-1}{w+1} \tag{F.15}$$

$$B_2 \equiv -2(w-r)(w-1) + 2k_2(w-1)^2 \tag{F.16}$$

$$D_2 \equiv (w-1)^2 \tag{F.17}$$

then

$$\tilde{h}_+^2 + \tilde{h}_-^2 + \tilde{h}_0^2 = A + B_1 R_1 + D_1 R_1^2 + B_2 R_2 + D_2 R_2^2 \tag{F.18}$$

If we further define

$$\begin{aligned} E_1 &\equiv (w^2-1)^{1/2}(w+1)^2(1 - 15z^2 + 91z^3)^2 \\ E_2 &\equiv 2(w^2-1)^{1/2}(w+1)^2(1 - 15z^2 + 91z^3)(8z - 53z^2 + 231z^3) \\ E_3 &\equiv (w^2-1)^{1/2}(w+1)^2(8z - 53z^2 + 231z^3)^2 \end{aligned} \tag{F.19}$$

and

$$I_1 \equiv \int AE_1 dw \tag{F.20}$$

$$I_2 \equiv \int AE_2 dw \tag{F.21}$$

$$I_3 \equiv \int AE_3 dw \tag{F.22}$$

$$I_4 \equiv \int B_1 E_1 dw \tag{F.23}$$

$$I_5 \equiv \int B_1 E_2 dw \tag{F.24}$$

$$I_6 \equiv \int B_1 E_3 dw \tag{F.25}$$

$$I_7 \equiv \int C_1 E_1 dw \tag{F.26}$$

$$I_8 \equiv \int C_1 E_2 dw \tag{F.27}$$

$$I_9 \equiv \int C_1 E_3 dw \tag{F.28}$$

$$I_{10} \equiv \int B_2 E_1 dw \tag{F.29}$$

$$I_{11} \equiv \int B_2 E_2 dw \tag{F.30}$$

$$I_{12} \equiv \int B_2 E_3 dw \tag{F.31}$$

$$I_{13} \equiv \int C_2 E_1 dw \tag{F.32}$$

$$I_{14} \equiv \int C_2 E_2 dw \tag{F.33}$$

$$I_{15} \equiv \int C_2 E_3 dw \tag{F.34}$$

and also

$$C \equiv \sqrt{\frac{48\pi^3}{G_F^2 m_B^5 \tau_B r^3}} \tag{F.35}$$

$$\begin{aligned}\mathcal{F}(1)|V_{cb}| = C\mathcal{B}(B \to D^*\ell\nu)^{1/2}[&I_1 - I_2\rho^2 + I_3(\rho^2)^2 \\ &+I_4R_1 - I_5R_1\rho^2 + I_6R_1(\rho^2)^2 \\ &+I_7R_1^2 - I_8R_1^2\rho^2 + I_9R_1^2(\rho^2)^2 \\ &+I_{10}R_2 - I_{11}R_2\rho^2 + I_{12}R_2(\rho^2)^2 \\ &+I_{13}R_2^2 - I_{14}R_2^2\rho^2 + I_{15}R_2^2(\rho^2)^2]^{-1/2}\end{aligned} \tag{F.36}$$

Thus, using fit results $\mathcal{B}(B \to D^*\ell\nu)$, R_1, R_2 and ρ^2, we can calculate $\mathcal{F}(1)|V_{cb}|$. We use the following numerical value in addition to the ones given in Equation (F.8)

$$m_{D^{*0}} = 2.0067 \ \ \text{GeV} \tag{F.37}$$

F.3 Uncertainties

To calculate uncertainties and correlations, for simplicity, we define

$$\begin{aligned} y_1 &\equiv \mathcal{G}(1)|V_{cb}| \\ y_2 &\equiv \mathcal{F}(1)|V_{cb}| \\ y_3 &\equiv \rho^2 \\ y_4 &\equiv \rho_D^2 \\ y_5 &\equiv R_1 \\ y_6 &\equiv R_2 \\ x_1 &\equiv \rho_D^2 \\ x_2 &\equiv \rho^2 \\ x_3 &\equiv R_1 \\ x_4 &\equiv R_2 \\ x_5 &\equiv \mathcal{B}(B \to D\ell\nu) \\ x_6 &\equiv \mathcal{B}(B \to D^*\ell\nu) \end{aligned} \tag{F.38}$$

then, Equation (F.7) becomes

$$y_1 = C^D x_5^{1/2} (I_1^D - I_2^D x_1 + I_3^D x_1^2)^{-1/2} \tag{F.39}$$

and Equation (F.36) becomes

$$\begin{aligned} y_2 = C x_6^{1/2} [& I_1 - I_2 x_2 + I_3 x_2^2 \\ & + I_4 x_3 - I_5 x_3 x_2 + I_6 x_3 x_2^2 \\ & + I_7 x_3^2 - I_8 x_3^2 x_2 + I_9 x_3^2 x_2^2 \\ & + I_{10} x_4 - I_{11} x_4 x_2 + I_{12} x_4 x_2^2 \\ & + I_{13} x_4^2 - I_{14} x_4^2 x_2 + I_{15} x_4^2 x_2^2]^{-1/2} \end{aligned} \tag{F.40}$$

The error matrix M(y) of y_1 - y_6 is determined by

$$M(y) = \left(\frac{\partial y_i}{\partial x_j} \right) M(x) \left(\frac{\partial y_i}{\partial x_j} \right) \tag{F.41}$$

where $M(x)$ the error matrix of x_1 - x_6, which can be extracted from fit, and

$$\frac{\partial y_1}{\partial x_1} = \frac{C}{2} x_5^{1/2} (I_2^D - 2I_3^D x_1)(I_1^D - I_2^D x_1 + I_3^D x_1^2)^{-3/2} \tag{F.42}$$

$$\frac{\partial y_1}{\partial x_5} = \frac{C}{2} x_5^{-1/2} (I_1^D - I_2^D x_1 + I_3^D x_1^2)^{-1/2} \tag{F.43}$$

$$\frac{\partial y_2}{\partial x_2} = -\frac{C}{2} x_6^{1/2} (-I_2 + 2I_3 x_2 - I_5 x_3 + 2I_6 x_3 x_2 - I_8 x_3^2 + 2I_9 x_3^2 x_2 - I_{11} x_6 + 2I_{12} x_6 x_2 - I_{14} x_6^2 + 2I_{15} x_6^2 x_2) F^{-3/2} \tag{F.44}$$

$$\frac{\partial y_2}{\partial x_3} = -\frac{C}{2} x_6^{1/2} (I_4 - I_5 x_2 + I_6 x_2^2 + 2I_7 x_3 - 2I_8 x_3 x_2 + 2I_9 x_3 x_2^2) F^{-3/2} \tag{F.45}$$

$$\frac{\partial y_2}{\partial x_4} = -\frac{C}{2} x_6^{1/2} (I_{10} - I_{11} x_2 + I_{12} x_2^2 + 2I_{13} x_4 - 2I_{14} x_4 x_2 + 2I_{15} x_4 x_2^2) F^{-3/2} \tag{F.46}$$

$$\frac{\partial y_2}{\partial x_6} = \frac{C}{2} x_6^{-1/2} F^{-1/2} \tag{F.47}$$

$$\frac{\partial y_3}{\partial x_1} = 1 \tag{F.48}$$

$$\frac{\partial y_4}{\partial x_2} = 1 \tag{F.49}$$

$$\frac{\partial y_5}{\partial x_3} = 1 \tag{F.50}$$

$$\frac{\partial y_6}{\partial x_4} = 1 \tag{F.51}$$

where

$$\begin{aligned} F = {} & I_1 - I_2 x_2 + I_3 x_2^2 + I_4 x_3 - I_5 x_3 x_2 + I_6 x_3 x_2^2 + I_7 x_3^2 - I_8 x_3^2 x_2 + I_9 x_3^2 x_2^2 \\ & + I_{10} x_4 - I_{11} x_4 x_2 + I_{12} x_4 x_2^2 + I_{13} x_4^2 - I_{14} x_4^2 x_2 + I_{15} x_4^2 x_2^2 \end{aligned} \tag{F.52}$$

and all other partial derivatives are zero.

The correlation coefficient, for example, between $\mathcal{G}(1)|V_{cb}|$ and $\mathcal{F}(1)|V_{cb}|$ can be calculated by

$$\frac{\mathrm{cov}(y_1, y_2)}{\sigma_{y_1} \sigma_{y_2}} \tag{F.53}$$

Appendix G

Leibovich Ligeti Stewart Wise (LLSW) model

The LLSW model is described in [45,46]. We will summarize the part which is related to our analysis.

The relevant kinematic variables are w and θ. This θ is the angle between the charged lepton and the charmed meson in the rest frame of the virtual W boson. Thus $\theta = \pi - \theta_\ell$,

$$\cos\theta = \cos(\pi - \theta_\ell) = -\cos\theta_\ell \tag{G.1}$$

In the paper [46], they use different approximations : Approximation A and B. In Approximation A, they treat $w - 1$ as order $\Lambda_{\rm QCD}/m_Q$ and expand decay rates in these parameters. Thus, Approximation A is useful only when $w \simeq 1$. This is not appropriate to our analysis. In Approximation B, they keep the known order $\Lambda_{\rm QCD}/m_Q$ contributions to form factors as well as the full w-dependence of decay rates. Thus, we consider only Approximation B.

In the paper two parameters are defined as follows

$$\varepsilon_b \equiv \frac{1}{2m_b}, \quad \varepsilon_c \equiv \frac{1}{2m_c} \tag{G.2}$$

with numerical values

$$m_b = 4.8\text{GeV}, \quad m_c = 1.4\text{GeV} \tag{G.3}$$

The difference between a hadron mass and a heavy quark mass in the first order :

$$\begin{aligned} &\bar{\Lambda} \text{ for ground state doublet } (D \text{ and } D^*) \\ &\bar{\Lambda}' \text{ for exited } \tfrac{3}{2}^+ \text{ doublet } (D_1 \text{ and } D_2^*) \\ &\bar{\Lambda}^* \text{ for exited } \tfrac{1}{2}^+ \text{ doublet } (D_0^* \text{ and } D_1') \end{aligned} \tag{G.4}$$

with numerical values

$$\begin{aligned} &\bar{\Lambda} = 0.4\text{GeV} \\ &\bar{\Lambda}' - \bar{\Lambda} = 0.39\text{GeV} \\ &\bar{\Lambda}^* - \bar{\Lambda} = 0.35\text{GeV} \end{aligned} \tag{G.5}$$

G.1 $B \to D_1 \ell \nu$

The matrix elements are

$$\frac{< D_1(v',\varepsilon)|V^\mu|B(v) >}{\sqrt{m_{D_1} m_B}} = f_{V_1}\varepsilon^{*\mu} + (f_{V_2} v^\mu + f_{V_3} v'^\mu)(\varepsilon^* \cdot v) \tag{G.6}$$

$$\frac{< D_1(v',\varepsilon)|A^\mu|B(v) >}{\sqrt{m_{D_1} m_B}} = i f_A \epsilon^{\mu\alpha\beta\gamma} \varepsilon^*_\alpha v_\beta v'_\gamma \tag{G.7}$$

The differential decay rate is

$$\begin{aligned} \frac{d^2\Gamma_{D_1}}{dw\, d\cos\theta} = 3\Gamma_0 r_1^3 \sqrt{w^2-1}\{&\sin^2\theta[(w-r_1)f_{V_1} + (w^2-1)(f_{V_3} + r_1 f_{V_2})]^2 \\ &+(1 - 2r_1 w + r_1^2)[(1+\cos^2\theta)(f_{V_1}^2 + (w^2-1)f_A^2) \\ &-4\cos\theta\sqrt{w^2-1} f_{V_1} f_A]\} \end{aligned} \tag{G.8}$$

where

$$\Gamma_0 = \frac{G_F^2 |V_{cb}|^2 m_B^5}{192\pi^3}, \quad r_1 = \frac{m_{D_1}}{m_B} \tag{G.9}$$

In approximation B, the form factors are given by

$$\begin{aligned}
\sqrt{6}f_A &= -(w+1)\tau - \varepsilon_b\{(w-1)[(\bar{\Lambda}'+\bar{\Lambda})\tau - (2w+1)\tau_1 - \tau_2] + (w+1)\eta_b\} \\
&\quad -\varepsilon_c[4(w\bar{\Lambda}'-\bar{\Lambda})\tau - 3(w-1)(\tau_1-\tau_2) + (w+1)(\eta_{\rm ke} - 2\eta_1 - 3\eta_3)] \\
\sqrt{6}f_{V_1} &= (1-w^2)\tau - \varepsilon_b(w^2-1)[(\bar{\Lambda}'+\bar{\Lambda})\tau - (2w+1)\tau_1 - \tau_2 + \eta_b] \\
&\quad -\varepsilon_c[4(w+1)(w\bar{\Lambda}'-\bar{\Lambda})\tau - (w^2-1)(3\tau_1 - 3\tau_2 - \eta_{\rm ke} + 2\eta_1 + 3\eta_3)] \\
\sqrt{6}f_{V_2} &= -3\tau - 3\varepsilon_b[(\bar{\Lambda}'+\bar{\Lambda})\tau - (2w+1)\tau_1 - \tau_2 + \eta_b] \\
&\quad -\varepsilon_c[(4w-1)\tau_1 + 5\tau_2 + 3\eta_{\rm ke} + 10\eta_1 + 4(w-1)\eta_2 - 5\eta_3)] \\
\sqrt{6}f_{V_3} &= (w-2)\tau + \varepsilon_b\{(2+w)[(\bar{\Lambda}'+\bar{\Lambda})\tau - (2w+1)\tau_1 - \tau_2] - (2-w)\eta_b\} \\
&\quad +\varepsilon_c[4(w\bar{\Lambda}'-\bar{\Lambda})\tau + (2+w)\tau_1 + (2+3w)\tau_2 \\
&\quad +(w-2)\eta_{\rm ke} - 2(6+w)\eta_1 - 4(w-1)\eta_2 - (3w-2)\eta_3]
\end{aligned} \tag{G.10}$$

where τ is the leading $m_Q \to \infty$ Isgur-Wise function, which is assumed to be a linear form:

$$\tau(w) = \tau(1)[1 + \hat{\tau}'(w-1)] \tag{G.11}$$

where

$$\tau' = \frac{d\tau}{dw}, \quad \hat{\tau}' = \frac{\tau'}{\tau(1)} \tag{G.12}$$

The uncertainty in the $\Lambda_{\rm QCD}/m_Q$ corrections is parametrized by τ_1 and τ_2.

In Approximation B_1,

$$\tau_1 = 0, \quad \tau_2 = 0 \tag{G.13}$$

In Approximation B_2,

$$\tau_1 = \bar{\Lambda}\tau, \quad \tau_2 = -\bar{\Lambda}'\tau \tag{G.14}$$

These are the two end values of τ_1 and τ_2. True τ_1 and τ_2 reside somewhere in between.

η_i comes from the correction to the HQET Lagrangian. In Approximation B,

$$\eta_1 = \eta_2 = \eta_3 = 0 \tag{G.15}$$

Also, in this Approximation, $\eta_1^{(b)} = \eta_2^{(b)} = \eta_3^{(b)} = 0$. Thus

$$\eta_b \equiv \eta_{\rm ke}^{(b)} + 6\eta_1^{(b)} - 2(w-1)\eta_2^{(b)} + \eta_3^{(b)} = \eta_{\rm ke}^{(b)} \tag{G.16}$$

Hence, the form factors are

$$\begin{aligned}
\sqrt{6} f_A &= -(w+1)(\tau + \varepsilon_c \eta_{\rm ke} + \varepsilon_b \eta_{\rm ke}^{(b)}) - \varepsilon_b (w-1)[(\bar{\Lambda}' + \bar{\Lambda})\tau - (2w+1)\tau_1 - \tau_2] \\
&\quad -\varepsilon_c [4(w\bar{\Lambda}' - \bar{\Lambda})\tau - 3(w-1)(\tau_1 - \tau_2)] \\
\sqrt{6} f_{V_1} &= (1-w^2)(\tau + \varepsilon_c \eta_{\rm ke} + \varepsilon_b \eta_{\rm ke}^{(b)}) - \varepsilon_b (w^2-1)[(\bar{\Lambda}' + \bar{\Lambda})\tau - (2w+1)\tau_1 - \tau_2] \\
&\quad -\varepsilon_c [4(w+1)(w\bar{\Lambda}' - \bar{\Lambda})\tau - 3(w^2-1)(\tau_1 - \tau_2)] \\
\sqrt{6} f_{V_2} &= -3(\tau + \varepsilon_c \eta_{\rm ke} + \varepsilon_b \eta_{\rm ke}^{(b)}) - 3\varepsilon_b [(\bar{\Lambda}' + \bar{\Lambda})\tau - (2w+1)\tau_1 - \tau_2] \\
&\quad -\varepsilon_c [(4w-1)\tau_1 + 5\tau_2] \\
\sqrt{6} f_{V_3} &= (w-2)(\tau + \varepsilon_c \eta_{\rm ke} + \varepsilon_b \eta_{\rm ke}^{(b)}) + \varepsilon_b (2+w)[(\bar{\Lambda}' + \bar{\Lambda})\tau - (2w+1)\tau_1 - \tau_2] \\
&\quad +\varepsilon_c [4(w\bar{\Lambda}' - \bar{\Lambda})\tau + (2+w)\tau_1 + (2+3w)\tau_2]
\end{aligned} \tag{G.17}$$

$\eta_{\rm ke}$ and $\eta_{\rm ke}^{(b)}$ can be absorbed into τ by the replacement of τ by

$$\tilde{\tau} = \tau + \varepsilon_c \eta_{\rm ke} + \varepsilon_b \eta_{\rm ke}^{(b)} \tag{G.18}$$

Thus, the form factors are

$$\begin{aligned}
\sqrt{6}f_A &= -(w+1)\tilde{\tau} - \varepsilon_b(w-1)[(\bar{\Lambda}'+\bar{\Lambda})\tau - (2w+1)\tau_1 - \tau_2] \\
&\quad -\varepsilon_c[4(w\bar{\Lambda}'-\bar{\Lambda})\tau - 3(w-1)(\tau_1-\tau_2)] \\
\sqrt{6}f_{V_1} &= (1-w^2)\tilde{\tau} - \varepsilon_b(w^2-1)[(\bar{\Lambda}'+\bar{\Lambda})\tau - (2w+1)\tau_1 - \tau_2] \\
&\quad -\varepsilon_c[4(w+1)(w\bar{\Lambda}'-\bar{\Lambda})\tau - 3(w^2-1)(\tau_1-\tau_2)] \\
\sqrt{6}f_{V_2} &= -3\tilde{\tau} - 3\varepsilon_b[(\bar{\Lambda}'+\bar{\Lambda})\tau - (2w+1)\tau_1 - \tau_2] \\
&\quad -\varepsilon_c[(4w-1)\tau_1 + 5\tau_2] \\
\sqrt{6}f_{V_3} &= (w-2)\tilde{\tau} + \varepsilon_b(2+w)[(\bar{\Lambda}'+\bar{\Lambda})\tau - (2w+1)\tau_1 - \tau_2] \\
&\quad +\varepsilon_c[4(w\bar{\Lambda}'-\bar{\Lambda})\tau + (2+w)\tau_1 + (2+3w)\tau_2]
\end{aligned} \tag{G.19}$$

The other τ can also be replaced by $\tilde{\tau}$ in the same order of approximation. For simplicity, we omit the tilde, then

$$\begin{aligned}
\sqrt{6}f_A &= -(w+1)\tau - \varepsilon_b(w-1)[(\bar{\Lambda}'+\bar{\Lambda})\tau - (2w+1)\tau_1 - \tau_2] \\
&\quad -\varepsilon_c[4(w\bar{\Lambda}'-\bar{\Lambda})\tau - 3(w-1)(\tau_1-\tau_2)] \\
\sqrt{6}f_{V_1} &= (1-w^2)\tau - \varepsilon_b(w^2-1)[(\bar{\Lambda}'+\bar{\Lambda})\tau - (2w+1)\tau_1 - \tau_2] \\
&\quad -\varepsilon_c[4(w+1)(w\bar{\Lambda}'-\bar{\Lambda})\tau - 3(w^2-1)(\tau_1-\tau_2)] \\
\sqrt{6}f_{V_2} &= -3\tau - 3\varepsilon_b[(\bar{\Lambda}'+\bar{\Lambda})\tau - (2w+1)\tau_1 - \tau_2] \\
&\quad -\varepsilon_c[(4w-1)\tau_1 + 5\tau_2] \\
\sqrt{6}f_{V_3} &= (w-2)\tau + \varepsilon_b(2+w)[(\bar{\Lambda}'+\bar{\Lambda})\tau - (2w+1)\tau_1 - \tau_2] \\
&\quad +\varepsilon_c[4(w\bar{\Lambda}'-\bar{\Lambda})\tau + (2+w)\tau_1 + (2+3w)\tau_2]
\end{aligned} \tag{G.20}$$

The numerical value for the slope is

$$\hat{\tau}' = -1.5 \pm 0.5 \tag{G.21}$$

G.2 $B \to D_2^* \ell \nu$

The matrix elements are

$$\frac{< D_2^*(v',\varepsilon)|V^\mu|B(v) >}{\sqrt{m_{D_2^*} m_B}} = i k_V \epsilon^{\mu\alpha\beta\gamma} \varepsilon^*_{\alpha\sigma} v^\sigma v_\beta v'_\gamma \tag{G.22}$$

$$\frac{< D_2^*(v',\varepsilon)|A^\mu|B(v) >}{\sqrt{m_{D_2^*} m_B}} = k_{A_1} \varepsilon^{*\mu\alpha} v_\alpha + (k_{A_2} v^\mu + k_{A_3} v'^\mu) \varepsilon^*_{\alpha\beta} v^\alpha v^\beta \tag{G.23}$$

The differential decay rate is

$$\begin{aligned} \frac{d^2\Gamma_{D_2^*}}{dw\, d\cos\theta} &= \tfrac{3}{2}\Gamma_0 r_2^3 (w^2-1)^{3/2} \{ \tfrac{4}{3}\sin^2\theta [(w-r_2)k_{A_1} + (w^2-1)(k_{A_3} + r_2 k_{A_2})]^2 \\ &+ (1 - 2r_2 w + r_2^2)[(1+\cos^2\theta)(k_{A_1}^2 + (w^2-1)k_V^2) - 4\cos\theta\sqrt{w^2-1} k_{A_1} k_V] \} \end{aligned} \tag{G.24}$$

where

$$r_2 = \frac{m_{D_2^*}}{m_B} \tag{G.25}$$

In Approximation B, the form factors are given by

$$\begin{aligned} k_V &= -\tau - \varepsilon_b[(\bar\Lambda' + \bar\Lambda)\tau - (2w+1)\tau_1 - \tau_2 + \eta_b] - \varepsilon_c(\tau_1 - \tau_2 + \eta_{\rm ke} - 2\eta_1 + \eta_3) \\ k_{A_1} &= -(1+w)\tau - \varepsilon_b\{(w-1)[(\bar\Lambda' + \bar\Lambda)\tau - (2w+1)\tau_1 - \tau_2] + (1+w)\eta_b\} \\ &\quad -\varepsilon_c[(w-1)(\tau_1 - \tau_2) + (w+1)(\eta_{\rm ke} - 2\eta_1 + \eta_3)] \\ k_{A_2} &= -2\varepsilon_c(\tau_1 + \eta_2) \\ k_{A_3} &= \tau + \varepsilon_b[(\bar\Lambda' + \bar\Lambda)\tau - (2w+1)\tau_1 - \tau_2 + \eta_b] \\ &\quad -\varepsilon_c(\tau_1 + \tau_2 - \eta_{\rm ke} + 2\eta_1 - 2\eta_2 - \eta_3) \end{aligned} \tag{G.26}$$

We use the same tricks for ηs, then

$$\begin{aligned}
k_V &= -\tau - \varepsilon_b[(\bar{\Lambda}' + \bar{\Lambda})\tau - (2w+1)\tau_1 - \tau_2] - \varepsilon_c(\tau_1 - \tau_2) \\
k_{A_1} &= -(1+w)\tau - \varepsilon_b(w-1)[(\bar{\Lambda}' + \bar{\Lambda})\tau - (2w+1)\tau_1 - \tau_2] \\
&\quad -\varepsilon_c(w-1)(\tau_1 - \tau_2) \\
k_{A_2} &= -2\varepsilon_c\tau_1 \\
k_{A_3} &= \tau + \varepsilon_b[(\bar{\Lambda}' + \bar{\Lambda})\tau - (2w+1)\tau_1 - \tau_2] - \varepsilon_c(\tau_1 + \tau_2)
\end{aligned} \tag{G.27}$$

G.3 $B \to D_0^* \ell\nu$

The matrix elements are

$$\frac{< D_0^*(v',\varepsilon)|V^\mu|B(v) >}{\sqrt{m_{D_0^*} m_B}} = 0 \tag{G.28}$$

$$\frac{< D_0^*(v',\varepsilon)|A^\mu|B(v) >}{\sqrt{m_{D_0^*} m_B}} = g_+(v^\mu + v'^\mu) + g_-(v^\mu - v'^\mu) \tag{G.29}$$

The differential decay rate is

$$\frac{d^2\Gamma_{D_0^*}}{dw\, d\cos\theta} = 3\Gamma_0 r_0^{*3}(w^2-1)^{3/2}\sin^2\theta[(1+r_0^*)g_+ - (1-r_0^*)g_-]^2 \tag{G.30}$$

where

$$r_0^* = \frac{m_{D_0^*}}{m_B} \tag{G.31}$$

In Approximation B, the form factors are given by

$$\begin{aligned}
g_+ &= \varepsilon_c\left[2(w-1)\zeta_1 - 3\zeta\tfrac{w\bar{\Lambda}^* - \bar{\Lambda}}{w+1}\right] - \varepsilon_b\left[\tfrac{\bar{\Lambda}^*(2w+1) - \bar{\Lambda}(w+2)}{w+1}\zeta - 2(w-1)\zeta_1\right] \\
g_- &= \zeta + \varepsilon_c\left[\chi_{\rm ke} + 6\chi_1 - 2(w+1)\chi_2\right] + \varepsilon_b\chi_b
\end{aligned} \tag{G.32}$$

We can use the same tricks for χs as ηs, then

$$\begin{aligned} g_+ &= \varepsilon_c \left[2(w-1)\zeta_1 - 3\zeta\tfrac{w\bar{\Lambda}^*-\bar{\Lambda}}{w+1}\right] - \varepsilon_b \left[\tfrac{\bar{\Lambda}^*(2w+1)-\bar{\Lambda}(w+2)}{w+1}\zeta - 2(w-1)\zeta_1\right] \\ g_- &= \zeta \end{aligned} \tag{G.33}$$

where

$$\zeta(w) = \frac{w+1}{\sqrt{3}}\tau(w) \tag{G.34}$$

Thus,

$$\begin{aligned} \zeta(1)[1+\hat{\zeta}'(w-1)] &= \tfrac{2+(w-1)}{\sqrt{3}}\tau(1)[1+\hat{\tau}'(w-1)] \\ &\simeq \tfrac{1}{\sqrt{3}}\tau(1)[2+2\hat{\tau}'(w-1)+(w-1)] \\ &= \tfrac{2}{\sqrt{3}}\tau(1)\left[1+\left(\hat{\tau}'+\tfrac{1}{2}\right)(w-1)\right] \end{aligned} \tag{G.35}$$

Hence

$$\begin{aligned} \zeta(1) &= \tfrac{2}{\sqrt{3}}\tau(1) \\ \hat{\zeta}' &= \tfrac{1}{2}+\hat{\tau}' = -1 \pm 0.5 \end{aligned} \tag{G.36}$$

In Approximation B_1,

$$\zeta_1 = 0, \quad \zeta_2 = 0 \tag{G.37}$$

In Approximation B_2,

$$\zeta_1 = \bar{\Lambda}\zeta, \quad \zeta_2 = -\bar{\Lambda}^*\zeta \tag{G.38}$$

These are the two end values of ζ_1 and ζ_2. True ζ_1 and ζ_2 reside somewhere in between.

G.4 $B \to D_1^* \ell\nu$

The matrix elements are

$$\frac{< D_1^*(v',\varepsilon)|V^\mu|B(v) >}{\sqrt{m_{D_1^*}m_B}} = g_{V_1}\varepsilon^{*\mu} + (g_{V_2}v^\mu + g_{V_3}v'^\mu)(\varepsilon^*\cdot v) \tag{G.39}$$

$$\frac{< D_1^*(v',\varepsilon)|A^\mu|B(v) >}{\sqrt{m_{D_1^*}m_B}} = ig_A\epsilon^{\mu\alpha\beta\gamma}\varepsilon^*_\alpha v_\beta v'_\gamma \tag{G.40}$$

The differential decay rate is

$$\begin{aligned}\frac{d^2\Gamma_{D_1^*}}{dwd\cos\theta} &= 3\Gamma_0 r_1^{*3}\sqrt{w^2-1}\{\sin^2\theta[(w-r_1^*)g_{V_1}+(w^2-1)(g_{V_3}+r_1^* g_{V_2})]^2 \\ &+(1-2r_1^* w+r_1^{*2})[(1+\cos^2\theta)(g_{V_1}^2+(w^2-1)g_A^2)-4\cos\theta\sqrt{w^2-1}g_{V_1}g_A]\}\end{aligned} \tag{G.41}$$

where

$$r_1^* = \frac{m_{D_1^*}}{m_B} \tag{G.42}$$

In Approximation B, the form factors are given by

$$\begin{aligned} g_A &= \zeta + \varepsilon_c\left[\tfrac{w\bar\Lambda^*-\bar\Lambda}{w+1}\zeta+\chi_{\rm ke}-2\chi_1\right]-\varepsilon_b\left[\tfrac{\bar\Lambda^*(2w+1)-\bar\Lambda(w+2)}{w+1}\zeta-2(w-1)\zeta_1-\chi_b\right] \\ g_{V_1} &= (w-1)\zeta+\varepsilon_c\left[(w\bar\Lambda^*-\bar\Lambda)\zeta+(w-1)(\chi_{\rm ke}-2\chi_1)\right] \\ &\quad -\varepsilon_b\left[(\bar\Lambda^*(2w+1)-\bar\Lambda(w+2))\zeta-2(w^2-1)\zeta_1-(w-1)\chi_b\right] \\ g_{V_2} &= 2\varepsilon_c(\zeta_1-\chi_2) \\ g_{V_3} &= -\zeta-\varepsilon_c\left[\tfrac{w\bar\Lambda^*-\bar\Lambda}{w+1}\zeta+2\zeta_1+\chi_{\rm ke}-2\chi_1+2\chi_2\right] \\ &\quad +\varepsilon_b\left[\tfrac{\bar\Lambda^*(2w+1)-\bar\Lambda(w+2)}{w+1}\zeta-2(w-1)\zeta_1-\chi_b\right] \end{aligned} \tag{G.43}$$

We use the same tricks for χs, then

$$\begin{aligned} g_A &= \zeta+\varepsilon_c\left[\tfrac{w\bar\Lambda^*-\bar\Lambda}{w+1}\zeta\right]-\varepsilon_b\left[\tfrac{\bar\Lambda^*(2w+1)-\bar\Lambda(w+2)}{w+1}\zeta-2(w-1)\zeta_1\right] \\ g_{V_1} &= (w-1)\zeta+\varepsilon_c(w\bar\Lambda^*-\bar\Lambda)\zeta \\ &\quad -\varepsilon_b\left[(\bar\Lambda^*(2w+1)-\bar\Lambda(w+2))\zeta-2(w^2-1)\zeta_1\right] \\ g_{V_2} &= 2\varepsilon_c\zeta_1 \\ g_{V_3} &= -\zeta-\varepsilon_c\left[\tfrac{w\bar\Lambda^*-\bar\Lambda}{w+1}\zeta+2\zeta_1\right] \\ &\quad +\varepsilon_b\left[\tfrac{\bar\Lambda^*(2w+1)-\bar\Lambda(w+2)}{w+1}\zeta-2(w-1)\zeta_1\right] \end{aligned} \tag{G.44}$$

University of Victoria

Partial Copyright License

Title of Dissertation: Measurement of Branching Fractions and Form Factor Parameters of $B \to D\ell\nu$ and $B \to D^*\ell\nu$ Decays at BaBar.

Author: _____

Kenji Hamano

October 3, 2008